AFOSR-109

AIR FORCE OFFICE OF SCIENTIFIC RESEARCH

TECHNICAL REPORT

Contract No. AF 29(600)-1711
Project No. 7856
Task No. 78548

DYNAMICS OF SEPARATING BODIES

VOLUME I

THEORETICAL ANALYSIS

by
A. H. Solarski
R. Turner
F. Doerr

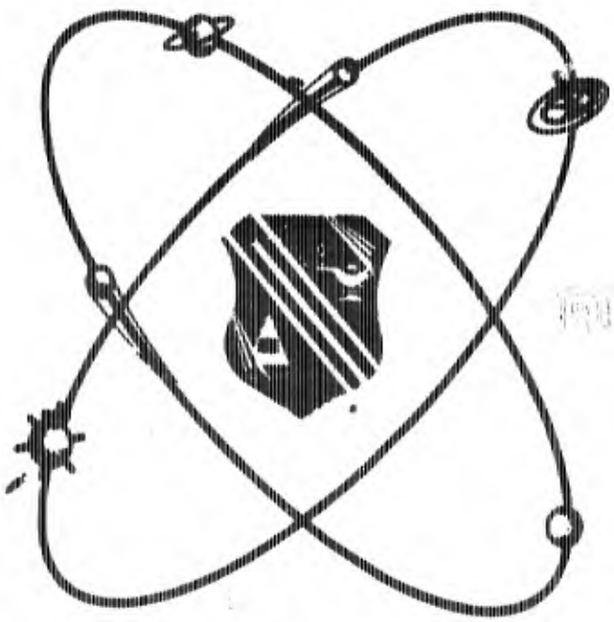

DIRECTORATE OF RESEARCH ANALYSIS

HOLLOMAN AIR FORCE BASE

NEW MEXICO

MARCH 1961

AFOSR-109

Contract No. AF 29(600)-1711
Project No. 7856
Task No. 78548

DYNAMICS OF SEPARATING BODIES

VOLUME I

THEORETICAL ANALYSIS

by

A. H. Solarski
R. Turner
F. Doerr

Cook Research Laboratories
A Division of
Cook Electric Company

Science and Engineering Division
Directorate of Research Analysis

AIR FORCE OFFICE OF SCIENTIFIC RESEARCH
OFFICE OF AEROSPACE RESEARCH
UNITED STATES AIR FORCE
Holloman Air Force Base, New Mexico

MARCH 1961

FOREWORD

This report, Volume I of the series DYNAMICS OF SEPARATING BODIES, was prepared under Air Force Contract No. AF 29(600)-1711, Project No. 7856, Task No. 78548, by the Cook Research Laboratories, a division of the Cook Electric Company, Chicago, Illinois. This contract is monitored by the AFOSR Directorate of Research Analysis, Science and Engineering Division. The contract monitor is Mr. F. Utech.

The work was conducted in the Aerodynamics Section of the Cook Research Laboratories under the direction of Mr. R.O. Fredette, Associate Director, with Messrs. H.L. Wackelin and later F.J. Doerr as Project Engineers. The treatment of wake characteristics is the work of Dr. R. Hoglund; Dr. J.S. Thale is the principal contributor in the presentation of the equations of motion. Messrs. L. Sims and P. Minerva participated in the study effort.

With respect to subsequent volumes of the series DYNAMICS OF SEPARATING BODIES, VOLUME II, MEASUREMENTS AT MACH 2, 4, AND 5, has been made available, and VOLUME III, MEASUREMENTS AT MACH 8 AND RESULTS, will be published at a later date after completion of these tests. A series of ejection tests at the above Mach numbers will be conducted in the future, and the results of thse tests will also be published at a later date.

ABSTRACT

The theoretical foundations of a detailed study of the dynamics of separating bodies at supersonic speeds are established. Carrier vehicle flow field characteristics are investigated to define the environment into which the ejected bodies are projected. The aerodynamic properties of representative capsule configurations in locally varying flows are documented, and the equations of motion pertinent to the several modes and techniques of ejection and separation are stated. Trajectory computations based upon a realistic summary of the problem inputs are discussed, and the relative importance of the operational parameters assessed. Separation system requirements are compared for the several ejection modes and capsule configurations considered. Particular emphasis is given to the section describing the wake structure behind a body representative of a carrier vehicle traveling at supersonic speeds.

TABLE OF CONTENTS

LIST OF ILLUSTRATIONS

LIST OF ILLUSTRATIONS

LIST OF TABLES

LIST OF SYMBOLS

d, D	Vehicle diameter, ft
g	Acceleration due to gravity, ft/sec^2
q, $Q = 1/2 \rho v^2$	Dynamic pressure, $lbs./ft^2$
q_w	Wake dynamic pressure, lbs/ft^2
r, y	Distance measured normal to wake axis; Radial coordinate, ft
r_o	Wake radius, ft
r_v	Vehicle radius, ft
t	Time, seconds
t_w	Thickness of wake throat, ft
u^*	Ratio of wake dividing streamline velocity to external flow velocity
x, X	Distance, axial coordinate, ft
x_1	Distance between vehicle base and first nodal point in wake, ft
x_o	Distance aft of wake minimum pressure coefficient, ft
x_t	Distance between vehicle base and wake throat, ft
A	Reference area, ft^2; Axial force, lbs
D	Drag force, lbs
K	Constant

L	Characteristic length, ft
M	Mach number; Pitching moment, lb. ft.
N	Normal force, lbs
P	Pressure, lbs/ft^2
R	Ratio of Carrier-to-capsule weight-to-drag ratios
$R_e = \frac{VL}{\nu}$	Reynolds number
U	Velocity defect in wake, ft/sec
V	Velocity, ft/sec
$V_{W_{\mathbb{E}}}$	Velocity along wake axis, ft/sec
W	Weight, lbs
X_{CP}	Axial coordinate of location of center of pressure, ft
$C_A = \frac{A}{(q\,A)}$	Axial force coefficient
$C_D = \frac{D}{qA}$	Drag force coefficient
$(C_M)_x = \frac{M}{qAL}$	Pitching moment coefficient referred to axial coordinate position, x
$C_N = \frac{N}{qA}$	Normal force coefficient
$C_p = \frac{\Delta P}{q}$	Pressure coefficient
C_{M_α}	Slope (with respect to) of pitching moment coefficient curve
C_{M_q}	Damping-in-pitch

C_{M_q}	Change in pitching moment coefficient due to rate of change of angle of attack
C_{N_α}	Slope (with respect to α) of normal force coefficient curve
α	Angle of attack, degrees
θ	Flow deviation; Wake convergence angle; Angular attitude, degrees
ν	Kinematic viscosity of air, ft^2/sec
ρ	Air density, $slugs/ft^3$
ϕ	Flow deviation from free stream direction, degrees;
	Velocity potential
	$\phi_x = \frac{\partial \phi}{\partial x}$, etc.
	$\phi_{xx} = \frac{\partial^2 \phi}{\partial x^2}$, etc.

DEFINITIONS

$C_D A$	"Drag area", ft^2
$\frac{W}{C_D A}$	"Weight-to-drag ratio", lbs/ft^2
∞	Denotes free stream conditions
Δ	Denotes incremental quantity

SECTION I

INTRODUCTION

An expedient means of recovering instrumentation, data, human or subhuman biological specimens, etc., from a rocket vehicle on a high-speed trajectory is to separate a part of the vehicle or a portion of its contents and bring that subordinate package safely to the surface of the earth. The process of separation and the requirements on the separation system are amenable to theoretical investigation to the extent that geometrical effects may be established, and those configurations deserving of experimental study may be limited to a practicable number. This report documents the results of such a theoretical investigation, which, taking originally a broad view, has delineated the areas in which practical solutions may be found. However, it must be emphasized that, with respect to aerodynamic considerations, the analytical treatment of capsule separation from a parent vehicle while in the sensible atmosphere at speeds ranging from supersonic to escape velocities requires the employment of techniques which differ radically from those employed to analyze a store drop from an aircraft. In these high velocity cases deviations from free stream conditions are of extreme importance, such that the velocity of the capsule with respect to the local flow environment during at least the initial portions of separation is generally quite different from the free stream velocity of the parent carrier vehicle. In addition, the gradients existing in the flow field experienced by a capsule ejected from a vehicle at hypersonic speeds may be of extreme importance in determining the separation characteristics of the ejected body. Also, for reasons of economy primarily, the feasibility of obtaining extensive experimental separation data with any configuration of carrier vehicle and capsule in the supersonic to escape velocity range is greatly reduced as compared to separation studies in the low speed regime. Thus, more reliance must be placed on analytical techniques and empirical results from previous cases requiring the use of more accurate means of estimating flow field effects in a dynamic situation.

An extensive search of the literature, performed in an effort to find a point of departure for this study, revealed that previous effort was largely limited to aircraft-type configurations at comparatively low speeds. A list of references is appended to this section which reports all known separation investigations related to the present study. Some comments are presented in following paragraphs on those works which influenced this study in one way or another.

Manuscript released by the author March 1961 for publication.

Though the data themselves are of limited applicability, the NASA store separation investigation (References 1 through 18) serves as a point of departure for the present study and provides guide lines for the procedures and techniques which have been adopted. References 1, 2, and 3 document a theoretical method of bomb motion prediction based upon experimentally determined static aerodynamic quantities for a store at various positions and attitudes in the separation region. Fair agreement with the results of wind tunnel dynamic tests (References 1 and 2) has so been obtained. Consequently, a measure of confidence has been derived that a similar procedure is valid in the present investigation.

Dynamic simulation of separated bodies, required for wind tunnel ejection tests, is comprehensively discussed in Reference 4. Procedures and techniques for separation testing employed by the NASA, which have application in the present program, are recorded in References 5 through 10. NASA flow field mapping experiments, performed for specific aircraft/store combinations are reported in References 11 through 18 and serve as a basis for the design of the experimental system required for the wind tunnel phase of this study.

Theoretical methods of estimating the loads on a separating body in a locally varying flow field are presented in Reference 19 for subsonic flows and in Reference 20 for supersonic flows. The latter approach has been adopted for estimating the interference loading on a body ejected from the side of a parent vehicle.

On the basis of the literature survey briefly reported and upon consideration of the possible alternatives, the following theoretical study approach has been evolved and pursued as part of the separation dynamics investigation.

(1) Establish limits on the scope of the study relative to carrier vehicle types and separating body configurations (capsules).

(2) Perform a preliminary aerodynamic analysis of candidate capsule configurations and reduce the number which must be considered in detail to cases of greatest interest.

(3) Estimate the properties of the flow fields around the carrier vehicles in those regions from which separation may be effected.

(4) Determine the aerodynamic properties of the capsules selected for detailed study under conditions of proximity.

(5) Derive the equations of motion pertinent to the established separation regions and modes for the capsule/region combinations of interest.

(6) Perform computations of separation trajectories for the selected capsule/region combinations over realistic ranges of the configuration/operational parameters. Establish thereby the relative separation efficiencies of the combinations so considered and the related requirements on the separation systems.

REFERENCES
(For Section I)

1. Carlson, H. W., Geier, D. J., and Lee, J. B., Comparison and Evaluation of Two Model Techniques Used in Predicting Bomb-Release Motions, NACA RM L57J23, 1957

2. Faget, M. A., and Carlson, H. W., Experimental Techniques for Predicting Store Motions During Release or Ejection, NACA RM L55L20b, 1956

3. Smith, N. F., and Carlson, H. W., Measurement of Static Forces on Internally Carried Bombs of Three Fineness Ratios in Flow Field of a Swept Wing Fighter Bomber Configuration at a Mach Number of 1.61 with Illustrative Drop Path Calculations, NACA RM L56I18, 1957

4. Sandahl, C. A., and Faget, M. A., Similitude Relations for Free-Model Wind Tunnel Studies of Store-Dropping Problems, NACA TN 3807, 1957

5. Lee, J. B., and Carter, H. S., An Investigation of Ejection Releases of Submerged and Semisubmerged Dynamically Scaled Stores from a Simulated Bomb Bay of a Fighter Bomber Airplane at Supersonic Speeds, NACA RM L56I10, 1956

6. Lee, J. B., Dynamic Investigation of Release Characteristics of a Streamlined Internal Store from a Simulated Bomb Bay of the Republic F-105 Airplane at Mac' .umbers of 0.8, 1.4, and 1.98, NACA RM SL56F01

7. Lee, J. B., Investigation of Ejection Release Characteristics of Four Dynamically Scaled Internal Store Shapes from a 1/17-Scale Simulated Bomb Bay of the Republic F-105 Airplane at Mach Number 1.39 and 1.98, NACA RM SL56I28a

8. Lee, J. B., Investigation of Ejection Release Characteristics of Bluff TX-28 and Turnabout TX-28 Stores from a 1/17-Scale Simulated Bomb Bay of the Republic F-105 Airplane at Mach Numbers of 1.39 and 1.98, NACA RM SL57B05

9. Lee, J. B., Investigation of Ejection Releases of an MB-1 Rocket from a 0.04956-Scaled Model of the Convair F-106A Airplane at Mach Number 1.59, NACA RM SL57E07

10. Lee, J. B., and Basford, R. C., Investigation of Ejection Releases of an MB-1 Rocket from a 0.04956-Scaled Model of the Convair F-106A Airplane at Several Mach Numbers and Simulated Altitudes, NACA RM SL57I11.

11. Smith, N. F., and Carlson, H. W., The Origin and Distribution of Supersonic Store Interference from Measurement of Individual Forces on Several Wing-Fuselage Store Configurations. III - Swept Wing Fighter-Bomber Configuration with Large and Small Stores, Mach Number 1.61, NACA RM L55H01, 1955

12. Morris, O. A., The Origin and Distribution of Supersonic Store Interference from Measurement of Individual Forces on Several Wing Fuselage Store Configurations. IV - Delta Wing Heavy Bomber Configuration with Large Store, Mach Number 1.61, NACA RM L55I27a, 1955

13. Smith, N. F., The Origin and Distribution of Supersonic Store Interference from Measurement of Individual Forces on Several Wing Fuselage Store Configurations. VI - Swept Wing Heavy Bomber Configuration with Stores of Different Sizes and Shapes, NACA RM L55L08, 1956

14. Morris, O. A., Aerodynamic Forces and Moments on a Large Ogive-Cylinder Store at Various Locations Below the Fuselage Centerline of a Swept Wing Bomber Configuration at a Mach Number of 1.61, NACA RM L56I25, 1957

15. Geier, D. J., and Carlson, H. W., Measurement of Static Forces on Externally Carried Bombs of Fineness Ratios 7.1 and 10.5 in the Flow Field of a Swept Wing Fighter Bomber Configuration at a Mach Number of 1.6. NACA RM L56K30, 1957

16. Geier, D. J., and Robins, A. W., Wind Tunnel Measurement of Static Forces on Internally Carried Bombs of Two Different Bluff Shapes in the Flow Field of a Swept Wing Fighter Bomber Configuration at a Mach Number of 1.6, NACA RM L57A23, 1957

17. Geier, D. J., An Investigation of Supersonic Store Interference in the Vicinity of a 22^{0} Swept Wing Fuselage Configuration at Mach Numbers of 1.61 and 2.01, NACA RM L57L18, 1958

18. Oehman, W. I., and Turner, K. L., Aerodynamic Characteristics of a 45° Swept Wing Fighter Airplane Model and Aerodynamic Loads on Adjacent Stores and Missiles at Mach Numbers of 1.57, 1.87, 2.16, and 2.53, NACA RM L58C17.

19. Strauss, L. H., Final Report on Study of External Store Separation, Aircraft Armaments, Inc., ER-561, 1955

20. Moskowitz, B., Approximate Theory for Calculation of Lift of Bodies, Afterbodies, and Combinations of Bodies, NACA TN 2669, 1952

SECTION II

CRITERIA OF THE STUDY

Separation problems can be characterized, in general, in terms of

(1) The environment to which the separated body is exposed (interpreted by the trajectory conditions of the carrier vehicle at separation)

(2) The physical circumstances of the separated body, i.e., its size, shape, placement on the carrier vehicle, and of its purpose or application.

The scope of the study relative to these criteria can be limited by practical considerations to those circumstances which occur more commonly. For example, the carrier vehicle which represents a parent payload section or re-entry body is assumed to be axisymmetric and at zero angle of attack in flight. Aside from the virtually unlimited cases that would arise, treatment of arbitrary shapes and vehicle attitudes would not fulfill the purpose of a general study program of this nature in that data and conclusions of extremely limited applicability would be generated in many cases. It is the purpose of this section to discuss the bounds of the separation problem and to establish the practical criteria under which the study is made.

A. Trajectory Carrier Vehicle

A representative number of trajectories, including those peculiar to sounding rockets, IRBM's, ICBM's, satellites and satelloids, identified by Table I, have been examined. Only pertinent portions of ascent and re-entry phases, i.e., those in which accelerations and dynamic pressures are significant are considered in any detail since the primary function of this program is to study the separation problem as influenced by aerodynamic effects. Thus, consideration is given to those altitude regimes in the sensible atmosphere where aerodynamic parameters are of prime consequence in determining separation characteristics.

Some remarks are advanced concerning the mechanics of extra atmosphere separation, wherein aerodynamic loads and carrier accelerations are not present. Two variant conditions arise, namely

(1) Satellite trajectory or superescape velocity

(2) Subescape velocity, suborbital velocity/direction.

In the latter case, separation may be effected merely by imparting to the separating body (capsule) a differential velocity, the magnitude and direction of the velocity being defined entirely by the desired subsequent capsule trajectory. For satellite conditions or superescape velocity; the magnitude and direction of the capsule differential velocity are restricted by the requirements of the de-orbiting maneuver. In general, there exists a minimum differential velocity which may be employed; however, dispersion is reduced as the differential velocity is increased. Heating and deceleration problems grow more severe with low dispersion re-entry trajectories. Carrier vehicle attitude at separation is critical to the subsequent capsule trajectory, and the act of separation must not be permitted to impose on the carrier vehicle forces and moments which would disturb its further orbiting and later de-orbiting maneuver.

Further consideration of the extra atmospheric separation problem is beyond the scope of the present study, and no further mention of it is made in this report. Representative trajectory conditions which have been used to implement the computations of this study are derived from the data of Figures 1 through 3 and are summarized in Table II.

B. Capsule Characteristics

In order to aid in the selection of capsule configurations of greatest interest which are to be analyzed, a catalog of representative examples has been prepared and is presented in this report as Table III. Specifically excluded from this tabulation are missile nose configurations – which are separated ordinarily outside the atmosphere – and human being-carrying capsules, the geometry of which is highly specialized and, therefore, outside the scope of the present broad study. The configurations appearing in Table III encompass ranges of capsule size, shape and aerodynamic properties, carrier vehicle placement, and separation environment pertinent to the study. Distinct groupings are seen to emerge from the compilation of capsule characteristics which reduce to a comparatively few the number of cases which must be considered independently. These general categories are given in Table IV and form the basis of the present investigation. A detailed discussion of capsule geometric characteristics, leading to the choice of representative shapes of interest to this study, is given in Section IV. B of this report.

TABLE I

REPRESENTATIVE TRAJECTORY CONDITIONS

Trajectory Number	Description
1	312 mile summit, sounding rocket 112, 689 feet burnout altitude, 2° from vertical launch angle
2	Single stage, 1, 500 nautical mile range ballistic
3	275 mile summit, sounding rocket, burnout altitude 103, 078 feet, 11° from vertical launch angle
4	1, 200 mile summit, sounding rocket, burnout altitude, 234, 713 feet, 2° from vertical launch angle
5	1, 200 mile summit, sounding rocket, burnout altitude, 238, 741 feet, 0° from vertical launch angle
6	Four-stage satellite launch for 190 nautical mile injection altitude
7	Satellite re-entry, 15, 600 feet per second velocity at 250, 000 foot re-entry angle 115° from vertical, W/C_DA = 20. 4
8	Satellite re-entry variable drag configuration, 23, 900 feet per second velocity at 316, 000 feet. Re-entry angle 93. 36° from vertical
9	Satellite re-entry, 23, 930 feet per second velocity at 316, 800 feet. Re-entry angle 93. 36° from vertical
10	Satellite re-entry, 24, 200 feet per second velocity at 316, 800 feet. Re-entry angle 90° from vertical
11	Three-stage, 3, 200 nautical mile range ballistic
12	Re-entry, 6, 000 nautical mile range, 24, 000 feet per second velocity at 400, 000 feet. Re-entry angle 110°
13	Satelloid re-entry, 18, 864 feet per second velocity at 195, 388 feet. Re-entry angle 90. 958° from vertical

TABLE II

CONDITIONS FOR SEPARATION ANALYSES

Separation Region	Mach No.	Altitude (ft)	Dynamic Pressure (lbs/ft^2)	Acceleration (g's)	Trajectory Angle Measured from Vertical (deg.)
BASE	5	0	37,000	-52.8	135
	5	25,000	13,750	-19.6	135
	5	50,000	4,250	-21.3	135
				- 6.08	
				- 3.54	
	10	50,000	17,000	-24.3	135
	15	50,000	38,300	-54.7	135
SIDE	2	50,000	680	0	45
				5	
				10	
	5	100,000	410	All Cases	45
	5	150,000	59		45
	15	85,000	7,430		45
	5	50,000	4,250		45
	5	0	37,000	-22.6	135
	5	5,000	30,800	-18.8	135
	5	25,000	13,750	- 8.4	135
	5	50,000	4,250	- 2.6	135
	10	50,000	17,000	-10.5	135
	15	50,000	38,300	-23.4	135

TABLE III

CHARACTERISTICS OF VARIOUS CAPSULE TYPES

Capsule	Purpose	Gross Weight (lbs)	Payload Weight (lbs)	Recovery System Weight (lbs)	Deceleration Device	Water or Land Impact	Configuration	Fineness Ratio	Length (ft)	Trajectory	Release Condition	Heating Protection	Capsule Launching Devices Used	Area of Separation	Capsule Shape
Sounding Rocket	Photographic Meteorological Investigation	85-98	45-58	30	Dive Brakes & Parachute	Land	Ogive-Cylinder	9.75	5.5	Ballistic	After Burnout	Fiberglass on Sides	Explosive Bolts	Nose	
Sounding Rocket	High Altitude Photographs	91	29	21	Nose Blunting & Paracoute	Land	Flared Cylinder	1.87	2.5	Ballistic	After Burnout	Heat Shield	Explosive Bolts	Nose	
Sounding Rocket	High Altitude IGY Investigation	30	20	None	———	———	Cone-Cylinder	6	3.3	Ballistic	After Burnout	Fiberglass	———	Nose	
Test Vehicle	Parachute Test Missile	240	75	30	Nose Blunting & Parachute	Water	Cylinder-Fins	8	6.0	Ballistic	After Burnout	———	———	Nose	
Medium Range Missile	Recover Recorded Information	26	6	10	Balloon Drag Skirt	Water	Flared Cylinder	0.91	0.84	Ballistic	Late Re-entry (Supersonic)	Fiberglass	Rocket Ejection	Base	
Data Capsule	Recover a Tape Recorder	40	10	12.0	Balloon Drag Skirt	Water	Cylinder	4.6	2.5	Ballistic	Late Re-entry (Supersonic)	Rear Heat Shield	Rocket Ejection	Base	
Satelloid	Recover a Data Package	47	8	12	Nose Blunting & Parachute	Water	Flared Hemisphere Cylinder	2.15	2.0	Horizontal Re-entry	Before Re-entry	Ablation Material	Pyrotechnic or Catapult	Side	
Earth Satellite	Recover a Data Package and/or Small Animal Occupant	500	130	40	Retrorocket & Parachute	Water	Flared Hemisphere	1.68	3.0	Re-entry	Space	Ablation Material	———	Nose	
IRBM Recovery Parachute Pack	Deceleration of Nose	11	11	——	Parachute	Water	Cylinder	2.0	1.6	Captive	Late Re-entry (Transonic)	None	Mortar	Base	
IRBM Recovery Parachute Pack	Deceleration of Nose	50	50	——	Parachute	Water	Cylinder	2.0	1.6	Captive	Late Re-entry (Transonic)	None	Mortar	Base	
ICBM Recovery Parachute Pack	Deceleration of Nose	65	65	——	Parachute	Water	Cylinder	1.8	2.0	Captive	Late Re-entry	None	Mortar	Base	
Nuclear Weapons Instrumentation Probes	Thermal Radiation Environment and Effects	260	70	40	Dive Brakes and/or Nose Blunting & Parachute	——	———	——	——	Ballistic	After Burnout	———	———	——	———
Nuclear Weapons Instrumentation Probes	Electro-magnetic Phenomena	160	80	None	———	——	Flared Hemisphere Cylinder	4.0	3.0	Ballistic	After Burnout	———	———	Nose	
Nuclear Weapons Instrumentation Probes	Atmospheric Physics	240	150	35	———	——	———	6.0	6.0	Ballistic	After Burnout	———	———	Nose	———
Hardtack Nuclear Probe	Nuclear Radiation Measure	175	65	——	———	——	Cone-Cylinder Fins	4.8	4.0	Ballistic	During Burnout	———	Pyrotechnic	Side	

TABLE IV

SUMMARY OF CHARACTERISTICS OF TYPICAL CAPSULES

Capsule Type	Recovery Circumstance	Weight (lbs)	Diameter (ft)	Weight-to-Drag Area Ratio W/C_DA	Capsule-to-Carrier Vehicle Diameter Ratio	Separation Region	Phase of Trajectory at Ejection
Data Capsules or Capsules with Small Animal Occupant	Recoverable Nonrecoverable	40-240 30	0.65-1.33 0.6	20-300 500	0.2-0.61 1.0	Nose, Side or Base Nose	Ascent, Space or Re-entry After Burnout
Nuclear Probe Capsules	Recoverable Nonrecoverable	240 160-175	1.0 0.75-0.80	300 1800	1.0 0.1-1.0	Nose or Side	Ascent Phase - during Burning or After Burnout
Recovery Packages		11-65	0.9-1.0	11-30	4-5	Base	Late Re-entry

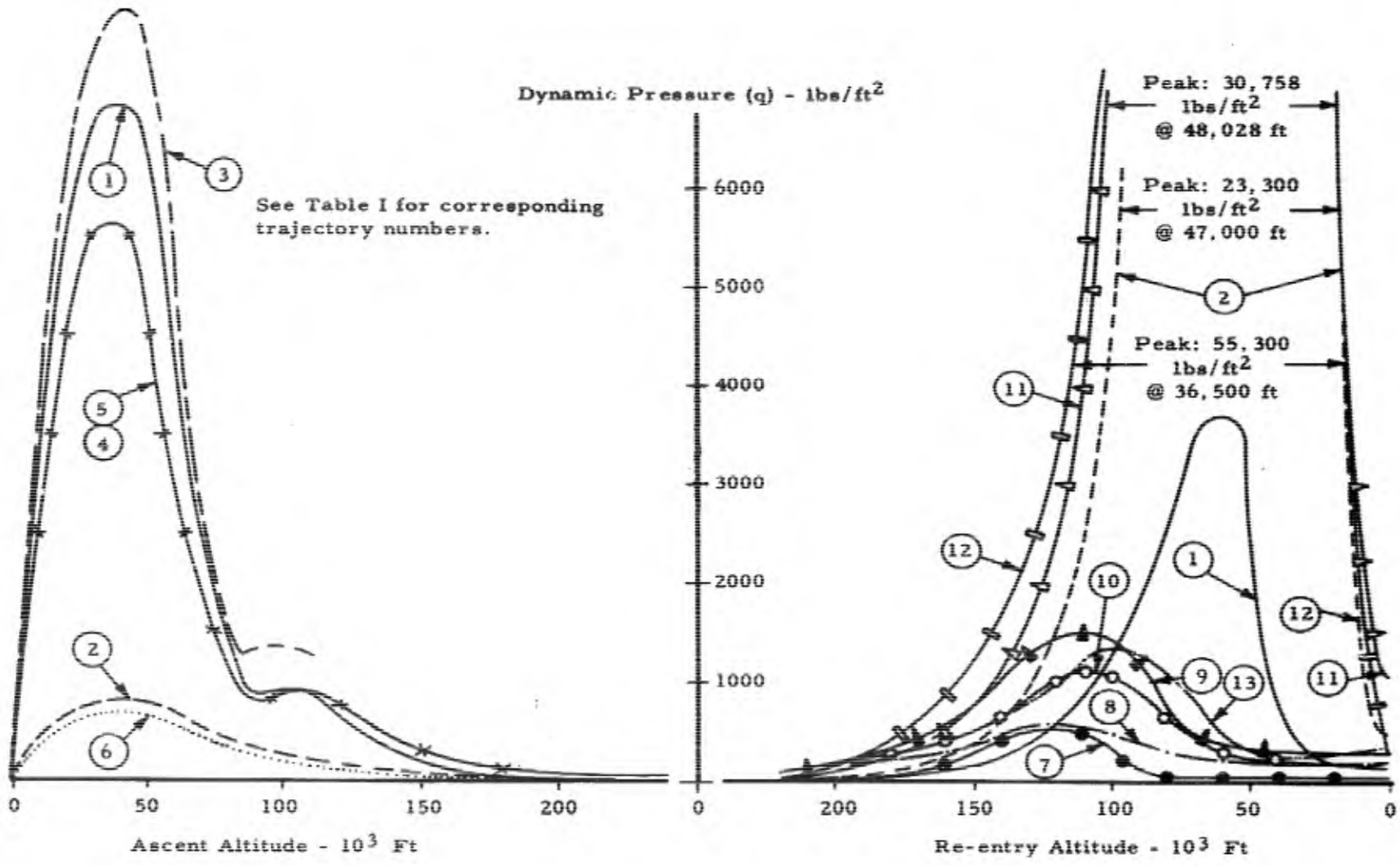

Figure 1. Dynamic Pressure Variation vs Altitude for Representative Trajectories

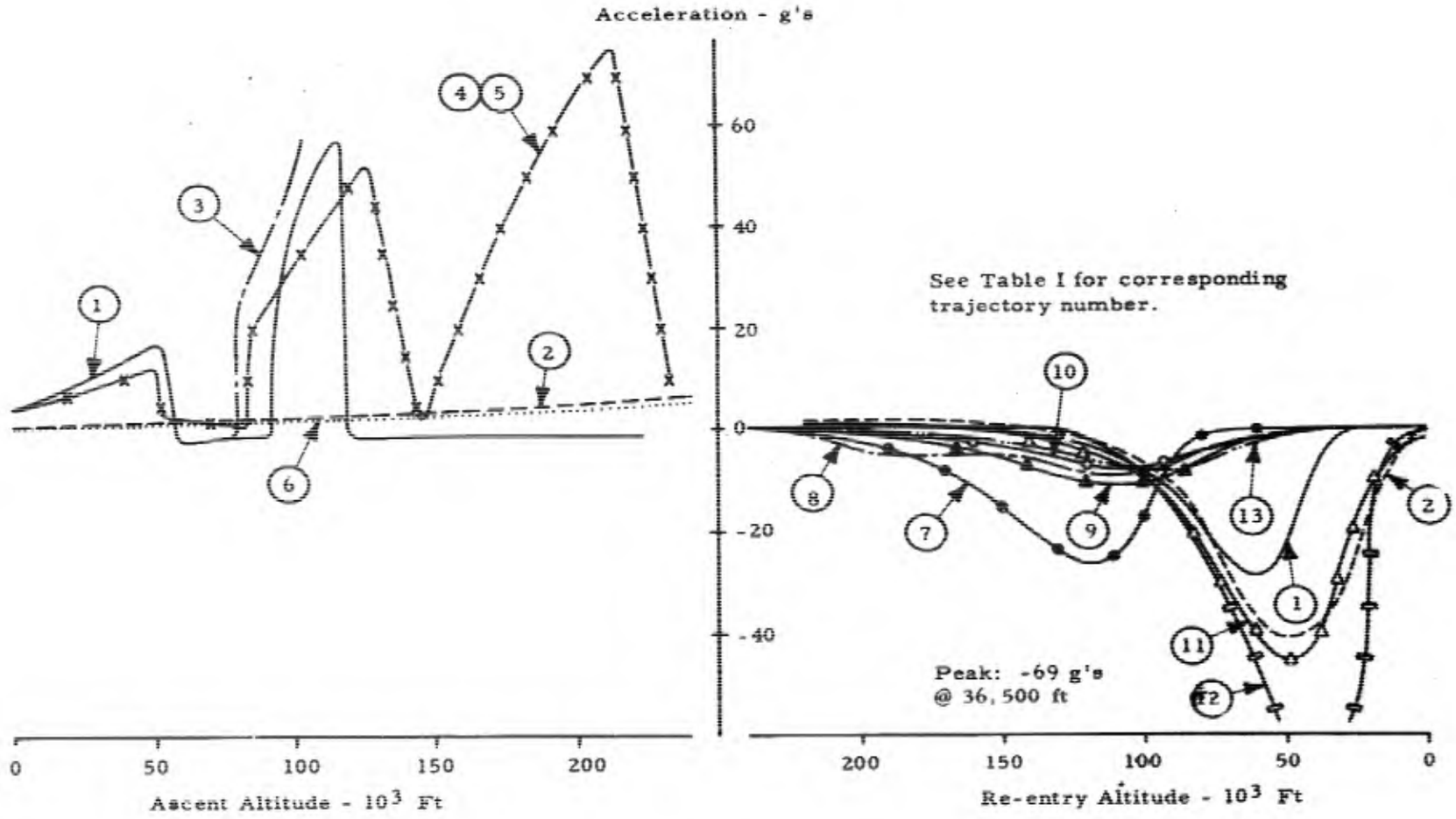

Figure 2. Acceleration Variation vs Altitude for Representative Trajectories

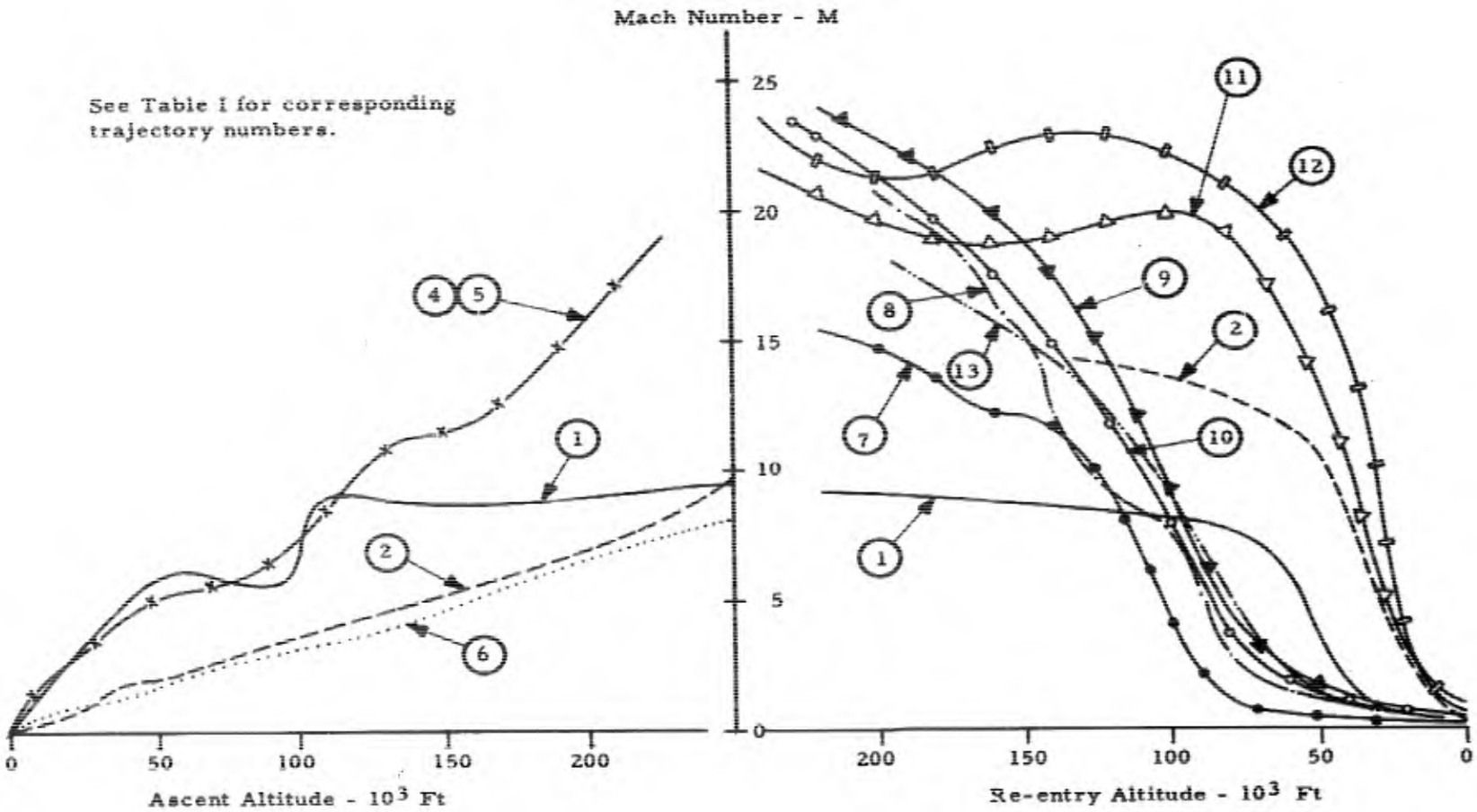

Figure 3. Mach Number Variation vs Altitude for Representative Trajectories

SECTION III

EQUATIONS OF MOTION

In order to predict the motion of a capsule ejected from a carrier vehicle into a particular region of the flow about the vehicle, the governing equations of motion must be established. The motion equations express the capsule dynamics in all physically pertinent degrees of freedom and the position-attitude-velocity dependent forces and moments which are impressed upon the capsule in a spatially varying flow field. As such, it is convenient to employ motion equations specifically appropriate to the particular ejection or flight mode.

It is determined in Section II that capsule separation may be effected from the carrier vehicle nose, from its side or from its base, or the nose itself may be separated. Applicable motion equations have been derived for each of these modes. Details of the formulations of the separation equations are presented in the Appendix of this report. In addition, the general equations for the motion of a capsule in free flight have been derived. The formulation of these equations is not presented in this report since they are not directly pertinent to separation analysis. The following subsections summarize briefly the salient characteristics of the respective sets of equations.

A. Nose Separation Equations

The mechanism of nose separation involves the use of a thrust force on the nose directed, in general, at some angle to the nose longitudinal axis. Aside from any relative longitudinal displacement, the effect of this force system is, in general, to cause the nose to slide laterally relative to the afterbody (carrier vehicle) and to rotate if the thrust axis is displaced off the center of gravity of the nose section. Thus, two effects are present which must be taken into account, namely

(1) The contact and frictional forces present during the contact phase of the process in circumstances where the magnitude of thrust in the longitudinal direction is not sufficient to immediately cause separation.

(2) The change in aerodynamic forces and moments on the afterbody as an increasingly greater amount of its blunt face is exposed to the flow during the progress of nose separation.

Three-degree-of-freedom equations have been derived for the nose and for the afterbody which describe their respective planar motions. Since the

separation process is of short duration the Mach number change is negligible, and the aerodynamic coefficients change with angle of attack only.

B. Base Separation Equations

Separation from the base of a carrier vehicle may be effected either (1) axially along the wake core, or (2) at an angle to the wake axis such as to cause penetration of the wake boundary. One-dimensional motion is applicable in the first instance. The equations in this case were purposely made general to provide for various combinations of ejected bodies. One equation each is written for the carrier vehicle, for the capsule, and for any devices that may be employed for extracting the capsule. An elastic line is assumed to interconnect each element of the train. Provision is made for a programmed increase in drag area of the pilot device, if used. In cases where no interconnecting lines or pilot devices are used, appropriate terms in the equations of motion are "zeroed" or suppressed.

The equations which represent capsule motion under the condition of ejection from the carrier base at an angle to the wake axis are a conventional three-degree-of-freedom system. Due, however, to the extreme variations in the base flow field, especially across the wake boundary, the force and moment representation is complex. In crossing the wake boundary the capsule is subject to large aerodynamic moments which produce large angular velocities and change markedly the local flow velocities over the capsule surface. To account for this velocity variation the capsule surface is divided into eight transverse "faces." The loading on the capsule, then, is the summation of the loads averaged over the respective faces. The center of pressure on each face is assumed to be at the centroid of the face; flow conditions over the face are assumed to be those associated with the centroid.

C. Side Separation Equations

The motion of a capsule ejected laterally from the side of a carrier vehicle is analyzed in two phases, namely

(1) During partial exposure to the flow

(2) After complete exposure to the local flow.

In the former case the capsule is subject to a rotational restraint imposed by the carrier vehicle which is assumed to be released at or before complete exposure, dependent upon capsule geometry. During restraint, two

degree-of-freedom equations apply; after release of restraint, three-degree-of freedom motion is employed. Frictional forces appear while the capsule is restrained, and a time-position dependent ejection force can be applied during the partial exposure phase. As a necessary computational subroutine, the exposed capsule area is monitored and employed as the reference area for the applicable aerodynamic force and moment system. During the partial exposure phase, the basic "capsule-free" local flow field surrounding the carrier vehicle is used in the computation of aerodynamic parameters.

After exposure to the local flow is complete, three-degree-of-freedom motion is continued except that additional force and moment terms appear. These terms express the interference effects of the capsule and the carrier flow field, and the effect of encounter with shock waves in the appropriate region (specifically, the carrier nose shock).

D. Free-Flight Equations of Motion

In order to predict the dispersion of a separated capsule subject to initial conditions resulting from the ejection process, equations of motion in six-degree-of-freedom have been derived. In the formulation of these equations, an axisymmetrical capsule is assumed; otherwise the resulting equations are very general and provide:

(1) That the gravitational constant may be expressed as a function of altitude

(2) That the wind (assumed horizontal) is variable in magnitude and direction with altitude

(3) That aerodynamic quantities may be expressed as nonlinear functions of local Mach number and angle of attack over a complete (±180 degrees) range of capsule angles of attack.

SECTION IV

AERODYNAMICS

The problem of separating a body from a carrier vehicle is approached by predicting, with the equations of motion, the path of the ejected body relative to the parent carrier and the associated linear and angular accelerations or loads applied to the separating body. These equations of motion require the determination of aerodynamic derivatives which apply during the separation process.

Basic to the establishment of these aerodynamic quantities is the determination of the resultant or combined flow field caused by the two bodies in proximity to each other. In principle the resultant, combined field may be determined by solving the fluid flow equations including viscous effects, or by conducting experimental programs to either observe the flow field or measure directly the forces and moments induced on the bodies in this field. The analytical determination of the combined flow field is extremely difficult, and even when computed as rigorously as possible will involve certain assumptions or data, for example on shock-viscous layer interaction, that are incompletely known and therefore can only be applied approximately.

Fortunately, the circumstances under which separation from the side or base of a carrier vehicle are of main interest permit simplification of the problem. Generally the separated body (capsule) will be small relative to the size of the carrier vehicle so that only when the capsule virtually touches the carrier or when it is in the region of the carrier field where extreme gradients exist will the interaction (interference) of the two flow fields produce a combined or resultant field which differs significantly from a simple superposition of the individual fields. In this case (and again relative to side or base capsule ejection), the primary characteristics of the field will generally be established by the larger carrier vehicle, and the capsule's own flow field will result from the local conditions established by this primary field (at each distinct capsule location in the field); at least as a first order approximation. During most of the separation period the gradients generated by the carrier field, at any given point, will result in moderate changes in flow parameters over the region occupied by the capsule. Thus the forces and moments on the capsule under local conditions may be derived by adding incremental terms to account for the effects of local field gradients and stream curvature to its basic characteristics at the average local conditions, assuming that the carrier field is unaffected by the presence of the capsule. Linear perturbation methods or simple numerical strip theory techniques are applicable under these conditions.

A further simplification is possible at capsule positions in the flow field where field changes over the physical extremities of the capsule are quite small. When this condition is satisfied the capsule may be treated at that point as effectively immersed in a uniform field corresponding to the average of the local field parameters in the neighborhood of that point.

In summary, with respect to side and base ejection, the present study of separation dynamics assumes capsule configurations which are small relative to the parent carrier vehicle and separation modes which will place the capsule predominantly in areas where the resultant or combined flow field may be obtained by simple superposition of the individual fields, the primary field being established by the carrier vehicle. Consequently separation characteristics in this study are largely predicated on these assumptions. The specialized considerations which apply to nose separation are noted in Section IV. A and IV. C of this report.

Discussion of the above aerodynamic phenomena is contained in the first three major subdivisions of this section. These subsections include a description of representative carrier flow fields, a summary of capsule configuration physical and aerodynamic characteristics, and discussions of interference effects relative to the manner in which they affect the loading on the separated body or on the carrier vehicle. Conditions where experimental aerodynamic data are needed, particularly to establish the effects of complex interactions, are indicated. The fourth major subdivision of this section completes the aerodynamic discussion by summarizing certain statements made in the previous sections and defining specific methods, results, and assumptions which are applied in the present analyses.

A. Carrier Flow Fields

Separation may be effected from three locations on the carrier vehicle, namely

(1) From (or of) the nose

(2) From the sides

(3) From the base.

It is possible, on a practical basis, to eliminate consideration of capsule separation from the nose of a carrier vehicle. Rather it is the entire nose that requires separation, and it is this circumstance which is assumed to exist and

for which a separation analysis is made. There is no purpose, therefore, in defining the flow over the nose as an environment for the ejected nose. In effect the environment for the nose is undisturbed air into which it advances, initially at flight speed. What happens to this flow during the ejection process is a result, in part, of what has happened to the nose and of the effect of the afterbody with which the flow must, during ejection, interact and is treated in Section IV. C. 1. The flow fields over the sides and at the base of a carrier vehicle are discussed in the following two subordinate sections.

1. Carrier Side Flow Field

The geometry of a vehicle nose has an important effect upon the flow over the cylindrical afterbody. Rather broadly different nose configurations, i. e., sharp or blunt, may be pertinent in various side ejection situations; therefore, corresponding flow field types must be established in each instance. The flow fields associated with pointed nosed and blunt nosed bodies are discussed in the following two parts of this section.

a. Pointed Nosed Bodies

Flow field variables for bodies having attached shock waves may be predicted more or less accurately by means of theoretical methods of commensurate complexity. The first and second order theories, as e.g., of Von Karman and Moore(Reference 1) and Van Dyke (Reference 2), predict the magnitudes of the flow field variables reasonably well close to the body but fail to estimate correctly shock-wave position and shape of the Mach lines. As discussed in Reference 3, Whitman has improved the linear theory by calculating a second approximation to the Mach line, the resulting increase in accuracy requiring a relatively modest increase in computational complexity.

The ultimate rigor in supersonic inviscid flow calculations is provided by the method of characteristics, which is applicable to the nonlinear hyperbolic equations of supersonic flow. This technique is equally applicable in rotational and irrotational flows. Ferri (Reference 4) has considered the former extension, which applies - e.g. - for high Mach number flows where strong curved shock waves occur with accompanying variation in entropy along them. Real gas effects have been accounted for by Gravolos (Reference 5). Though the characteristics method involves the greatest

computational complexity, its use (and inherent accuracy) is made practical by the employment of machine computational methods.

Typical pointed bodies, cone-cylinder configurations, have been analyzed by Liepmann and Clippinger (References 6 and 7) using the characteristics method. The specific cases and results are documented and plotted in Figures 4 to 6. Representative calculations only of Clippinger are included; the conclusions derived therefrom apply in all his results. It is found, relative to the cone-cylinder body in supersonic flow, that:

(1) At least in regions not near the shock wave and aft of the shoulder in the range of Mach 2 to 7 for the cases considered, velocities throughout the flow field are within approximately 95 percent of free stream.

(2) A significant departure from free-stream conditions exists for low length-to-diameter ratio bodies at low Mach numbers, and at high Mach numbers for longer bodies.

(3) Where approximate free-stream conditions exist on the body the environment for capsule ejection is essentially uniform at a Mach number and dynamic pressure somewhat reduced from that of free stream.

b. Blunt Nosed Bodies

Nose blunting becomes pertinent for high-speed flight applications where stagnation heating becomes critical. The strong detached shock wave associated with blunt configurations imposes large increases in entropy. The flows associated with such configurations are given in several references such as Lees and Bogdonoff (References 8 and 9).

The flow field is mixed subsonic-supersonic, and the methods of calculation previously discussed are inadequate in the subsonic parts of the region. A relaxation method due to Wang (Reference 10) has been used by Gravalos (Reference 5) to determine the properties of the subsonic-transonic flow field. In the supersonic region, any of the previous methods are applicable with preference given to the characteristics method where practicable. A representative hypersonic case has been calculated by the method of Gravalos and the

characteristics method assuming real gas effects. The vehicle is a hemisphere-cone-cylinder having a cone half angle of 30 degrees. The flight Mach number is 15.0, and the altitude is 85,000 feet. Figure 7 (a and b) is presented which exhibits, respectively, the spatial variations of pressure, density, flow direction, and Mach number in the flow field about the vehicle up to 6 diameters from the vehicle nose. The following observations are drawn relative to this case, which illustrates – typically – flow field characteristics in a hypersonic environment.

(1) Near the shock wave pressure gradients are large but diminish rapidly with radial and axial distances. Beyond about 6 diameters from the nose approximately free stream static pressure exists throughout the flow field.

(2) Density gradients behave similarly as do pressure gradients. Density ratios (relative to free stream) are very low in the regions near the body aft of the shoulder and, at high Mach numbers, everywhere in the region aft of about 5 diameters from the nose.

(3) Flow direction approaches free stream in the region behind about 4 diameters from the nose. However, radial flow direction gradients remain large even at 6 diameters from the vehicle nose.

(4) Mach number gradients axially are relatively small behind about 4 diameters from the vehicle nose. Further, as indicated by Powers (Reference 11) the Mach number at distances from the nose which correspond to the lengths of practicable hypersonic vehicles does not appreciably exceed 5.0.

2. Carrier Wake Flow Field

In order to determine the environment for a base ejected body, the structure of the dissipative wake and the associated external flow of a carrier vehicle is discussed, and a practical model of the flow field is established. The principal information derived from a survey of the status of wake technology is reported in this section. The supersonic wake is the subject of present concern. Further, for bodies ejected from moderately decelerating carrier vehicles, the wake structure

immediately behind the body is of prime importance; hence, emphasis will be placed upon description of this region.

The quantitative description of wake flow remains today virtually inadmissible to analytical treatment. Approximations which have been useful in solving the equations of fluid motion (e.g., Navier-Stokes) for boundary layers, say become inadequate in wake analysis, since the interaction of the inviscid external flow with the internal dissipative region may not be neglected. The unsteady nature of the (practical) turbulent wake further complicates the theoretical problem with implications of the statistical approach.

Presently, therefore, wake characteristics must be determined primarily in an empirical manner. However, considerable progress towards description of the wake has been made in the last decade. In particular, efforts to correlate and explain observed base pressure data have necessarily resulted in models of the wake structure. These models and the work of Chapman (References 12 and 13), Crocco and Lees (Reference 14), Korst and Love (References 15 and 16) provide the greatest insight into the mechanism of wake flow and its quantitative description. Of these works, only the very general theory of Crocco and Lees is founded upon a firm theoretical basis. By emphasizing the importance of mixing in establishing an equilibrium between the external flow and the dissipative region, these authors are able to explain the qualitative behavior of base pressure (and thus wake structure) for various Reynolds number regimes. Unfortunately, the Crocco-Lees theory depends critically upon empirical values of mixing coefficients for various flows and upon determination of the laminar-turbulent transition point, both little known quantities. Practical computational difficulties further limit the usefulness of the theory. Nevertheless, the Crocco-Lees theory is considered to be the most important modern contribution to wake determination since it embodies implicity or explicitly virtually all of the models or ideas used by the other investigators.

In the following paragraphs, the structure and characteristics of wakes are discussed with emphasis on those features important for bodies ejected into wakes. For convenience, the discussion of wake characteristics is divided into three subsections. The first subsection is concerned with the generally converging region immediately behind the body up to and including the wake "throat" or "critical region." The second subsection discusses the spreading downstream wake, and the third subsection describes the representation of wake structure used for this program.

a. The Wake Immediately Behind a Blunt Body

The general features of the wake are depicted in Figure 8. As shown in this figure, the boundary layer flow ahead of the base of the body expands around the corner and separates from the surface at the corner. A weak lip shock terminates the corner-centered expansion fan. Entrainment of air from the region behind the base by the jet pump action of this stream lowers the pressure behind the base. The resulting pressure difference across the stream causes it to be deflected inward towards the axis of the body. Upon reaching the axis of the body the stream is again deflected (and hence recompressed) back to the longitudinal direction. An equilibrium state is reached wherein the flow expands at an angle such that the dissipative flow can negotiate the resulting recompression.

The region of the flow recompression, or the wake throat, is critical and controls both the upstream and downstream wake structure. Figure 9 is a schematic diagram of the region between the blunt base and the wake throat. The general features of this region are common to two-dimensional and to axisymmetric flows. For convenience the wake region is discussed relative to two-dimensional flow. The important differences which arise in three-dimensional, axisymmetric flow are discussed later.

Referring to Figure 9, the boundary layer (of thickness AB) formed on the surface of the body spreads downward into the region behind the base. Entrainment of air from the base region increases the thickness of the mixing layer. At the point where the streamlines from opposite sides of the body converge, one of the streamlines must stagnate at the point D. Streamlines having a total pressure greater than that of streamline BD pass downstream, while those of lesser total pressure are reversed and recirculated in the base region. For steady flow, no mass flow is added to or removed from the base region. The streamline, BD, is therefore a boundary through which fluid particles cannot cross. The essential mechanism then, is that of a balance between mass flow scavenged or entrained from the base region and mass flow reversed back into the region by the pressure rise through the recompression zone.

This concept of the base flow mechanism was developed independently by Chapman (Reference 13), Korst (Reference 15) and Kirk (reported in Reference 17). Its correctness has been

verified by several investigators, e.g., by Rouse (Reference 18), who detected a small recirculating eddy within the base region and by Charwat and Yakura (Reference 19). With this model of the wake structure direct calculation of the base pressure and hence, of the all-important angle of streamline separation is permitted.

Referring to Figure 9 it is seen that between points B and C along the dividing streamline the process is one of viscous mixing or air entrainment. Between points B and C the bounding streamline is nearly straight and the static pressure in the region is virtually constant and equal to base pressure. Hastings (Reference 20) has determined, experimentally, that behind both two and three-dimensional bodies, the static pressure remains nearly constant for about 0.8 diameter behind the body (at Mach number 2.0). Between points C and D, however, there must occur a pressure rise of sufficient magnitude to destroy the momentum of the entrained air. The line CD is therefore curved and a series of compression waves are set up which coalesce to form a trailing shock.

It is possible to calculate the wake separation angle and obtain the flow structure by setting the total pressure on the dividing streamline equal to the pressure after recompression. The only piece of information required is the velocity along the dividing streamline. This velocity, or better the ratio of this velocity to that of the local external flow, u^*, depends solely on the process of viscous mixing. The classical problem of mixing of parallel streams provides the needed information. Napolitano (Reference 21) has shown that uniplanar mixing problems, with the usual boundary-layer type assumptions, can be reduced to solution of the familiar Blasius boundary-layer equation (with unfamiliar boundary conditions). If, at the beginning of mixing, the velocity distribution is uniform, no reference dimension appears and there is no Reynolds number effect. The solutions are members of a one parameter family and can be obtained by numerical solution of the Blasius equation or by coefficient determination in assumed polynomial solutions to the integrated equations. For compressible mixing the usual Stewartson-Illingsworth transformation (see for example Reference 22) can be used to define an equivalent incompressible problem for isoenergetic streams. In the case of turbulent mixing, either the Prandtl momentum transport theory or the Taylor vorticity transfer theory (References 23, 24, and 25) can be employed to convert the turbulent equations to laminar-like forms. Though theoretically unsound, either theory has been fairly successful in correlating experimental data.

The presence of a nonuniform velocity profile at the beginning of mixing introduces a reference dimension and thus destroys the one parameter similarity of the mixing solutions. A method of solution for these cases was given by Goldstein (Reference 26). A numerical calculation is required for each case to be analyzed.

The solutions for zero boundary-layer thickness may be thought of as applicable to cases where the ratio of boundary-layer thickness to base height is small, or for a given body to flow at very high Reynolds numbers. Chapman and Korst have utilized such solutions to provide the dividing streamline velocity and thus to deduce the base pressures (and hence the wake separation angle). Very satisfactory correlation with appropriate experimental data has been obtained for both laminar and turbulent flow, further substantiating the correctness of the assumed model.

Several empirical methods of accounting for finite base boundary-layer thickness have been proposed. In his original correlation, Chapman used the ratio of boundary-layer thickness to base height. Fuller and Reid (Reference 17) obtain a linear correlation of their data with the ratio of boundary-layer momentum thickness to base height (for turbulent boundary layers). In the laminar region, Charwat and Yakura (Reference 19) obtain the most satisfactory correlation with the boundary-layer thickness proper. The limited available data suggest no preference for any of these correlation methods, and their utility is academic.

The manner in which the wake mechanism in the base region is affected by configurational and flow parameters is discussed in the following subdivisions of this section.

(1) Three-Dimensional Effects

For three-dimensional flow about an axisymmetric body, a meridian section of the base flow is identical to a section of the two-dimensional flow shown in Figure 9. The conceptual model used for the two-dimensional case can be immediately applied to the three-dimensional case. In view of the axial symmetry, for a meridian section, the dividing streamline, recompression zone and stagnation point are formally the same in two and three dimensions. In fact, the base pressure and the flow separation angle can still be calculated by the

same simple technique, i.e., equating the total pressure of the dividing streamline to the recompression pressure.

Two-dimensional and axisymmetric flows differ in their external flow fields (except for changes in u*, the ratio of the dividing streamline velocity to the external flow velocity, which will be discussed later). The differences are a consequence of the lack of a simple relationship between deflection angle and Mach number for three-dimensional flow as exists (Prandtl-Meyer function) for two-dimensional flow. Flow along a constant pressure converging section must be curved; flow along a conical section must have pressure variation. Photographs of the axisymmetric wake show that the boundaries are nearly conical. Recompression along the converging wake is thus expected, and experimental data (Reference 16) verify that it exists. The recompression pressure for axisymmetric flow can, in fact, rise above the free-stream value before returning to that value.

Now the expansion at the corner of the base is locally two-dimensional, as is the recompression at the critical region if this region is small. Thus, the methods and data used to calculate the two-dimensional wake are directly applicable to the axisymmetric case if the Mach number ahead of the critical region is known. Since this Mach number is dependent upon wake angle, an iteration solution becomes necessary. To circumvent this difficulty, which involves successive solutions by the method of characteristics, Love (Reference 16) has suggested a correlation of wake convergence angle with the effective two-dimensional angle as calculated from base pressure data. In the range Mach 1.0 to 4.0 (where data exist), Love obtains good correlation (for turbulent boundary layers) using the relationship

$$0.85\,(\theta)_{\text{axisymmetric}} = (\theta)_{\text{two-dimensional}}$$

where $(\theta)_{\text{two-dimensional}}$ is calculated from the Prandtl-Meyer relationship and measured base pressure. The values of wake angle so obtained are plotted in Figure 10. It should be noted that this correlation does not imply a fundamental

difference between the two-dimensional and axisymmetric wake models. Rather it is a method of accounting, empirically, for the recompression and conical flow area variation along the converging region.

Since recompression occurs along the wake boundary behind an axisymmetric body, it is apparent that in order to realize the same value of Mach number ahead of the critical region in axisymmetric and two-dimensional flow (for identical wake convergence angles) the Mach number ahead of the base must be higher for the body of revolution. Because of the nonlinear character of the Prandtl-Meyer function the two-dimensional wake angle first increases with Mach number, reaches a maximum at a low supersonic Mach number and then decreases.

The manner in which the dividing streamline velocity (ratio), u^*, of the axisymmetric case differs from that of the two-dimensional flow has been examined. Recognizing that in the case where the radius from the body axis to the mixing layer is large compared to the mixing layer thickness, the mathematical formulation of the mixing problem is similar to that for boundary-layer flow over a body of revolution. By analogy, therefore, the Mangler transformation is employed and the following results established:

(1) The dividing streamline u^* is unchanged from that of the two-dimensional case.

(2) The insensitivity of u^* to Mach number change suggests that the effect of the axisymmetric recompression pressure gradient is small. The difficulty of obtaining a solution for the problem of mixing in an adverse pressure gradient (Reference 27) dictates the employment of such an expedient assumption.

(3) The transverse (induced) velocity is higher in the axisymmetric case than in the two-dimensional case.

(2) Effect of Forebody Shape

The unique functional relationship between Mach number

and streamline angle that exists for two-dimensional flow eliminates the effect of forebody shape (apart from all boundary-layer effects). That is, the Mach number ahead of the critical region, which is the determining factor for the wake structure, is unaffected whether the expansion takes place in one or several steps. However, in axisymmetric flow, no such simple function exists.

Fortunately, successful correlation of the wake structure on a wide variety of body shapes can be achieved by referencing the wake characteristics to a reference Mach number and pressure in the region of the base. Various investigators have proposed various reference points, such as on the body surface just upstream of the base or on a hypothetical cylindrical extension of the body beyond the base. For cylindrical afterbodies there is little difference between the methods; cones without afterbodies seem to be best treated as the limit of a cone-cylinder rather than as an example of a diverging afterbody.

(3) Boundary-Layer Effects

In the foregoing discussion the boundary layer and wake flow have been considered as either completely laminar or completely turbulent. However, the complete history of the boundary layer and the location of boundary layer or wake transition has a marked effect on the wake structure. This fact is the single feature that so drastically complicates determination of the structure of the wake. For example, lack of knowledge of the transition location is the factor mainly responsible for the quantitative failings of the Crocco-Lees theory. In addition, the growth and state of the boundary layer is dependent, in some imperfectly known manner, on a combination of effects of flow history, pressure gradients, surface roughness, heat transfer history and shockwave interaction as well as the usual Mach number and Reynolds number effects.

The Crocco-Lees theory provided the first indication of the dependence of base pressure upon the Reynolds number throughout the range of practical interest. Experimental data throughout the Reynolds number range exist only for a Mach number near 2.9 and are due to the coordinated research of

Bogdonoff (Reference 28) and Kavanau (References 29 and 30). A summary of these data is given in Figure 11 (after Hastings, Reference 20). Figure 12 (after Hastings) and Van Hise (Reference 31) shows a similar plot for various Mach numbers in the practical Reynolds number range, i.e., around 10^6 to 10^7 based on total length of boundary-layer run. The Mach numbers shown in this figure are true base Mach numbers except for the curves labeled M_∞. In these cases, characteristic solutions are not available for determination of the true Mach numbers at the base. Except for the data of Van Hise (labeled $M_\infty = 2.0$ and $M_\infty = 2.62$) which, as he noted in Reference 31, appear shifted to higher Reynolds numbers, a reasonable amount of correlation is seen to exist. The wake angle can be obtained from the base pressures by using the linear relationship of Love above or by an exact characteristics calculation for each case.

Referring to Figure 11, the qualitative behavior of base pressure (and hence wake angle) can be physically explained by the wake model described in subsection IV. A. 1. a. Because of its fuller velocity profile and consequent higher kinetic energy, the turbulent boundary-layer flow has a greater capacity for negotiating a pressure gradient than does the laminar. Therefore, a greater portion of a laminar flow will be reversed by a given pressure gradient; the base region is larger, and the expansion around the base corner is less in order that balance be maintained between mass reversed and mass scavenged. The lesser expansion serves to increase the base pressure. Increase of Reynolds number has two opposing effects. The boundary layer is thinned, reducing the quantity of low energy fluid and tending to increase the expansion and reduce the base pressure; the rate of boundary-layer growth or rate of mixing is decreased, tending to decrease the rate of scavenging, decrease the expansion angle and increase the base pressure.

Starting at low Reynolds numbers, then, the decrease in mixing predominates over the thinning of the boundary-layer causing an increase in base pressure with increasing Reynolds number (Region AB of Figure 11). As the Reynolds number increases, transition moves forward in the wake. When transition has moved into the critical recompression

region, it causes increased mixing and a fuller velocity profile in this all-important region. The reversed mass is thus decreased; for equilibrium, the scavenged mass must also decrease. Therefore, the wake expansion angle must increase and the base pressure is lowered.

It should be noted that the point of maximum base pressure, C, does not necessarily correspond exactly to the point where transition reaches the critical region. First, transition does not occur at a sharply defined, steady point; rather, it extends over a finite distance. Secondly, there are indications (Reference 20) that the maximum can be reached, because of the increasing effect of boundary-layer thinning, before transition reaches the critical region. In any case, the sharp decrease in base pressure (C to D) is due to the effect of transition reaching the critical recompression region.

As the Reynolds number is further increased, transition creeps along toward the base. The mixing action in the wake is increased, the scavenged mass is increased, and the wake expansion angle increases further (base pressure decreases). At or near point D, the transition point reaches the base of the body. Between points D and E, the transition point moves forward on the body. The turbulent mixing in the wake is only slightly affected but the boundary layer at the base is rapidly thickened. Thus, a minimum in base pressure occurs at D followed by a rise from D to E. At point E the transition point is far upstream, near the body nose. The boundary layer and wake flow are now fully turbulent and point E becomes the turbulent analog of point C for laminar flow.

Beyond point E, the decrease in thickness predominates since the mixing rate associated with the turbulent transport mechanism is little affected by increasing Reynolds number. Consequently, base pressure decreases only slightly at these high Reynolds numbers. Various power law expressions have been fitted to data in that regime, $R_e^{-1/2}$ giving the closest fit (except at large Reynolds numbers, of course, since base pressure does tend to a nonzero limit).

The minimum in transitional base pressure (point D) seems to shift to lower Reynolds numbers as the Mach number is increased (Figure 12). Judging from the data at M = 4.18, the minimum tends to disappear altogether at higher Mach numbers. As is the case with boundary-layer transition, the data for high Mach numbers and blunt bodies may turn out to be correlated better by basing the Reynolds number on boundary-layer momentum thickness (Reference 32).

(4) The Recirculation Zone

It has already been indicated that the region between the separating streamlines behind a blunt base, which is frequently referred to as the "dead air" region, might better be called the recirculation zone. The balance between scavenged mass and reversed mass calls for a vortex-like flow (see Figure 9) consisting of reversed flow from the recompression region and scavenged flow into the mixing region. Because of the boundary imposed by the dividing streamline, the recirculating mass consists of the same fluid particles.

Although such a recirculation has frequently been observed, attempts to measure the recirculation velocity distribution (References 17, 33 and 34) have met with little success. Charwat and Yakura (Reference 19) have detected large aperiodic fluctuations at the edge of the mixing layer which apparently are impressed on the recirculation flow. Although the periods of these waves are long with respect to the mixing layer flow, they are short with respect to the slow moving recirculation flow and they cause it to break up. The time dependence of recirculation flow is neglected in arriving at a model of wake flow for the present study. Attempts have been made to deduce recirculation velocities from the variations in base pressure across the base. Application of the Bernoulli equation to such data (References 16 and 35) indicates reverse flow velocities of about one-fourth to one-third of free stream.

It is indicated that variations in base pressure are greater behind an axisymmetric body than behind a two-dimensional base due, evidently (References 16 and 19), to the greater nonuniformity of pressure in the three-dimensional recirculation region.

Reverse flow velocities may be estimated from the pressure distribution in the recirculation zone. Referring to Figure 9, it is recalled that the dividing streamline has a total pressure just equal to the recompression pressure. The streamline just below the dividing streamline then has a total pressure almost equal to the recompression pressure. It is stagnated near the end of the recompression zone, point D. Between this stagnation point and the base, flow is accelerated back toward the base by the pressure difference between approximately the recompression pressure and the base pressure. The flow in this stream tube is capable of attaining a relatively high reverse velocity.

Since the highest velocity reverse flow stream tube must lie near the axis or center line, the magnitude of the velocity is important for small objects ejected in this region. An estimate of the maximum reverse velocity may be obtained by using one-dimensional isentropic flow relations for the stream tube recompressed just at the end of the recompression zone. Results of such calculations are plotted in Figure 13. These results are based upon the recompression pressure and base pressure obtained by Love (Reference 16) for the axisymmetric bodies having turbulent boundary layers. (Above M = 3, the recompression pressures were assumed equal to the free-stream pressure - see Figure 14 and section IV. A.-2. a. (5).)

While reverse flow velocities of sizeable magnitude can exist at the wake centerline near the beginning of the recompression region, the associated dynamic pressures drop off very rapidly with increasing Mach number.

An order of magnitude idea of the mean recirculation velocities induced in the mixing or fluid entrainment region ahead of the recompression zone can be obtained from the mixing calculations used to determine u^*, the velocity along the dividing streamline. It has been mentioned that the mixing problem can be put in the form of the laminar incompressible case. Under the usual boundary-layer assumptions (constant pressure, longitudinal variations much less than transverse variations) the governing two-dimensional equations (Reference 21) may be put into the form of the familiar Blasius

equation for a flat plate boundary layer with appropriate boundary conditions. The equation has been numerically solved by several investigators (see References 15, 21, 23, and 36) using either a series or integral approach. The result of present interest is the induced velocity at the edge of the mixing zone. Napolitano's solution (Reference 21), e.g., indicates that the induced velocity is inversely proportional to the square root of the Reynolds number based on length of the mixing region. In laminar compressible or incompressible flow, for practical Reynolds numbers, the induced velocities are less than one percent of free stream. Kavanau's experiments (References 29 and 30) bear out this Reynolds number dependence.

Prandtl's representation of the character of the eddy viscosity (Reference 37) leads to the result that the induced velocity is inversely proportional to a Mach number-dependent experimentally determinable scale factor (as opposed to the Reynolds number-dependency of the laminar case). On the basis of experimental values of the scale factor in the subsonic and supersonic ranges (References 19, 38 and 39), induced velocities in the turbulent case are of the order two percent to four percent of the external flow velocity.

In the axisymmetric case induced velocities are somewhat greater than those in the two-dimensional case. Near the base, however, the difference is negligible.

It is thus documented that the mixing induced mean recirculation velocities in the constant pressure region just behind the base are small compared to the external flow velocities. However, for local regions (in particular, near the body centerline at the upstream edge of the recompression zone) the reverse flow velocities can be quite large, although the associated dynamic pressure falls off rapidly with Mach number.

An as yet unproved model of the wake core reverse flow structure has been formulated and is included here, parenthetically, subject to experimental verification.

The variation in static pressure along the wake core is predicted on the basis of the following data:

(1) Love (Reference 16) has observed, at Mach numbers 1.62, 1.93 and 2.41, that the static pressure along the wake core is either constant at the value of base pressure or decreases slightly for a distance aft of the base of 0.5 caliber. Data at Mach 1.33 (Reference 40) confirm this circumstance. Apparently there is no Mach number effect.

(2) The maximum recompression pressure coefficient for turbulent boundary layers occurs, according to the data of Howarth (Reference 40) and Heinrich (Reference 41), at a distance of 0.25 caliber aft of the wake throat, independently of Mach number. The location of the wake throat has been given by Love (Reference 16) as a function of Mach number.

(3) Love has established a trend of maximum recompression pressure coefficient, Cp_{max}, with Mach number, M, which - fitted to the data contained in Howarth (Reference 40) - is expressed as

$$Cp_{max} = e^{\frac{0.335}{(M + 0.35)^{2.42}}} - 1$$

(4) Zero pressure coefficient occurs (References 41 and 42) midway between the base and the point of maximum recompression pressure coefficient.

The data contained in Howarth suggest that the static pressure variation along the wake core between the points of minimum and maximum pressure coefficient has the form

$$Cp\,(M) = \frac{x_o/d + A}{B\,(x_o/d)^2 + C\,(x_o/d) + D}$$

where (x_o/d) is the distance, measured in calibers, aft of the

point of minimum pressure coefficient, i.e., aft of the station at 0.5 caliber. The constants appearing in this equation are evaluated by using the data of (1), (2) and (3), and (4) above. The equation is maximized (by differentiating with respect to (x_o/d) and setting the result equal to zero) to provide the fourth relationship for coefficient determination and, thereby, to constrain the maximum to occur at the experimentally observed location (2). The axial pressure variation so determined establishes the buoyancy effect on a body residing in the recirculation region.

Data due to Eiffel, contained in Hoerner (Reference 43), provide the best available insight into the variation of reverse dynamic pressure in the recirculation region. The variation suggested by these data is sinusoidal, with maximum reverse dynamic pressure occuring at a point 56 percent of the distance, x_t, between the base and the wake throat. In terms of the maximum reverse dynamic pressure, $(q_w)_{max}$, and the distances (measured in calibers from the base), x_1/d and x_t/d, of the nodal points, this variation as a function of the distance from the base, x/d, is given by

$$q_w\,(M) = (q_w)_{max} \sin\left[\frac{(x/d) - x_1/d}{(x_t/d - (x_1/d)}\,\pi\right]$$

Maximum reverse dynamic pressure is calculated by means of the incompressible Bernoulli equation, applied between the wake throat stagnation point and the position of maximum reverse dynamic pressure. The equation for pressure coefficient, $C_p = C_p\,(x_o/d)$, provides the values of pressure required for this calculation. Velocity and density are obtained with the energy equation and the perfect gas, say, equation of state under the assumption that total temperature is everywhere equal to free stream total temperature.

From the above parenthetical representation of the recirculation region an estimate of the two factors (reverse flow and horizontal buoyancy) which hinder the separation of a capsule from the base of a vehicle can be appraised.

Considering the two factors separately, it seems to be that the reverse flow contribution is most detrimental at low Mach numbers and diminishes rapidly as Mach number is increased; the horizontal buoyancy term is most critical when the base pressure is near zero and the recompression pressure is maximum. Both terms, however, become significant only when the integrated force-time (change in momentum) curve exceeds the probable error (factor of safety of the separation device) in the impulse required for separation due to carrier vehicle deceleration.

It is reiterated that the considerations of this section apply only to steady flow or (by assumption) to the time mean average of unsteady flow. Actually, all tests which have attempted to define the characteristics of the recirculation zone have found it to be intermittent and irregular (References 19 and 34). With respect to the above procedure for evaluating the effects of horizontal buoyancy and reverse flow, a further detailed discussion and results of computations are contained in the work of Broderick and Turner (Reference 44).

Some features of the high Mach number wake are prominent. At high Mach numbers three-dimensional effects are minimized and the external flow is given closely by the Prandtl-Meyer function. In order to verify this point a solution of the flow field about a conical afterbody (for $M = 4.95$) using the method of characteristics was obtained. Only slight variations were detected from the constant property solution associated with a Prandtl-Meyer expansion at the base corner. Thus, the recompression pressure gradient along the converging wake is at a minimum at high Mach numbers. Also, the pressure overshoot (to above free stream) found for low supersonic Mach number flow along a converging region virtually disappears at higher Mach numbers. To illustrate this, the data obtained by Love (Reference 16) in the recirculation region behind a cylindrical semibody of revolution are plotted in Figure 14 along with the correlated base pressure coefficients from the same report. When these curves coincide (at approximately Mach 3.0), the recompression pressure equals the free-stream pressure. Because of the lesser recompression and (mostly) because of the reduction in dynamic pressure (Figure 13) the importance of the

recirculation or reversed flow velocities is minimized at high Mach numbers.

The effects on wake structure of the changes in state (dissociation, ionization, formation of new species) associated with real gas flows at high enthalpy levels appear, tentatively, to be negligible. Liepmann's (Reference 6) shock tube experiments provide preliminary evidence for this statement. At high Mach numbers or low Reynolds numbers the inherent stability of the flow would be expected to minimize the unsteadiness of the recirculation flow.

(5) Hypersonic and Transonic Effects

A hypersonic body must necessarily have a blunt leading edge or nose in order to withstand the heating associated with high Mach number flight. A strong bow shock wave is produced at the nose of such bodies, causing large entropy increases and total pressure losses for streamlines passing through the shock wave. The associated energy dissipation takes the form of temperature rise; hence, those streamlines which pass through the bow shock do not recover the losses. Since the streamlines important for wake flow are those close to the body surface, it is apparent that the flow just upstream of the base will have a lesser total pressure than the external flow far from the body. Thus, even for bodies long enough that the static pressure ahead of the base is equal to the free-stream pressure, the associated Mach numbers will be less than free stream.

A remarkable feature of high Mach number flow is its inherent stability. Thus, the wake pattern would be expected to be most sharply defined at high Mach numbers, the recirculation pattern would be at its steadiest. On the other hand, low Mach number flows exhibit a minimum of steadiness. Fluctuations in the wake pattern and in the recirculation pattern will be quite prevalent for these flows. Furthermore, the recirculation velocities are of more importance because of their higher dynamic pressure.

However, in a time averaged sense, the previously discussed model of the wake is still applicable to transonic (or lower speed) flows. Both Chapman and Korst (References 13

and 15) correlate appropriate data through the transonic regime. In fact, by taking the limit of Chapman's expression for base pressure as $M \to 0$, he obtains suprisingly good correlation of incompressible data. The difficulty with subsonic flows is that no simple function like the Prandtl-Meyer function relates streamline deflection to pressure. Instead, a potential flow problem must be solved for the external flow in each case, and this solution is highly dependent on the assumed boundaries of the viscous region. The "recompression" pressure is thus difficult to obtain.

b. The Spreading Downstream Wake

The spreading wake downstream of the throat or critical region is less well known than is the converging wake ahead of the throat. The latter region is of greater interest since it determines the base pressure and hence, in part, vehicle performance. Consequently research has been focused upon the base region; that which is known about the downstream wake may, for the most part, be attributed to Prandtl and his associates.

Practically, only turbulent flow in the downstream wake needs to be considered since the downstream laminar wake becomes unsteady or turbulent at very low Reynolds numbers. Solutions of the momentum equation for distances far away from the body (where the velocity defect is small compared to the free-stream velocity) result in asymptotic velocity profiles all similar to a single "universal" velocity profile. Further, dimensional analysis (Schlichting, Reference 37) specifies velocity defect, U, and wake width (radius), r_o, as functions of downstream coordinate, x, as

$$U_{max} = U_{axial} \backsim x^{-p}$$

$$r_o \backsim x^{1-p}$$

where p has the value, 2/3, for axisymmetric flow and 1/2 for

two-dimensional flow. Two empirically determined constants are available for correlating experimental data. One is the constant of proportionality, K, (known if the viscosity is known); the other is the origin for the x coordinate.

By applying Prandtl's mixing length theory for turbulent momentum transfer and assuming the mixing length to be constant across the width of the wake and proportional to the width, there results the following expression for velocity (defect) transverse distribution in the axisymmetric case:

$$\frac{U}{U_{max}} = \left[1 - \left(\frac{r}{r_o}\right)^{3/2} \right]^2$$

Alternatively, if it is assumed that the eddy viscosity is constant across the wake, the simplified turbulent momentum equation is identical with the laminar and there results a velocity distribution given by the error function. Such a Gaussian asymptotic velocity distribution is common to mixing problems governed by the boundary-layer type of equations, since these equations are of the diffusion type. The Gaussian velocity distribution avoids several esthetic deficiencies of the velocity distribution given by the above equation, namely the discontinuities in curvature at the edges of the wake and on the wake centerline. Also, the constant eddy viscosity assumption avoids the difficulty inherent in the mixing length theory that the eddy viscosity vanishes on the wake centerline (where actually it is a maximum).

However, either distribution matches experimental data very well. The above equation has the advantage (because it calls for a finite wake width) that it can be readily integrated to give average velocities across the wake without requiring explicit knowledge of the wake width. With it the average velocity defect in the axisymmetric case has been computed as 0.257.

The average velocity defect to which a body ejected along the wake core is subject can be computed by applying limits of integration appropriate to the body size.

These equations apply to incompressible flow. However, since two constants are capable of individual determination, there seems to be little point in attempting a compressible solution. The available constants provide sufficient freedom to enable fitting of the very limited data that are available.

A second approximation to the wake width and velocity distributions has been obtained by Swain (Reference 45) by using the above expressions as the first term in a series. This second approximation results in a wake width larger than that given by the first approximation in regions near to the wake producing body. However, the second approximation for velocity distribution includes still another empirical constant to be obtained from experimental data. In view of the lack of such data and because of the basic unsoundness of the asymptotic methods for regions near the body, this second approximation is not used here.

Although the simple analysis just described is useful in that it provides an indication of the sort of wake behavior to be expected, some serious deficiencies should be pointed out. Careful measurement by Townsend (Reference 25) have shown that the wake velocity profiles are not truly similar until very large distances distances downstream of the wake producing body. However, by assuming different origins for the x-coordinate for different regions of the downstream flow, similarity is closely obtained over limited regions.

Also, observations of the turbulent wake indicate that the growth of the wake, or the lateral transfer of momentum, is due primarily to large, intermittent jet-like puffs of fluid extending out from the wake axis. These puffs of fluid appear at a given point in the flow in a random fashion. However, more nearly uniform small scale eddies which lie in various directions carry most of the turbulent energy and are responsible for most of the apparent viscosity, or eddy viscosity.

Considering, in particular, the large eddies or puffs of fluid, the flow at a given point in the wake is intermittently turbulent. Townsend has measured intermittency factors and found them to fall off from unity (continuous) at the center of the wake to zero at the edges.

The momentum transfer theory used to obtain expressions for wake spreading and wake velocity ignores this intermittency. Also, it assumes the same mechanism or length scale for effective viscosity and for wake spreading, ignoring the difference between the large and small scales of eddies.

In spite of these defects, the velocity distributions derived from Prandtl's momentum transfer theories agree closely with the experimental data and hence are quite useful here. The results for wake spreading provide the form of the relationship to be fit with experimentally determined constants.

c. Representation of Wake Structure

The preceding discussion has shown that the wake structure for a given body depends upon a number of factors, e.g., the Mach number, Reynolds number, a description of the boundary layer at the base of the body, and a description of the location of transition, if it occurs in the wake. The effects of various bodies are manifested in all of these parameters. The practical bounds of the present study require that the description of wake structure be as simple as it is consistent with the attainment of reasonable accuracy. These simplifications and restrictions which have been adopted are briefly discussed.

Because of their more frequent practical occurrence, turbulent boundary layers are assumed. Necessarily, the downstream wake is also considered as turbulent. Again, because of their more frequent practical occurence, axisymmetric bodies of revolution aligned with the wind are considered.

Thus, the values of wake convergence angle given in Figure 10 are used to define the outlines of the converging wake region. Since the boundaries of the region are assumed to be conical, the converging region is completely defined once the width of the viscous region after convergence is known. This width (labeled t_w in Figure 8) is most readily obtained from examination of wake photographs, on which the wake width at this point is usually defined quite sharply. Chapman (Reference 12) values of wake thickness so obtained, given in Figure 15, are used in the present program.

Since the Prandtl-Meyer function has been demonstrated to give an approximation to a more exact characteristics calculation

for the flow past a conical afterbody at the Mach numbers of primary interest in the present study ($M \geq 5$), the external flow properties along the conical boundary are considered to be constant and equal to those given by a Prandtl-Meyer expansion to the base pressure. Thus, the pressure in the recirculation region is also considered constant and equal to the base pressure, and the recirculation velocities and static pressure gradients which actually exist in the "dead air" region are neglected. In the interest of simplicity, the external flow along the conical converging section is assumed to have its properties vary linearly with angle back to those associated with the free-stream direction (undeflected extension of the cylindrical body).

To calculate the properties of the downstream wake, the values of wake thickness at the wake throat given in Figure 15 are used. This value of wake thickness is kept constant independent of distance back of the wake throat since at supersonic Mach numbers the downstream wake divergence angle is of the order of two degrees or less.

The data contained in Howarth (Reference 40) for a body of revolution at $M = 1.33$ were used as a basis to determine the empirical constants for the wake centerline variation, V_{w_ℓ}, using the 2/3 power law for the variation in centerline velocity in the axisymmetric subsonic case as discussed in section IV. A. 2. b. The resulting expression for the axial wake centerline velocity is

$$\frac{V_{w_\ell}}{V_\infty} = 1 - \frac{0.684}{(x/D - x_A/D)^{2/3}}$$

where

$$x_A/D = x_t/D - (0.684)^{3/2}$$

$$V_{w_\ell} = (V_\infty - U_{max}) \text{ and}$$

$$x_t/D = \frac{1 - t_w/D}{2 \cos \theta}$$

As discussed in section IV. A. a. a. (4), the static pressure variation in the wake at high Mach numbers is small, justifying the approximation of constant static pressure equal to free stream static for the downstream wake. Using this approximation for the static pressure within the wake coupled with the velocity variation described above and further assuming that the wake total temperature is equal to that of free stream the wake centerline density, Mach number, and dynamic pressure can be computed. The results are shown in Figures 16 and 17. The wake properties for radial distances (r) other than the centerline values were obtained by using the following expression:

$$\frac{U}{U_{max}} = \left[1 - \left(\frac{r}{t_w}\right)^{3/2} \right]^2$$

where U_{max} is the centerline velocity defect evaluated from the above equations.

B. Capsule Characteristics

From an infinity of geometrical types it becomes necessary, for practical reasons, to narrow for consideration the possible capsule configurations to a reasonable number. For most realistic applications only the blunt shape is pertinent; symmetric and asymmetric shapes arise in specific instances. The manned capsule (see for example Reference 42) is an important example of the cases in which the asymmetric shape could have attractive advantages. The ability of an asymmetric shape to produce substantial lift forces can be put to use to assist in the separation procedure, and - of course - is beneficial in the deceleration and heating problems associated with re-entry. Since, however, the asymmetric shape is highly specialized and dependent upon the particular application, its geometrical variations are essentially infinite. It becomes impractical therefore to include the class of asymmetrical capsules in the present generalized study.

Restricting consideration to the symmetric capsule nevertheless permits the inclusion of a large number of diverse shapes. Broadly the candidate configurations may be characterized according to their drag characteristics, namely as low, moderate, or high drag shapes. In Table V, are illustrated schematically the geometric configurations which arise as representative capsule types, and which are considered more or less in detail in this report. According to their drag characteristics, these configurations group in the following manner:

(1) High drag

- (a) Cylinder
- (b) Spool

(2) Moderate drag

- (a) Sphere
- (b) Disk

(3) Low drag

- (a) Hemisphere - cone
- (b) Hemisphere - cone - flared cylinder (designated as "flared capsule").

Certain criteria may immediately be applied against these candidate shapes so as to reduce the number which must be considered in detail here.

On the basis of packaging efficiency, i.e., the packaging of the capsule onboard the carrier vehicle, the above capsules qualify approximately as follows. The cylinder and, to a somewhat lesser degree, the spool have excellent packaging characteristics and are adaptable either to side or to base ejection. The flared shape is reasonably adaptable to internal packaging such as to permit either side or base ejection and is further an appropriate vehicle nose configuration. Similarly, the hemisphere-cone is suitable as a vehicle nose and can be internally packaged. Less satisfactory as a vehicle nose due to its high drag is the disk shape, and its internal packaging efficiency, along with that of the sphere, is poor.

A further objection to the sphere lies in its neutral orientation stability (with its center of gravity at the centroid); the disk shape has erratic dynamic stability characteristics. The unfavorable stability characteristics of the sphere and disk, along with their poor packaging efficiencies, relegate them to a position of secondary importance as capsule configurations. Their detailed consideration in the present study is therefore minimized.

The aerodynamic characteristics (normal and axial force coefficients, center of pressure location, static and dynamic stability) of the capsule configurations of prime importance are considered in the following two subdivisions of this section. These subdivisions consider, respectively, free flight characteristics and interference effects. Salient free flight characteristics are summarized in Table V_2 which includes for purposes of comparison the aerodynamics of the sphere and disk configurations.

1. Capsule Free Flight Aerodynamic Characteristics

Evaluation of capsule shapes on the basis of their aerodynamic characteristics is most conveniently made independent of the effects of proximity to the carrier vehicle. The latter effects are treated as incremental to the free flight force and moment system and are discussed in Section IV. B. 2 of this report. The present section is organized in subdivisions, considering – respectively – the cylinder, spool, flared body, and cone.

a. Cylindrical Capsule

Static aerodynamic data at low angles of attack exist for a wide range of cylinder fineness ratios and over a Mach number

range from subsonic to moderately high supersonic. Dynamic stability derivatives are available in a limited number of cases and form the basis for extrapolation over the Mach number range of interest. Lack of experimental data at high angles of attack requires that theoretical estimation of static quantities be made. The modified Newtonian theory is adequate for this purpose. The following paragraphs discuss the available data as presented in this report.

Plotted in Figures 18 and 19 as functions of Mach number and cylinder fineness ratio (zero angle of attack) are center of pressure location and normal force coefficient slope, respectively. Figure 20 presents for a fineness ratio 2.0 cylinder, the variation of normal force, moment and drag coefficient with Mach number, the latter quantity being independent of fineness ratio in the range above Mach 2. Some remarks are pertinent in the interpretation of the data presented in these figures.

The location of center of pressure is observed to move forward on the body as fineness ratio is increased and rearward as Mach number is increased. As indicated by Potter (Reference 46) in subsonic flow at small angles of attack (and evidently in moderate supersonic flows) separation occurs as the flow attempts to negotiate the sharp (upper) corner at the forward end of the cylinder. Reattachment occurs at about three-quarters of a cylinder diameter beyond the shoulder with accompanying positive pressures. These pressures drop approximately to zero at a distance two diameters from the shoulder. Since this pressure distribution is independent of cylinder length it follows that the center of pressure must move forward (relative to the base) as length increases. The Mach number effect is attributed to weakening of the separated region behind the shoulder with increasing Mach number and consequent reduction in negative pressure there (loc. cit. Figure 25). The resultant of the normal force, which is reduced as a consequence of this mechanism, therefore lies further from the cylinder front surface. The data for cylinder fineness ratios between 2 and 5 indicate that center of pressure location varies approximately linearly with fineness ratio in that range. Comparison of the data of Potter and Felix (References 46 and 47) reveals that beyond Mach 2.5 the slope of the normal force coefficient curve is independent of fineness ratio.

From the paucity of dynamic stability data for cylindrical shapes there are noted some isolated measurements. It can be

surmized that this shape is dynamically unstable at subsonic speeds and stable at supersonic speeds. Additional data for a near-cylindrical configuration at supersonic Mach numbers suggest that there exists an exponential decay of the sonic value to zero dynamic stability at very high Mach numbers.

It is of interest to consider, parenthetically, the problem of aerodynamic heating wherein a cylindrical capsule, with its sharp face-edge, might be expected to be vulnerable. Representative calculations indicate that the edge heating rate is, in fact, considerably higher than the stagnation value (50 percent higher than the peak stagnation value). Even at these rates, however, adequate insulation may still be provided for many trajectory conditions.

b. Spool Capsule

A shape which has received some consideration as an airplane store and as an artillery shell is the so-called spool configuration, i.e., a cylinder surmounted at each end by circular flanges. The available data are examined to determine if there exists, for this configuration, a significant improvement, aerodynamically, over the simple cylinder. The meager information is summarized briefly as follows.

Subsonic and transonic experiments indicate that for a spool of moderate fineness ratio the center of pressure location, though favorable, is extremely sensitive to angle of attack in the low range. The supersonic data for simple and finned spools indicate the more favorable static stability of the spool at low supersonic Mach numbers as compared to a simple cylinder of the same fineness ratio, but the location of center of pressure on the spool moves unfavorably with increasing Mach number. Oscillation tests indicate that, dynamically, the pure cylinder is at least as satisfactory as the best variation of the simple spool (and that both shapes are inferior to the flared configuration).

A somewhat more sophisticated version of the spool is the so-called bicylinder configuration. Static aerodynamic data at supersonic speeds are plotted for an optimum variation of this configuration in Figure 21. Compared in the same figure are data for the pure cylinder of equivalent fineness ratio. It is indicated that, at the relatively high fineness ratio of the test configurations, the bicylinder

exhibits a substantial superiority over the simple cylinder. Furthermore, the unfavorable center of pressure travel (with Mach number) of the simple spool is absent with the bicylinder. Possible problem areas of the bicylinder lie in its probable sensitivity to Reynolds number effects on optimum slip ring location and in aerodynamic heating at the shoulder of the slip ring (see Figure 21).

c. Flared Capsule

Some of the geometric parameters which affect the aerodynamic characteristics of the flared capsule are:

(1) Flare angle, the most important geometrical variable; increasing flare angle tends to move center of pressure rearward relative to the nose

(2) Flare length has an effect similar to that of flare angle; however, to obtain a comparable change (say, increase) of center of pressure location with respect to the nose requires a substantial increase in flare length

(3) Concurrent with geometric considerations, nose blunting tends to move center of pressure forward relative to nose but rearward relative to cone-cylinder shoulder

(4) Increasing fineness ratio by increase of length of cylindrical portion tends to move center of pressure in percent of body length forward relative to the nose.

The Reynolds number-dependent phenomenon of boundary layer separation importantly affects flared body stability characteristics. Dennis (Reference 48) has investigated this Reynolds number affect on a flared body in the supersonic range. His data indicate that static stability is promoted by low Reynolds number while the reverse trend exists for dynamic stability.

A further indication of Dennis' data, verified by others, is that boundary layer separation, and hence static stability, is Mach number-dependent.

The aerodynamic quantities, $(C_{M_q})_{0.5L}$, C_{N_α} and C_A at zero angle of attack, are plotted in Figure 22 for a representative 20

degree flared body (illustrated therein). Experimental supersonic normal force and moment data are reflected in the supersonic range; normal force and moment data at subsonic and transonic speeds have been estimated based on data for another flared body from unpublished wind tunnel tests conducted at the Arnold Engineering Development Center and the Naval Ordnance Laboratory. Axial (drag) coefficient has been estimated from available data. At high angles of attack the modified Newtonian theory has been employed to estimate the above quantities. Results of the Newtonian calculations are presented in Figure 23.

The slender body theory of Tobak (Reference 49) has been employed to estimate the dynamic stability ($C_{M_q} + C_{M_{\dot{\alpha}}}$) for the assumed 20 degree flared body. The value so obtained is -2.5, which compares well with data for a similar configuration at supersonic speeds.

d. Cone

Whether for use as a nose cone or as an internally stored capsule, the several considerations of aerodynamic heating, drag and dispersion, and packaging efficiency generally will dictate the use of blunting for conical bodies. In certain instances blunting can result in reduced drag (over that of a pure cone), but, in general, the drag penalty must be taken.

Data for a conical configuration, which is representative of those which emerge after compromises among the above criteria are made, are illustrated in Figure 24. (Dynamic stability is well approximated by the slender theory in the supersonic range.) Approximation of aerodynamic data at higher angles of attack can be made by employing the modified Newtonian theory.

C. Interference Effects

The manner in which the flow fields of the separating body and of the carrier vehicle affect each other's loading distributions is discussed in this section. Interference effects arise differently according to the region on the carrier vehicle from which separation is effected. Consequently, this section is organized in three subdivisions, considering respectively, nose, side, and base field interference.

1. Nose Separation Interference

The interference effects arising in nose separation are manifested in the loading on the carrier vehicle (afterbody). Two counteracting conditions occur as the nose cone translates laterally and rotates about its point of contact with the afterbody.

(1) A portion of the cylindrical afterbody becomes immersed in the wake of the nose cone, with reduced pressure (relative to free-stream static) occurring over the affected area. Moments tending to rotate the afterbody axis in a direction corresponding to the direction of movement of the nose cone axis are thus induced.

(2) Simultaneously a portion of the afterbody nose becomes exposed to the air stream as the nose cone moves off the vehicle axis. The pressures occurring on this exposed area tend to rotate the carrier vehicle in a sense opposite to that of the interference normal force distribution (1).

The magnitude of the above pressure changes and the areas affected by them must be determined in order to calculate carrier vehicle motion during the nose separation process.

In order to render the above interference problem tractable, certain simplifying assumptions are made. These assumptions and the model of the resulting pressure field are described in the following paragraphs.

The nose cone wake is assumed to be unaffected by the presence of the afterbody. Consequently, the method discussed in sections IV. A. 2. c and IV. D for predicting wake angle in the convergent region is applicable in determining the area on the carrier vehicle blanketed by the nose. Along the cylindrical portion of the carrier, the blanketed area is assumed to be triangular in shape with base and altitude given by the maximum transverse and longitudinal extent of the wake-carrier intersection.

The pressure acting on the cylindrical portion of the carrier vehicle is assumed to be given by the base pressure coefficient of the nose cone, applied uniformly over the affected area. On the carrier nose, the pressure acting over the exposed surface is assumed to be that associated with a flat surface normal to free stream flow. Again the distribution of this pressure is assumed uniform. A possible "spike effect" due to the proximity of the nose cone (see e.g., Bogdonoff, Reference 9), which could act to reduce the pressure on the "exposed" front surface and concurrently alter the pressure distribution over the capsule, is neglected.

2. Side Ejection Interference

Interference effects in side ejection are considered within the two separate phases of the ejection process, namely

(1) During partial exposure

(2) In complete exposure

Boundary layer-shock wave interaction effects, which arise during the partial exposure phase and during the earlier portions of complete exposure, are discussed in sections IV. C. 2. a and b.

a. Partial Exposure Phase

During partial exposure the normal shock wave produced by the exposed portion of the capsule interacts with the boundary layer of the carrier vehicle. In general a stable system requires separation of the boundary layer upstream of the theoretical shock impingement point. The pressure that would otherwise exist on the front surface of the capsule is altered in accordance with the modified flow mechanism. The present problem, however, involves shock wave-boundary layer interaction, aggravated by the existence of a cavity with separated flow and with complex three-dimensional boundaries. These effects are not covered in the literature and are not presently feasible for analytical treatment. Aerodynamic effects existing under these conditions can only be profitably determined empirically. Therefore, in the present study the aerodynamic characteristics during the partial exposure phase, and also during the earlier portions of complete exposure where such interactions can occur, are obtained neglecting these interactions. The acceptability of such simplifications can only be determined by later

comparison with experimental data. The methods employed to determine aerodynamic "interference" effects are discussed in sections IV. C. 2. a. (1) and (2) for partial exposure and section IV. C. 2. b for complete exposure.

For reference purposes, relatively simple cases of shock wave-boundary layer interaction are contained in the literature. Chapman's data (Reference 13) indicate that the normal shock wave induced at high Mach number will separate both laminar and turbulent boundary layers. Moeckel (Reference 50) has shown that boundary-layer separation is a necessary condition for two-dimensional flow equilibrium. Some effects of separated flow have been observed by Lange and by Moeckel (References 35 and 50). The former investigator has measured a pressure coefficient on the forward face of a step (height equal to three boundary-layer thicknesses) equal to less than one-quarter of the value associated with the normal shock for the test Mach number, 3.03. For step heights equal to 12 boundary-layer thicknesses Moeckel has observed unsteady flow conditions with pressures fluctuating above and below the steady value. Presumably as the step height becomes large relative to boundary-layer thickness a detached shock will occur with the usual pressure distribution existing over most of the step face. Forces on a capsule during partial exposure arise from the following:

(1) The dynamic pressure of the carrier flow field

(2) The dynamic pressure due to ejection velocity

(3) The buoyancy effect of the static pressure differential existing between the capsule surfaces internal and external to the carrier vehicle.

The means of estimating these forces are documented in the following subsections where "normal" and "axial" directions are referred to the capsule longitudinal axis. In all instances pressure distributions are assumed uniform.

The partial exposure phase is considered relative to two modes of ejection, namely

(1) Capsule longitudinal axis normal to carrier axis, capsule base end outward

(2) Capsule longitudinal axis parallel to the carrier axis, capsule nose aligned in same sense as carrier nose.

Flared and cylindrical capsules are discussed with respect to the "normal" ejection mode; flared capsules only, in "parallel" orientation.

(1) Capsule Normal Orientation

Dependent upon capsule geometry, the carrier flow field can induce forces in both the normal and axial directions. The forces attributed to various effects have been computed independently and summed in their respective normal and axial directions. Normal forces arise over the cylindrical portions which can be estimated from Penland's data (Reference 51). Pressure distribution is based upon an averaged local dynamic pressure and upon exposed "plan" area. For the hemisphere-cone-flared cylinder capsule, normal and axial forces arise on the inclined surfaces which are estimated by means of the modified Newtonian theory based upon averaged local Mach number and dynamic pressure and upon exposed area.

An axial force arises due to ejection velocity and local density which acts uniformly over the capsule maximum cross-sectional area. The drag coefficient employed in the calculations for this effect was 0.8 for the cylinder, and a value pertinent to a disk in subsonic flow of 1.17 was assumed for the base end of the flared body.

The buoyancy effect, which is reflected in an axial force, is based upon the pressure differential existing between that on the farthest removed capsule external surface (the capsule base) and the carrier internal pressure (assumed ambient static). Thus, when the capsule base is tangent to the carrier surface (not yet exposed), the pressure differential becomes the difference of the "end" pressure over the capsule base and the ambient pressure assumed acting on the nose and flare of the capsule which is external to the carrier. The area on which this pressure differential acts for any capsule position is assumed to be that capsule cross-sectional area intercepted by a plane passing normal to the capsule axis and tangent to the carrier body. This assumption was made in an attempt to maintain

consistence with the assumption that Newtonian flow is acting over the exposed portion of the capsule flare during ejection. The pressure acting on the exposed capsule end is a function of Mach number. Pertinent data are available in the supersonic range and have been supplemented by a test conducted in the Cook Technological Center wind tunnel at a Mach number of 0.476.

The latter test indicates that the pressure coefficient over more than half the end surface (base of capsule in this case), is -1.0 and that a recompression occurs over the rearward part of the surface such as to bring the value to -0.4. This flow mechanism variation is reasonably consistent with the aforementioned results of Potter (Reference 46) which indicate that pressure coefficients on the shoulders of blunt cylinders oriented with longitudinal axes parallel to the flow follow essentially the same type of variation as cylinder end pressure coefficients in normal orientation. In search for additional data it is assumed that the pressure acting on the end of a body at $\alpha = 90$ degrees (normal orientation) would compare to base pressure for a cylinder in cross-flow. This assumption is consistent with conclusions drawn by Love in Reference 16 for relationships between separated flow axes and base pressure coefficients. Corresponding data have been gathered and are plotted, along with Hoerner's estimate (Reference 43) for shoulder pressure coefficient, in Figure 25. The curve faired through the data points is used in the present buoyancy calculations.

(2) Capsule Parallel Orientation

Axial and normal forces arise due to the carrier dynamic pressure field. The zero angle of attack axial force coefficient at the locally averaged Mach number (loc. cit section IV. C) is pertinent in the axial calculation; the area on which the force acts (uniformly) is the exposed cross-sectional area. The (uniform) normal force is assumed to be given by the conical flow pressure coefficient (see e.g., Reference 52) on the nose and flare sections, projected in the normal direction. Ambient static pressure is assumed to exist over the exposed cylindrical portion. Opposing this normal force is the carrier internal pressure (assumed ambient static), which acts upon an area

intercepted by a plane passing longitudinally through the capsule and tangent to the carrier body for any capsule position during ejection.

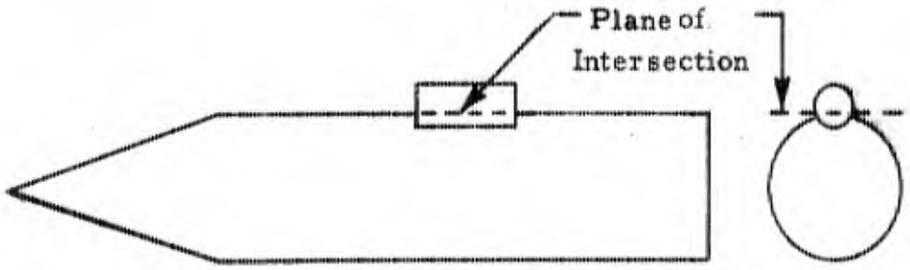

The normal force due to ejection velocity is calculated on the basis of the cross-flow drag coefficient, 1.2, and local density. This loading is assumed uniform over the capsule plan area.

b. Complete Exposure Phase

The capsule during the complete exposure phase will initially be within distances from the carrier surface where various proximity effects such as shock wave reflections and interactions with boundary-layer flows, etc., will exist which can produce significant changes in the local flow fields. Later the capsule will traverse regions of the basic carrier field where, in general, shock waves and continuous gradients and curvature of varying magnitudes occur.

In the former case when the separating body is close to the carrier vehicle, as it is during ejection and the earlier phases of separation, the flow field of this body can affect the parent vehicle flow field and therefore adjust the field to which the separating body itself is exposed. In this regime extreme flow gradients are generated and the interaction of the capsule flow field with that of the carrier can produce extremely significant alterations in the basic carrier flow field. The extent of this effect is, to a large degree, proportional to the size of the separating body with respect to the parent vehicle. As discussed in section IV.C.2.a, the phenomena associated with this type of interference are so complex, involving interactions between inviscid as well as boundary flows, as to

prevent any confidence in analytical attempts to define them. Consequently, the determination of these phenomena is relegated to experimental methods. For smaller capsule configurations which are of interest to the present study the effect of these interactions may be restricted to relatively short time periods during the separation interval so that the over-all effect of flow interaction on the separation process during complete exposure might approach secondary importance, or even be negligible in certain cases. In addition, the extent to which "steady state" interactions are approached may very well be a function of the relative velocity of the capsule as it traverses the close-in portion of the carrier field. Because of these considerations, capsule aerodynamic characteristics are computed assuming that the carrier flow field is unaffected by the presence of the capsule.

With this assumption that the presence of the capsule does not affect the carrier field, the changes in capsule characteristics due to basic field nonuniformities may be obtained from a perturbation potential analysis for continuous field variations (no discontinuities) with a relatively low drag body, or by employing a numerical "strip theory" in general. The perturbation potential analysis is first discussed assuming that the nonuniform field is compatible with the linear equation for the perturbation potential.

The linear equation for the perturbation potential associated with small disturbances in irrotational flow is

$$(1 - M_{\infty}^2)\,\phi_{xx} + \phi_{yy} + \phi_{zz} = 0$$

This equation is valid for subsonic or supersonic speeds; however, for $M_\infty \doteq 1$ or $M_\infty \gg 1$, some of the nonlinear terms which were neglected for this study must be included.

Slender body theory provides approximate solutions to the above equation under the assumption that

$$\sqrt{M_\infty^2 - 1} \quad R/x \ll 1$$

where R is the body radius and x is the body axial coordinate. Although this restriction is rather severe, results obtained with the slender body assumptions are nevertheless useful. Even for bodies of low fineness ratio, the slender body theory yields – in many cases – surprisingly good approximations to experimentally determined aerodynamic coefficients.

The total perturbation potential for the following analysis is then due to the capsule body angle of attack with respect to a uniform local stream and the interference upwash or downwash velocities which are deviations from the local average (uniform) flow field direction. Under the restriction that the sidewash generated by the parent body varies only with the axial coordinate of the separating body, Moskowitz (Reference 53) has shown that the sidewash velocity contributes nothing to the net lift on the separating body. The total perturbation potential may, therefore, be written as

$$\phi = \frac{R^2 \sin\theta}{r} \left[U\alpha + w(x) \right]$$

where

x = axial or longitudinal coordinate

r = radial coordinate

θ = tangential coordinate

R = body radius

U = uniform velocity of local stream (averaged over extremities of capsule)

α = angle of attack of capsule with respect to the local stream (averaged value)

w = upwash or downwash velocity increments due to stream curvature over the extremities of the immersed body, i.e., deviations from average local conditions along the capsule body.

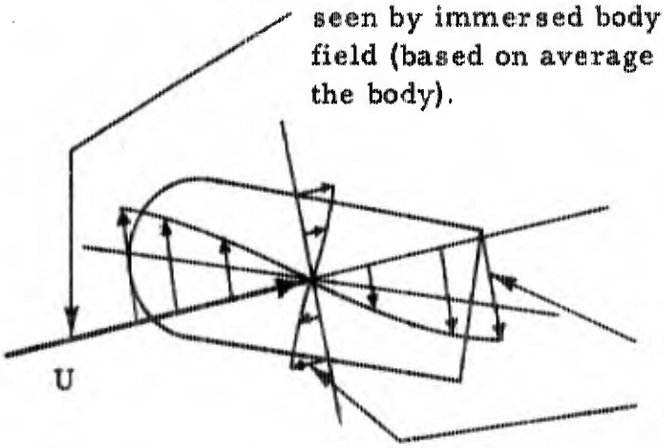

This total potential has been specified to satisfy the boundary condition that the cross-flow is cancelled at the surface of the body, i.e.,

$$(\phi_r)_{r=R} = -(U\alpha + w)\sin\theta$$

To the same order of accuracy the pressure coefficient is given by

$$Cp = \frac{-2(\phi_x + u)}{U}$$

where u, the longitudinal interference velocity component (deviation from the average local condition), is related to w by the irrotationality condition

$$\frac{\partial u}{\partial z} = \frac{\partial w}{\partial x}.$$

Integrating the pressure in the lift direction around and along the body results in an expression for total lift force which splits into three sets of terms representing (a) the lift due to angle of attack of

of the body immersed in an averaged "uniform" field, (b) the lift due to vertical velocity deviations (horizontal gradients) from the average field along the length (longitudinal extremities) of the capsule and (c) lift due to vertical gradients or deviations of the flow field velocity in the "uniform" field direction. The latter term may be expressed as a buoyant force due to immersion in a vertically varying field, or effectively, a variable pressure field. The expression for total lift is:

$$L = \frac{2Q\pi}{U}\left[\underbrace{\frac{Ua}{\pi}\,(A_2 - A_1)}_{a} + \underbrace{w_2 R_2^2 - w_1 R_1^2}_{b}\right.$$

$$\left. + \underbrace{\frac{1}{\pi}\int_{x_1}^{x_2} R\,dx \int_0^{2\pi} u \sin\theta\, d\theta}_{c}\right]$$

where Q is the local average dynamic pressure over the capsule extremities, A represents body cross-sectional area, and subscripts 1 and 2 refer to the nose and tail of the immersed body, respectively.

By expanding u in a Taylor's series, keeping the first two terms and applying the irrotationality condition, the second integral can be evaluated. Dropping the lift due to local angle of attack of the psuedo-uniform stream which can be epxressed by the actual lift characteristics of the body as $C_{L_\alpha}\,\alpha_{uniform}$, the interference lift is derived. For a closed nose body, $A_1 = 0$ and the final expression for interference lift is

$$C_{L_i} = \frac{2A_2}{SU}\left[w_2 + \frac{\overline{A}}{A_2}\,(w_2 - w_1)\right]$$

where

$\overline{A}$ = average body cross-sectional area (volume/length)

S = reference area

The closed nose condition actually implies $\frac{dA}{dx} = 0$ at $x = 0$, and hence for bodies of the form $r \sim x^n$, n should be greater than 1/2.

The expression for interference moment is derived in a generally similar vashion. The total moment about the body nose is given by

$$M = -\Bigg[\underbrace{\frac{U\alpha}{\pi}\,(A_2\,x_2 - A_1\,x_1 - V)}_{a} + \underbrace{R_2^2\,w_2\,x_2 - R_1^2\,w_1\,x_1}_{b}$$

$$+ \underbrace{\int_{x_1}^{x_2} R^2\,x\,dw - \int_{x_1}^{x_2} R^2\,w\,dx}_{c}\Bigg]\,\frac{2Q\pi}{U}$$

where V is the body volume and the other symbols are those used previously.

Assuming $A_1 = 0$ as before, defining an average body cross-section area and removing the moment due to local angle of attack of the psuedo-uniform field, there results the following expression for interference moment coefficient (about the nose)

$$C_{M_i} = -\frac{2w_2}{U}\,\frac{A_2\,l}{SC} - \frac{2\overline{A}}{USC}\left[w_2\,x_2 - w_1\,x_1 - \int_{x_1}^{x_2} w\,dx\right]$$

where $\bar{C}$ is the reference length for moments, and l is the total length of the immersed body.

It is apparent that the interference downwash velocity deviation distribution, w(x), must be known to perform the integration associated with the buoyancy term and other field variables must be established.

For the cases considered in the present study where the carrier angle of attack is zero and the angular displacements from free-stream direction of the pseudo-uniform local averaged field velocity vector are relatively small due to the position of ejection in the carrier flow field the interference downwash velocity distribution, w(x), may be approximated by taking the magnitude of these deviations from the "uniform" stream as being normal to the true free-stream direction (carrier longitudinal axis). This allows the w(x) values to be referenced to carrier body coordinates. In order to determine the local magnitude and direction of the "uniform" stream, the velocity components throughout the field must be known. For machine computation purposes, simple functions or tabulations can be made to describe the spatial variations of the velocity field in terms of components along and normal to the carrier vehicle longitudinal axis. In computing the spatial coordinates of the capsule in this field, the pseudo-uniform field velocity and direction is established by flow conditions existing at a reference "average" capsule location, say at the capsule center of gravity or half the capsule length. (The center of gravity is preferable since the actual total linear velocity of the capsule will be established at this point.) The interference velocity deviations, w(x), existing over the capsule extremities can then be determined by subtracting out the "uniform" field total vertical velocity component, $W_{y_{average}}$, which is the normal velocity of the local stream with respect to the carrier vehicle at the reference position:

$$w(x) = W_y(x) - W_{y_{average}}$$

$$w_1 = W_{y_1} - W_{y_{average}}, \text{ etc.}$$

Values of w(x) so existing over the capsule can then be integrated

over the capsule extremities to determine the interference downwash velocity distribution which must be known to evaluate the buoyancy term. Of course, the "uniform" velocity and angle of attack actually seen by the capsule as it traverses the carrier field is a result of vectorially combining the "uniform" field velocity components which are established relative to the carrier vehicle with the velocity of the capsule with respect to the carrier. However, the w(x) values may be established prior to this vector addition since the capsule separation velocity is small compared to stream velocity. Local Mach number and dynamic pressure can be determined by describing pertinent field variables such as density and ambient temperature with spatial tabulations or mathematical representations. When the carrier is accelerating or decelerating (changing Mach number), the flow field variables are altered accordingly. In this case, in addition to being dependent on the position in the carrier side flow field, the field parameters such as density and temperature must be represented as Mach number (and altitude) dependent quantities. The carrier field velocity components can be derived by employing corrections to free stream which would also be position and Mach number dependent. In many cases, however, the time required for the capsule to traverse the carrier flow field will be small enough that the effects of change in Mach number on flow field parameters may be neglected when the carrier is accelerating. In these cases, the employment of a time-averaged Mach number effect would be adequate.

It is, of course, assumed that in employing the above interference approximation the effects of the vertical velocity downwash deviations, w(x), over the capsule are divorced from the effects of pitch rate about the capsule center of gravity producing an additional linear velocity distribution. It is therefore assumed that these effects can be assessed separately, the latter being included as capsule damping in pitch.

Additional forces and moments appear when the separating body is intercepted by a shock wave. Pressure differences are caused by the intersection of the shock wave with the body and by the discontinuity in downwash velocity associated with the shock wave. The downwash discontinuity must be considered since the longitudinal downwash velocity component, u, was expanded in a Taylor's series to perform the integrations in the buoyant terms. Thus, the expressions obtained above are not valid at the discontinuity in u which occurs at the point of shock-wave intersection with the body.

The terms due to pressure differences are obtained by using the oblique shock relations to calculate the pressure rise across the shock. This pressure rise is assumed to act uniformly over the projected area intercepted by the shock wave. The resulting force is then projected in the lift direction to give the lift term and multiplied by the distance (along the body centerline) from the shock-wave intersection to the body nose to give the additional moment term. This is in essence an application of local field conditions to distinct sections or strips of the immersed body. This sectional or "strip theory" may also be applied instead of the perturbation potential analysis in other areas of the field.

The additional force due to the upwash distribution was shown by Moskowitz (Reference 53) to vanish for cases where the shock wave is weak and intersects the separating body at an angle approximately equal to the flow Mach angle. These conditions are closely fulfilled if the separating body is reasonably far from and nearly parallel to the parent body at shock-wave interception. For this reason and because of the difficulty involved in calculating these effects, the forces and moments due to the upwash discontinuity are not included in the present calculations.

In the digital computing scheme, the spatial disbribution of the interference field (and shock-wave locations, if present) is calculated and stored. The coordinates of the nose and tail of the separating body are computed and tested to see if they lie within the interference flow field. If the shock wave intersects the separating body, the coordinates of the intersection point are also computed. The downwash velocities at these locations are then computed from the stored spatial downwash field. These velocities are then inserted in the expressions for interference lift and moment.

3. Base Separation Interference Effects

The discussion in section IV. A. 2 has considered the wake behind a body with no other body influencing the flow field. In the case of separating bodies, however, the very presence of the separating body may alter the structure of the wake. It is of interest, first, to delineate those instances in which the presence of the body will not totally alter the basic wake structure.

Chapman's data (Reference 12) at Mach 2.0 and 2.9 for the effects of a support sting on wind tunnel models indicate little effect on the base pressure for sting diameters less than about 0.3 of the body diameter for both laminar and turbulent flow with larger sting diameters permissible at higher Mach numbers. For very low Reynolds numbers ($M = 3.9$, $R_{e_1} = 2960$), Kavanau (Reference 29) observes sting effects for all sting sizes;

however, for higher Reynolds numbers in the fully laminar regime (see Reference 30). little effect is noted for sting diameters about 0.2 of the body diameter. Crocco and Lees (Reference 14) have further demonstrated that, for the supersonic wake, small disturbances introduced aft of the wake throat have no effect on the region ahead of the throat. Thus, from these references it appears that disturbances produced by objects which lie within the viscous wake will not alter the basic object-free wake structure, although the pattern of velocities which exist in the recirculation zone ahead of the throat may be locally altered by objects located there.

Large alteration of the wake structure must be anticipated for those cases where the disturbance-producing body is large compared to the viscous wake diameter or where the body is ejected so as to penetrate the wake boundary – especially when the penetration occurs forward of the wake throat. Such changes in the body-free wake structure are even more involved than the interacting field difficulties encountered in side separation (as discussed in section IV. C. 2) and must be investigated experimentally.

In this study the investigation of base separation requirements is therefore based on the assumption that the basic wake structure of the carrier is unaltered by the presence of the separating body.

With this assumption the aerodynamic forces and moments induced on the separated capsule aft of the wake throat are calculated using the capsule-free axial wake flow parameters and weighted averages of the radial variations. The loads which may exist in the recirculation zone ahead of the wake throat due to static pressure gradients and reverse flow were considered sufficiently small to be neglected. Wake penetration is similarly treated; that is, the loads on the capsule were computed using capsule-free wake boundary characteristics. The characteristics of the capsule-free wake structure used for the present program are discussed in section IV. A. 2. c.

The extent to which these simplifications are admissible must await the performance of suitable experiments. Of particular importance to such experimentation is the determination of the role of relative velocity when altered carrier wake structures are induced due to the presence of the separating body. In other words, the fact that the separating capsule is moving at a relative velocity to the carrier vehicle may have an additional effect on the altered wake structure of the carrier.

D. Summary of Accepted Aerodynamic Characteristics

This section summarizes, for quick reference, the aerodynamic description of the capsules and the pertinent carrier flow fields for which separation trajectory computations are made. When a convenient summarization is not feasible, the sections wherein specific information is contained are referenced.

With respect to basic carrier-side flow fields, representative conditions are calculated by means of the characteristic theory (as applicable), and are documented - for typical pointed bodies - in Figures 4 through 6 and discussed in section IV.A.1. For the side separation trajectory cases calculated at Mach 5.0, uniform free-stream characteristics were assumed for the carrier side flow field. Conditions resulting from the method of characteristic analysis were employed for the side flow field in the Mach 15.0 case, with the effects of flow nonuniformities over the length of the capsule accounted for by the method of Monkewitz as discussed in section IV.C.2.b.

Basic wake properties and the pertinent assumptions are listed as follows and as discussed in section IV.A.2.c:

(1) Region ahead of throat is assumed conical with angle of convergence given by Figure 10.

(2) External flow properties along conical boundary given by Prandtl-Meyer expansion to base pressure, assumed constant within convergent region.

(3) Flow conditions vary linearly from conical boundary to streamwise direction, latter conditions associated with body just ahead of base.

(4) Throat thickness given by Figure 15; downstream wake thickness and velocity distribution given by Prandtl's mixing length theory; constants from Howarth as per data of Figure 16. Static temperature and pressure in downstream wake assumed equal to free-stream values.

Free-flight capsule characteristics for a cylinder, flared body, and blunted cone shape are given or referenced in Table VI. Also summarized in Table VI are the interference effects of an ejected nose cone on the carrier vehicle. Partial exposure loading in side ejection is summarized in Table VII Base ejection is assumed to be free of capsule-carrier interference effects, and side ejection is assumed free of capsule-flow field interactions with the carrier flow field.

TABLE V

CAPSULES' TYPICAL HIGH MACH NUMBER AERODYNAMIC CHARACTERISTICS

	Length-to Diameter Ratio	Axial Force Coefficient, C_A		*Normal Force Coefficient Slope $(C_{N_\alpha})_{\alpha=0}$, per degree	Location Center of Pressure, Percent Body Length from Nose	Dynamic Stability Derivatives, $C_{M_q} + C_{M_{\dot{\alpha}}}$	
		$\alpha = 0$	$\alpha = 90^\circ$				
Cylinder	2.0	1.68	0	0.020	50	-0.2	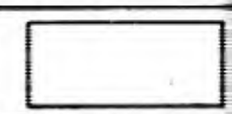
Cone	1.5	0.24	+0.34	0.025	65	-1.0	
Spool	2.5	1.70	0	0.020	45	-0.2	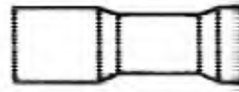
Flared Body	2.5	0.40	+0.35	0.027	60 to 70	-2.5	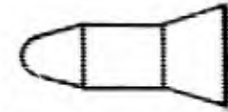
Sphere	1.0	0.92	0	0	-	0	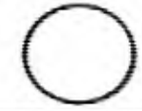
Disk	0.4	1.04	+0.24	0.023	70	-0.1	

TABLE VI

SUMMARY-CAPSULE AERODYNAMIC CHARACTERISTICS
AND NOSE CONE INTERFERENCE EFFECTS

	Cylinder	Flared Body	Blunted Cone	
	Free Flight	Free Flight	Free Flight	Interference-Nose Separation
C_{N_α}	Fig. 19, small α; Newtonian theory, large α.	Fig. 22, small α; Newtonian theory, large α.	Fig. 24, small α; Newtonian theory large α.	On carrier loading: Given by base pressure of nose cone uniformly distributed over "triangular" area of wake-body intersection.
Location Center of Pressure	Fig. 18, small α; Newtonian theory, large α.		Fig. 24, small α; Newtonian theory, large α.	On carrier loading: Normal force - centroid of triangular area; Axial force-centroid of exposed face.
C_{M_α}		Fig. 22, small α; Newtonian theory, large α.		
C_A	Fig. 20, small α; Newtonian theory, large α.	Fig. 22, small α; Newtonian theory, large α - Fig. 23.	Fig. 24, zero α; Newtonian theory, large α.	On carrier loading: Given by pressure coefficient on flat face in normal orientation.
$C_{M_q} + C_{M_{\dot{\alpha}}}$	Unstable sub-sonically and stable sonically with exponential decay to zero at hypersonic speeds.	-2.5	Fig. 24	

TABLE VII

PARTIAL EXPOSURE LOADING SUMMARY
(Uniform Pressure Distributions)

Forces, Moments Due to:	Normal Orientation		Parallel Orientation	
	Flared	Cylindrical	Flared	Cylindrical
Local Dynamic Pressure	C_N: Cylindrical Portion, Ref. 51 Inclined Surfaces, Newtonian Theory	C_N: Ref. 51	C_A: Fig. 22	C_A: Fig. 20
Ejection Velocity	C_A = 1.17 (Disk)	C_A = 0.8	C_D(Crossflow) = 1.2	C_D(Crossflow) = 1.2
Buoyancy	External Surface, Capsule Base (flat plate) Pressure Coefficient, Fig. 25 Internal Pressure, Static Ambient Affected Area, see Section IV. C. 2. a. (1)		Inclined External Surfaces, Conical Flow, Ref. 52; Cylindrical External Surfaces, Ambient Static Pressure Internal Pressure, Static Ambient Affected Area, see Section IV. C. 2. a. (2)	

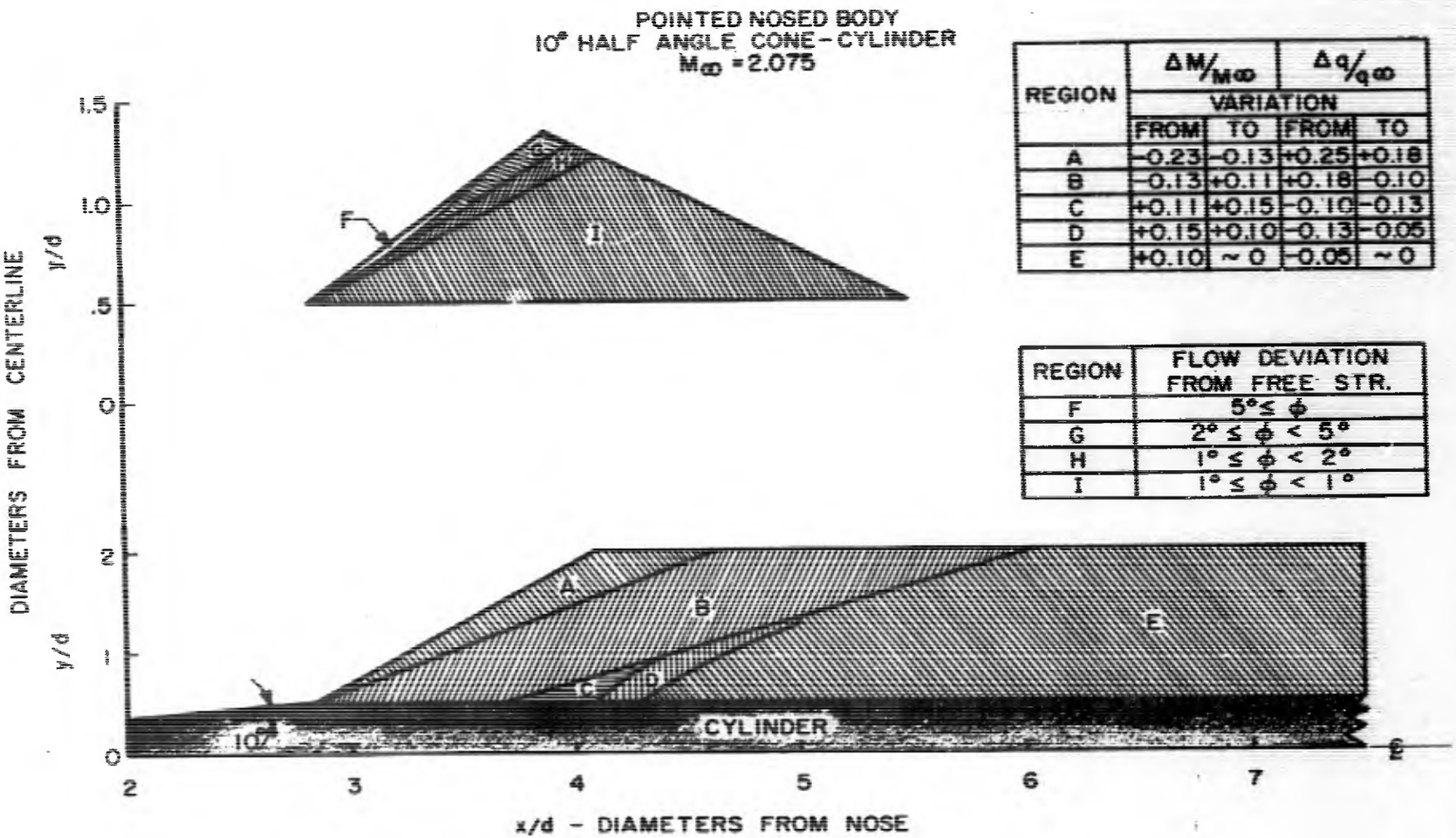

REGION	ΔM/M∞ VARIATION		Δq/q∞ VARIATION	
	FROM	TO	FROM	TO
A	-0.23	-0.13	+0.25	+0.18
B	-0.13	+0.11	+0.18	-0.10
C	+0.11	+0.15	-0.10	-0.13
D	+0.15	+0.10	-0.13	-0.05
E	+0.10	~ 0	-0.05	~ 0

REGION	FLOW DEVIATION FROM FREE STR.
F	$5° \leq \phi$
G	$2° \leq \phi < 5°$
H	$1° \leq \phi < 2°$
I	$1° \leq \phi < 1°$

Figure 4. Flow Deviation Angle, Mach Number, and Dynamic Pressure for Body Side Flow Field

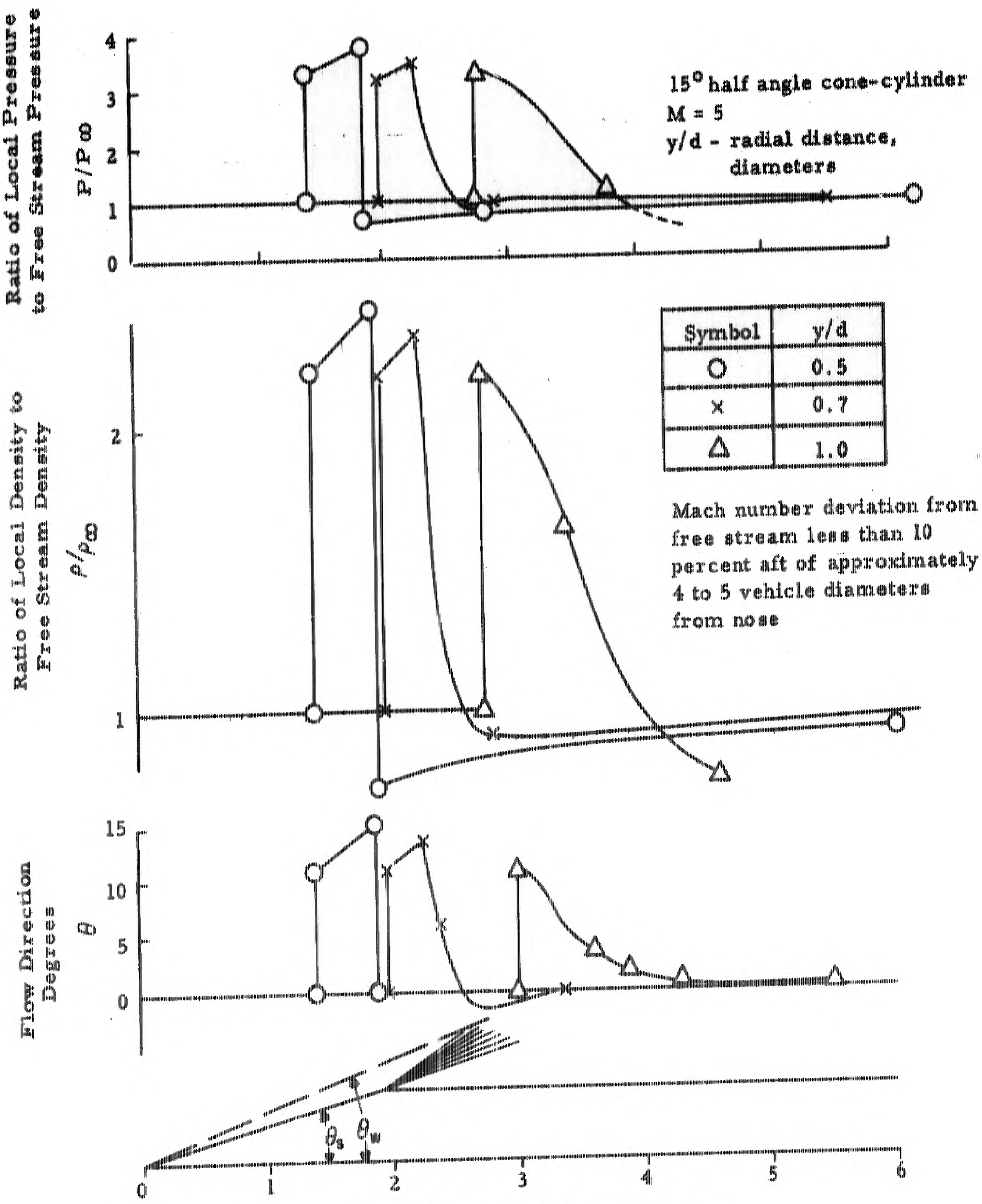

Figure 5. Flow Density, Pressure, and Direction, Body Side Flow Field, Pointed Nosed Body

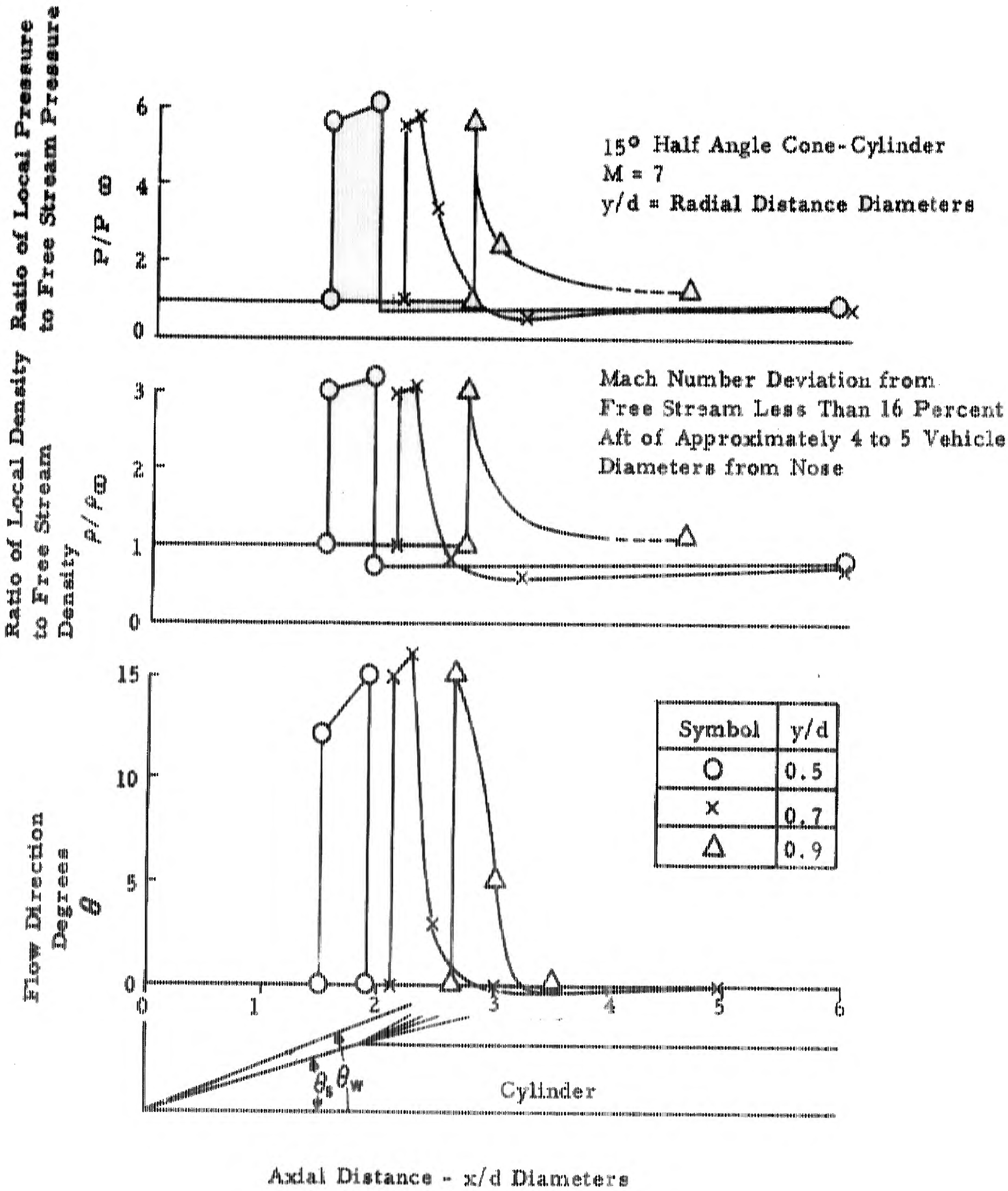

Figure 6. Flow Density, Pressure, and Direction, Body Side Flow Field, Pointed Nosed Body

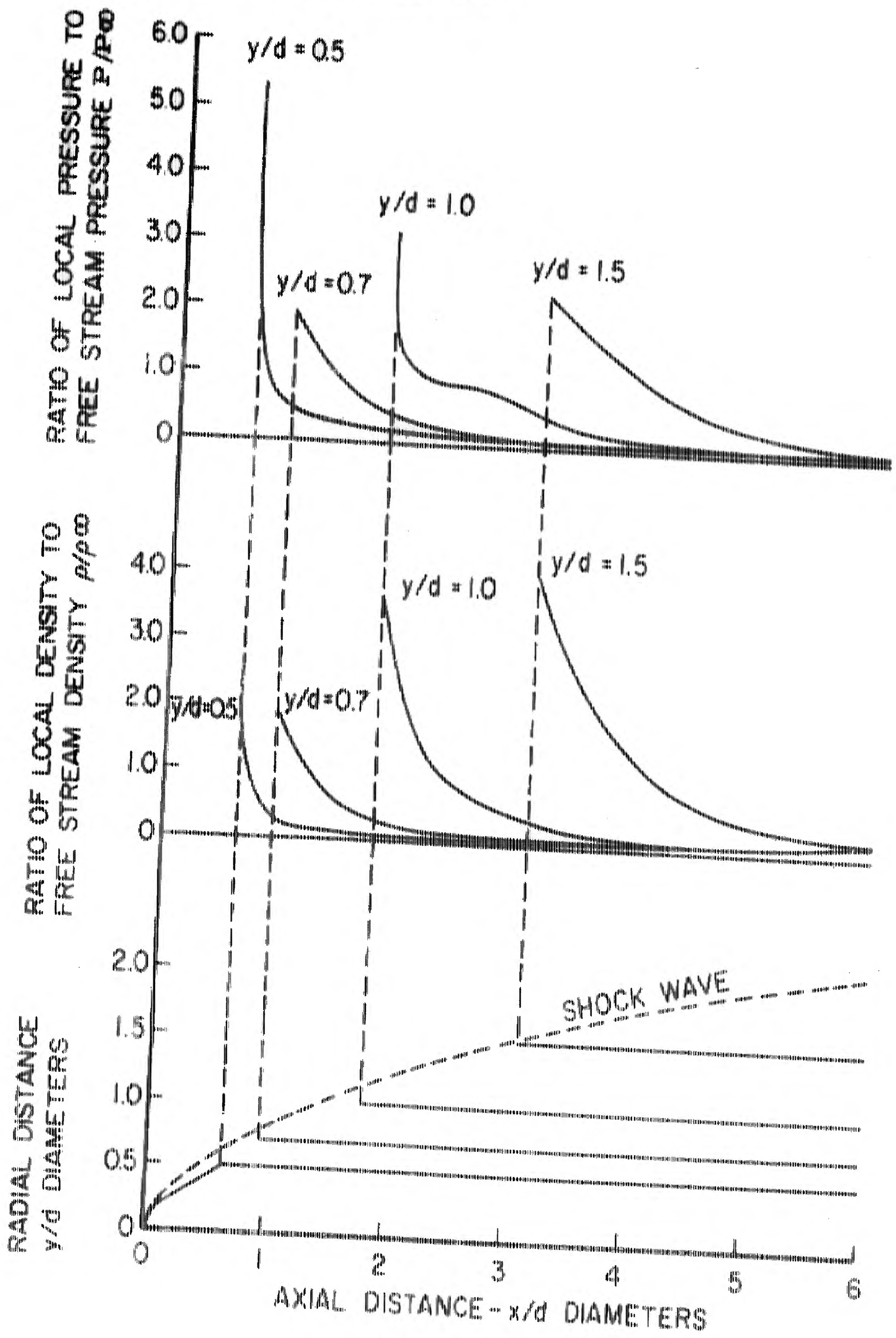

Figure 7a Density and Pressure Ratios-Body Side Flow Field for Real Gas

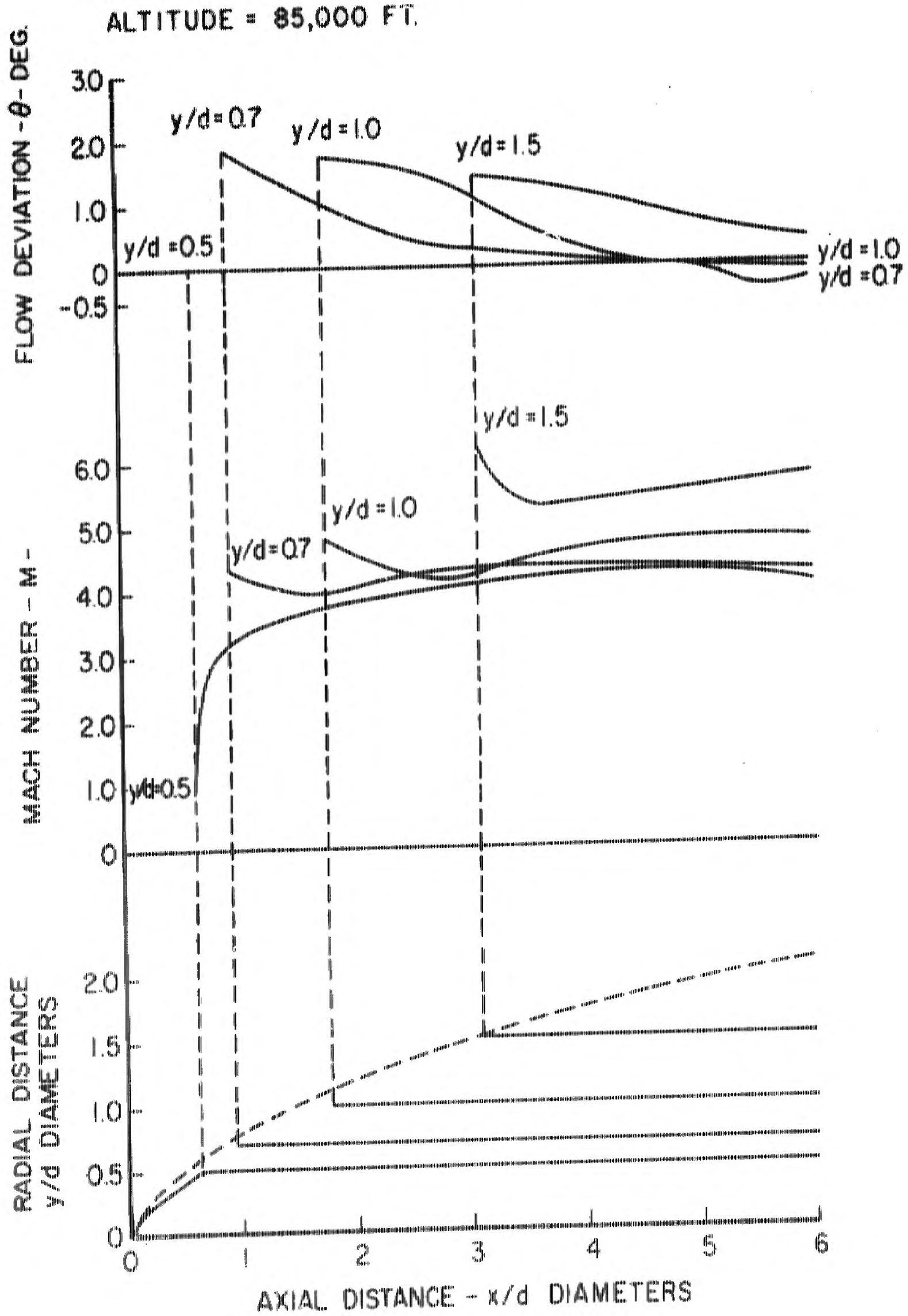

Figure 7b Local Flow Deviation and Mach Number-Body Side Flow Field for Real Gas

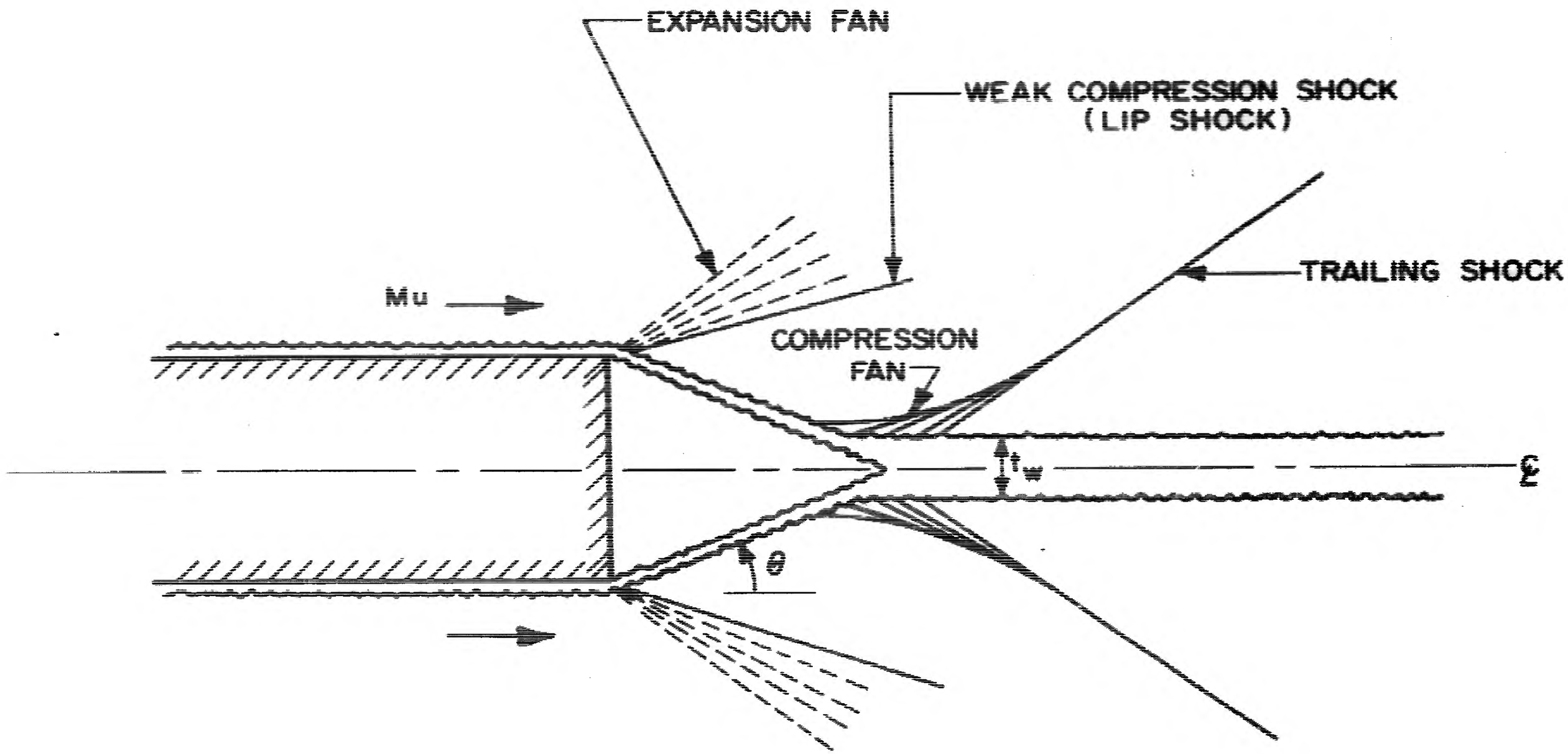

Figure 8. Schematic Diagram of the Flow Past a Blunt Base

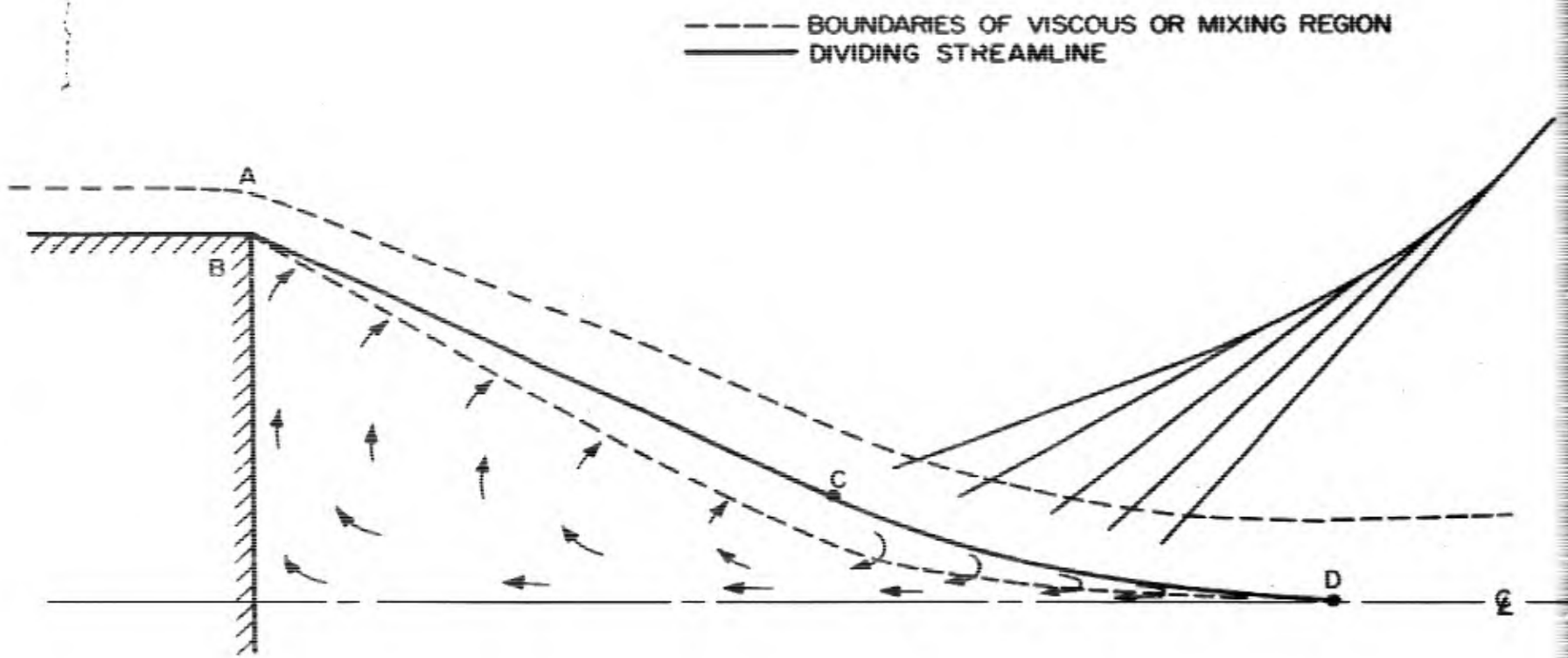

Figure 9. The Region Behind a Blunt Base

Figure 10. Axisymmetric Wake Convergence Angle, Turbulent Boundary Layer, After Love, Reference 16

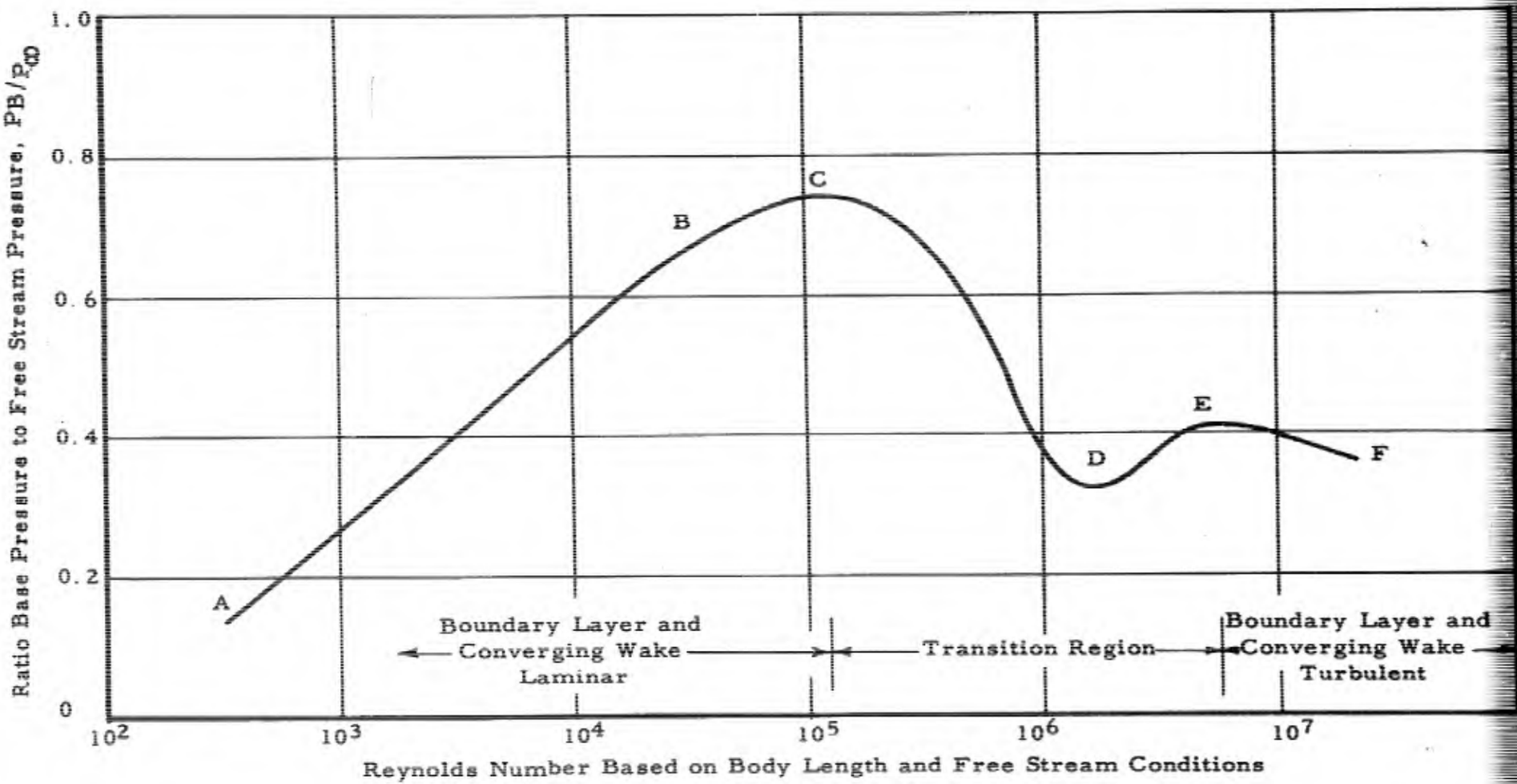

Figure 11. The Effect of Reynolds Number on the Base Pressure of a 30° Cone-Cylinder Body, Fineness Ratio, 3.5, for Mach Numbers Near 2.9

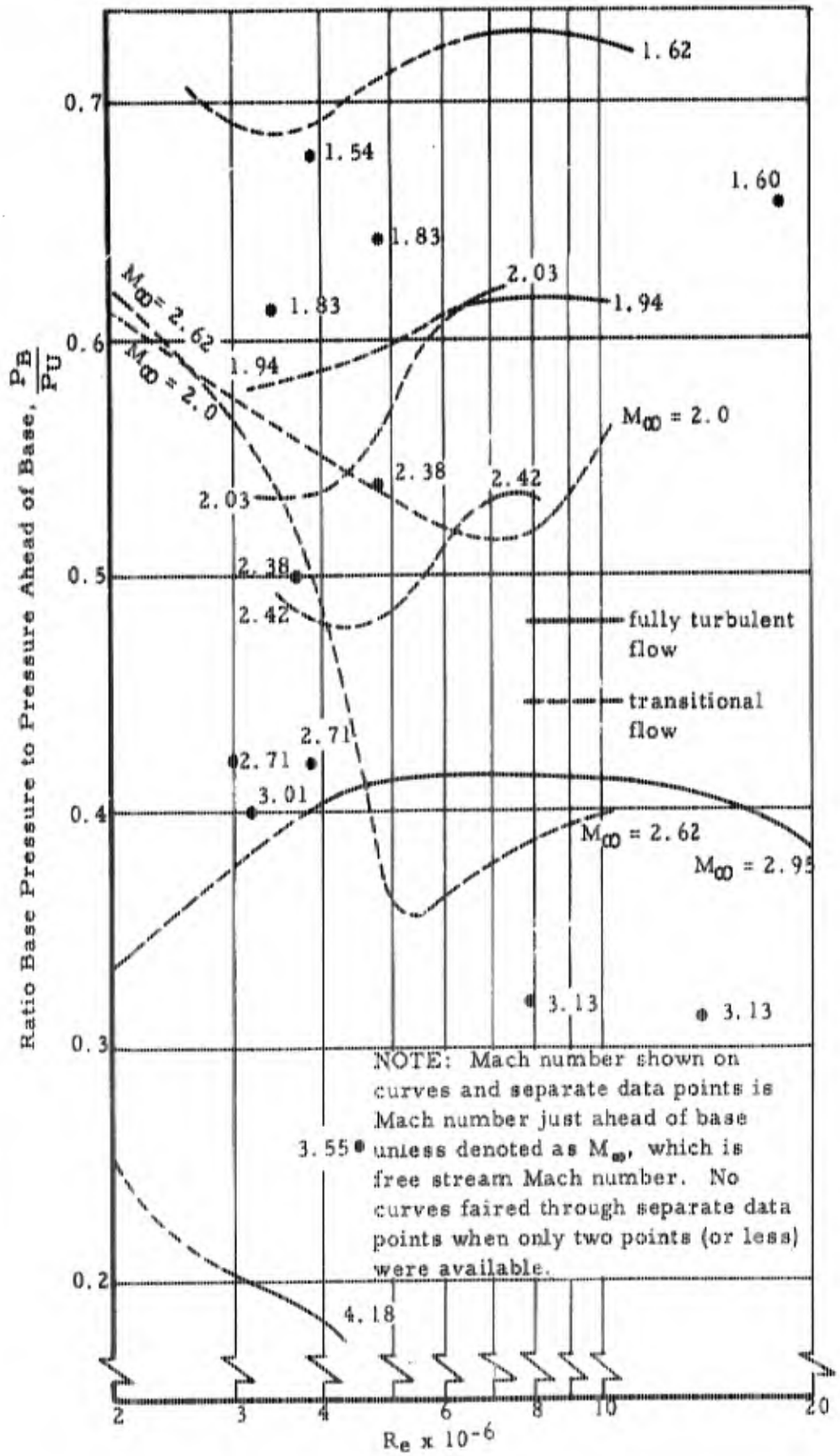

Figure 12. Cone-Cylinder Body Base Pressure Ratio as a Function of Reynolds Number for Various Mach Numbers

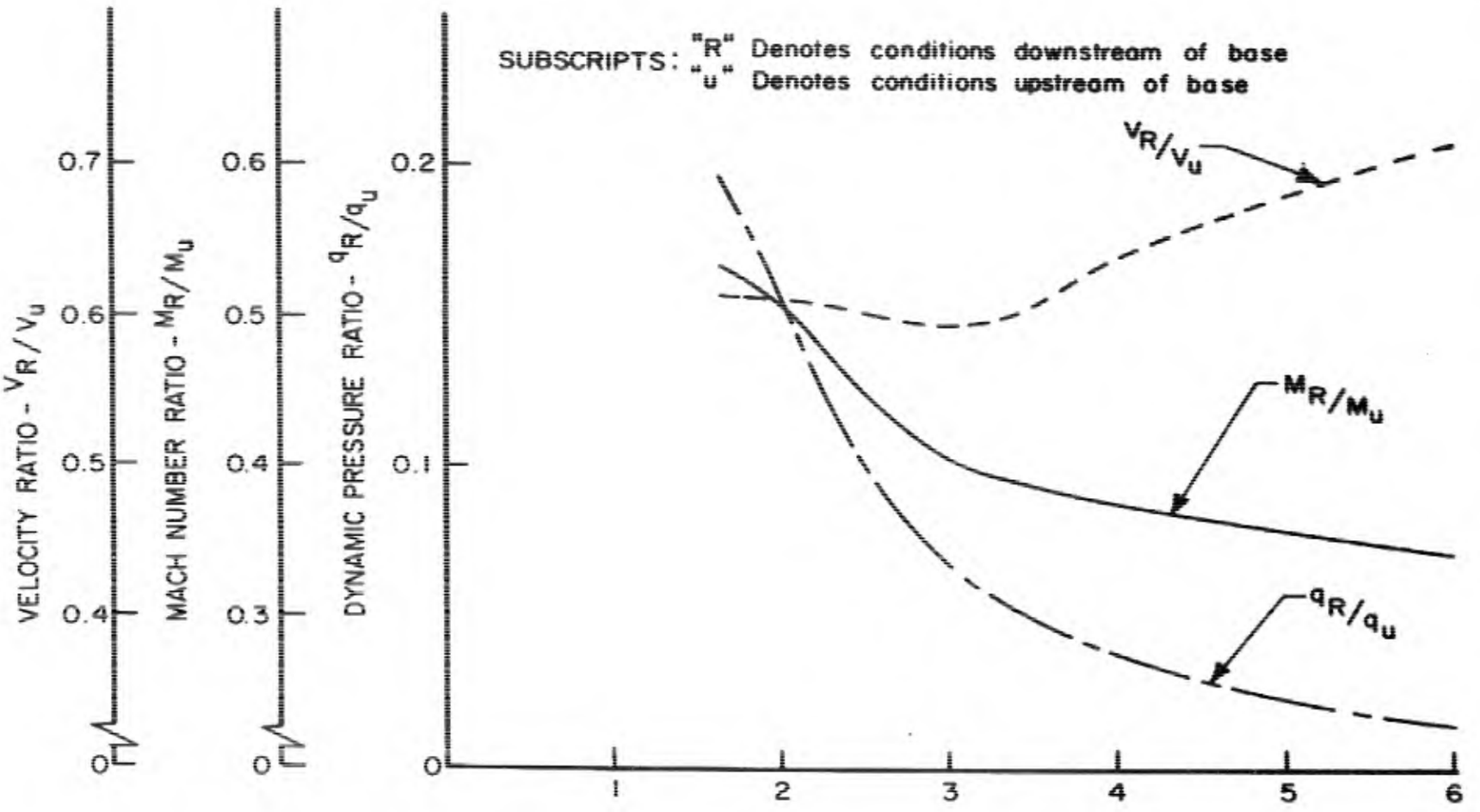

Figure 13. Maximum Reverse Flow Conditions (Highest Energy Reverse Flow Stream Tube Near the Wake Centerline)

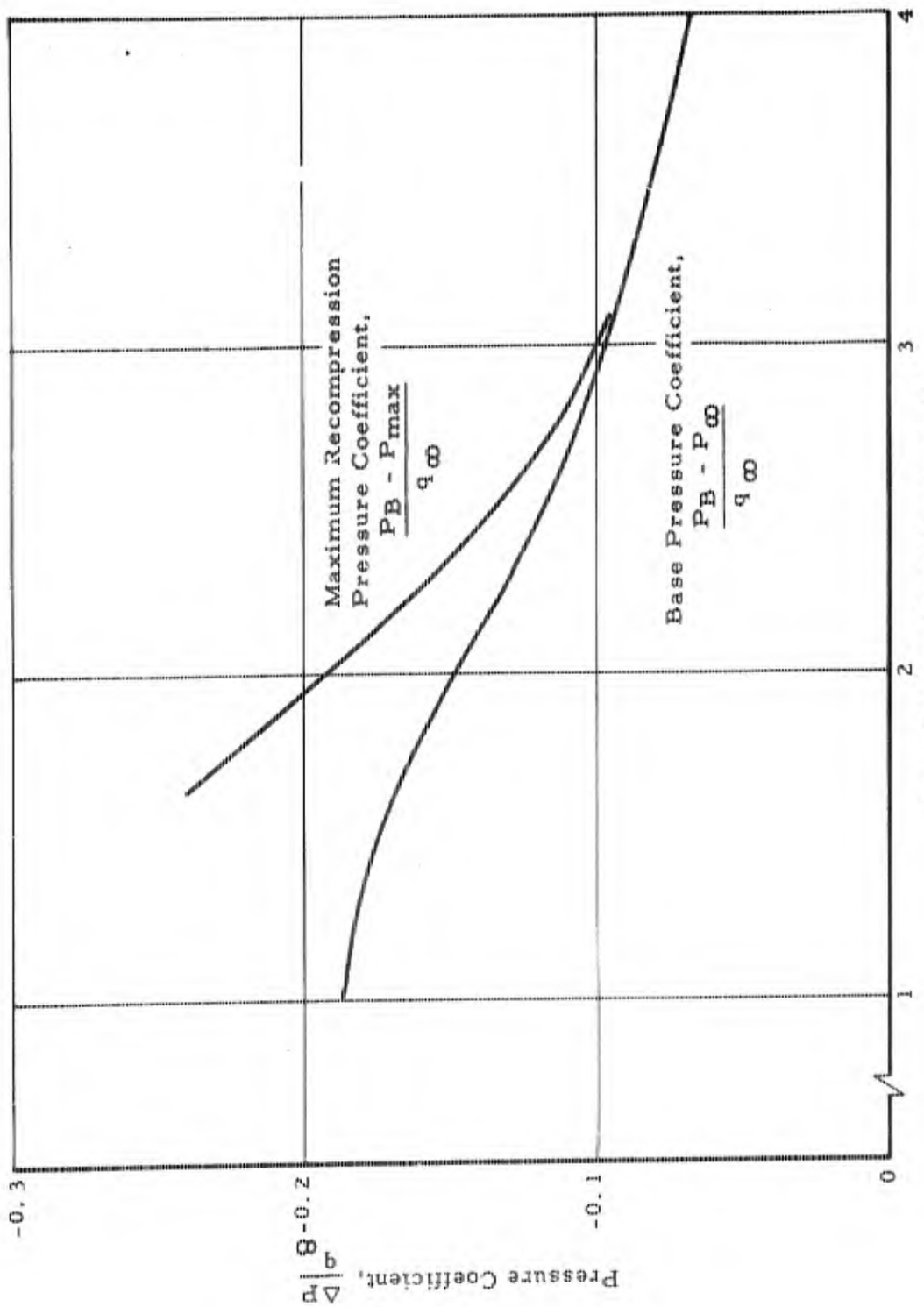

Figure 14. Base and Recompression Pressure as Functions of Mach Number, Axisymmetric Bodies, After Reference 16

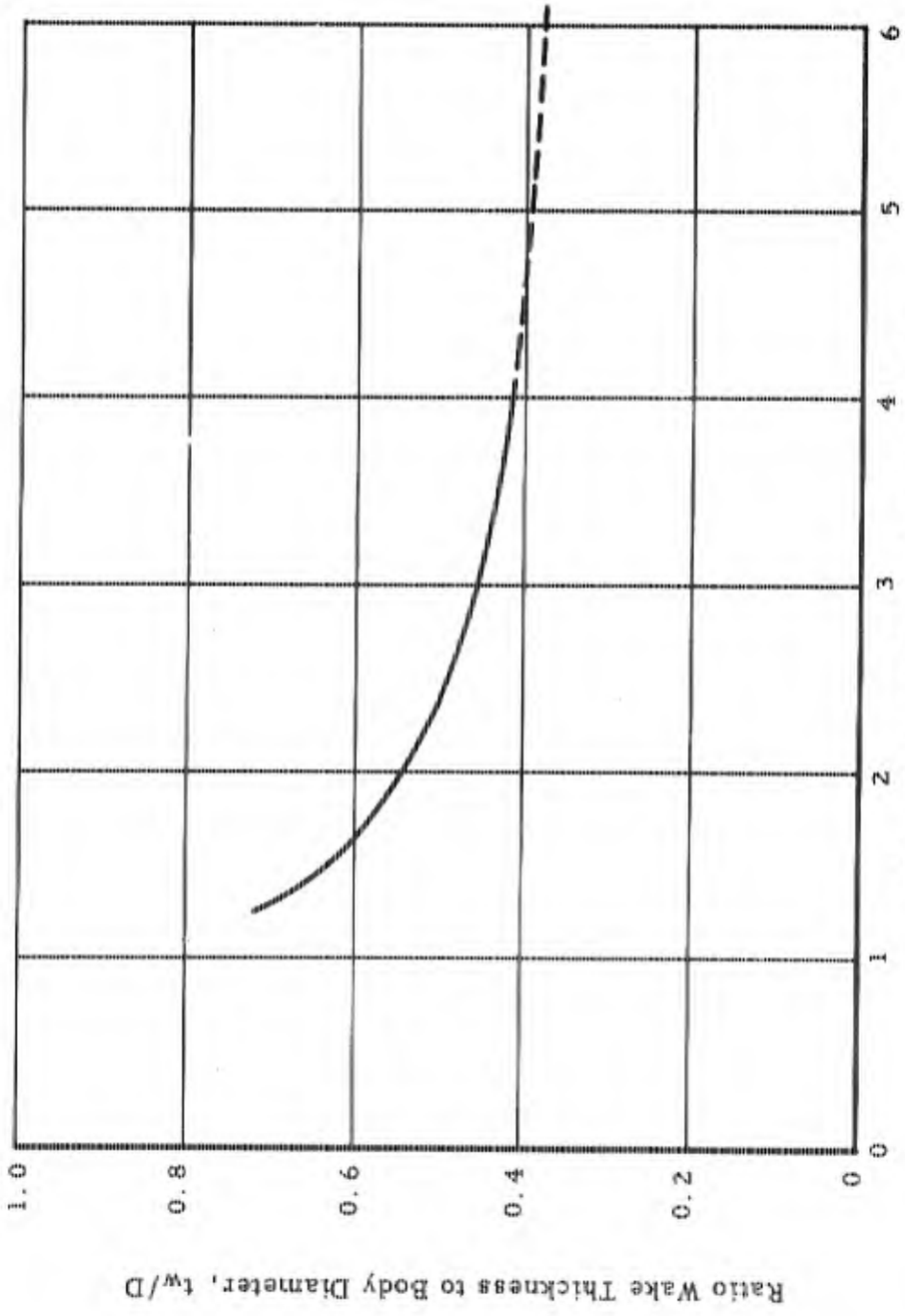

Figure 15. Wake Thickness at the Throat as a Function of Mach Number, Turbulent Boundary Layers. Bodies of Revolution; After Chapman, Reference 12

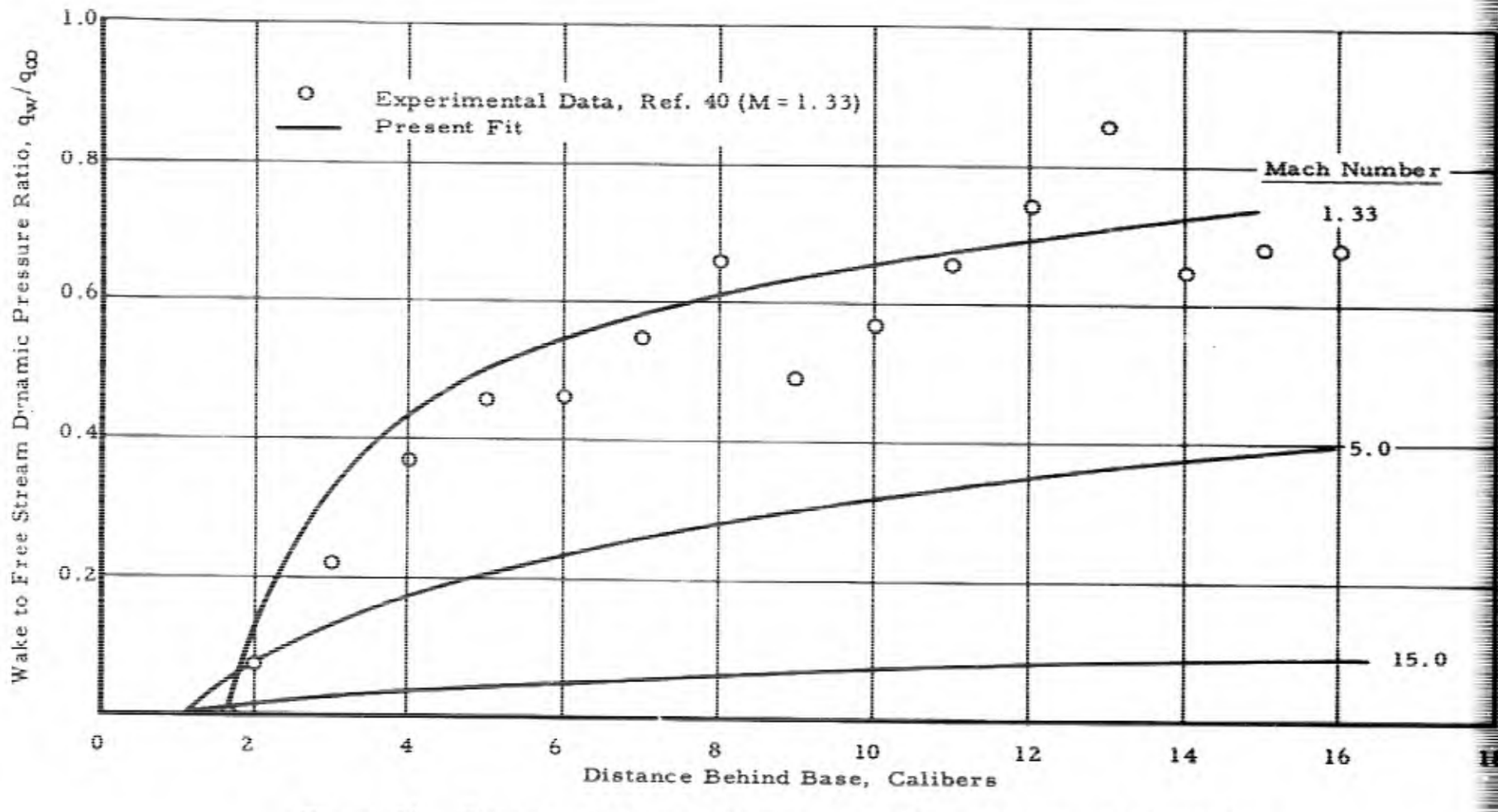

Figure 16. Dynamic Pressure Variation on Wake Axis Body of Revolution

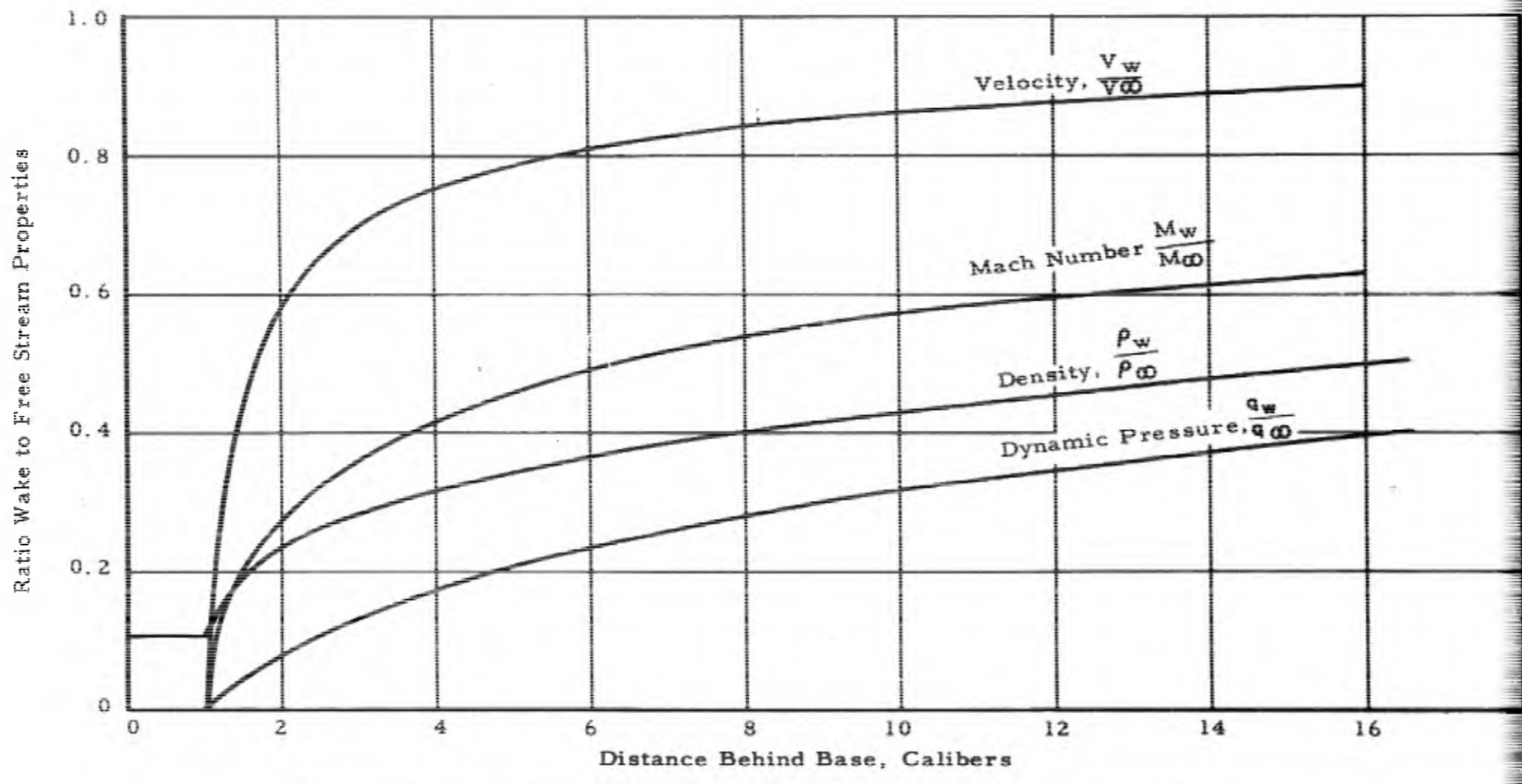

Figure 17. Properties Along the Wake Axis; Mach Number Ahead of the Base, 5.0

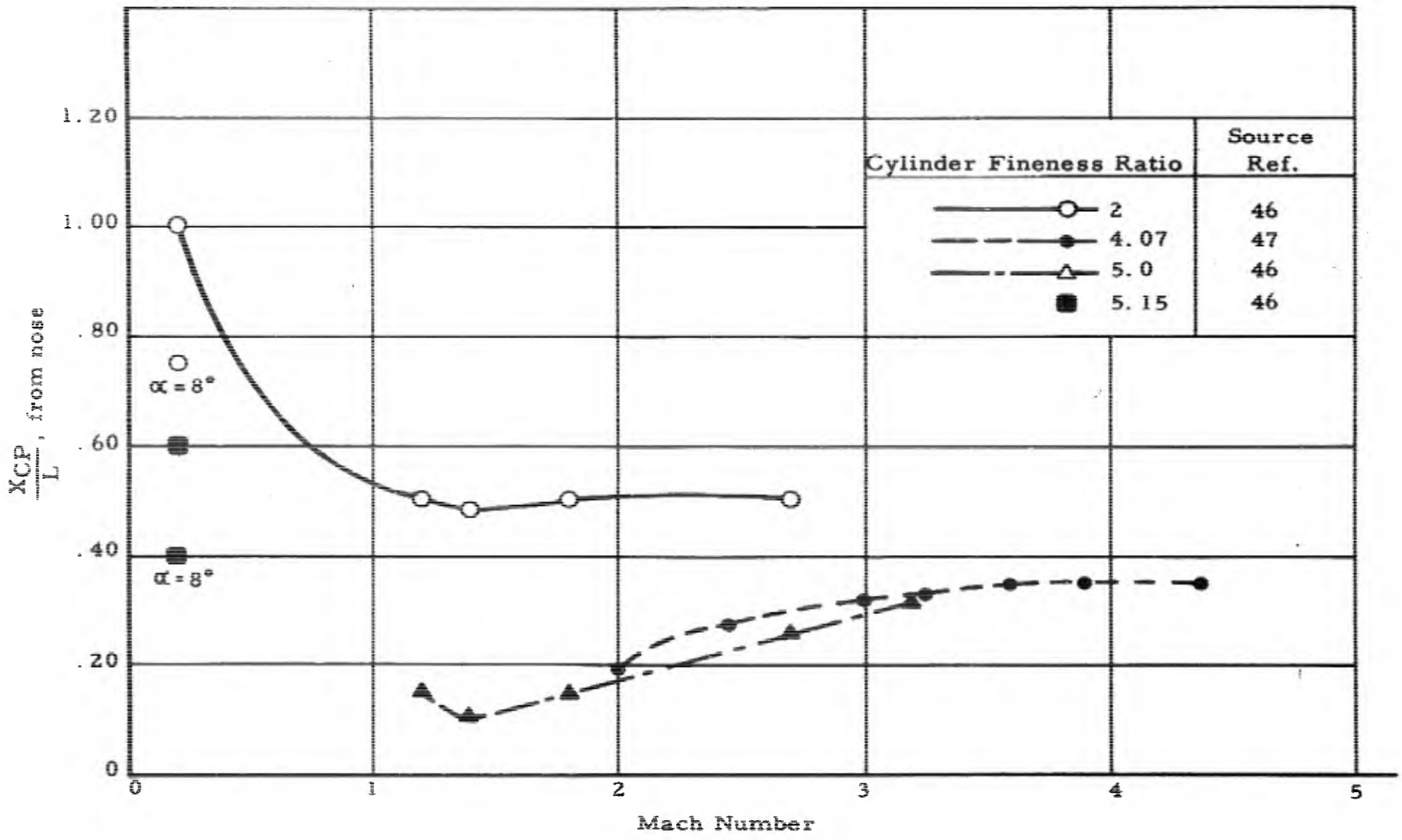

Figure 18. Location of Center of Pressure on Blunt Cylinder in Approximately Axial (Except as Noted) Flow as Function of Mach Number and Fineness Ratio

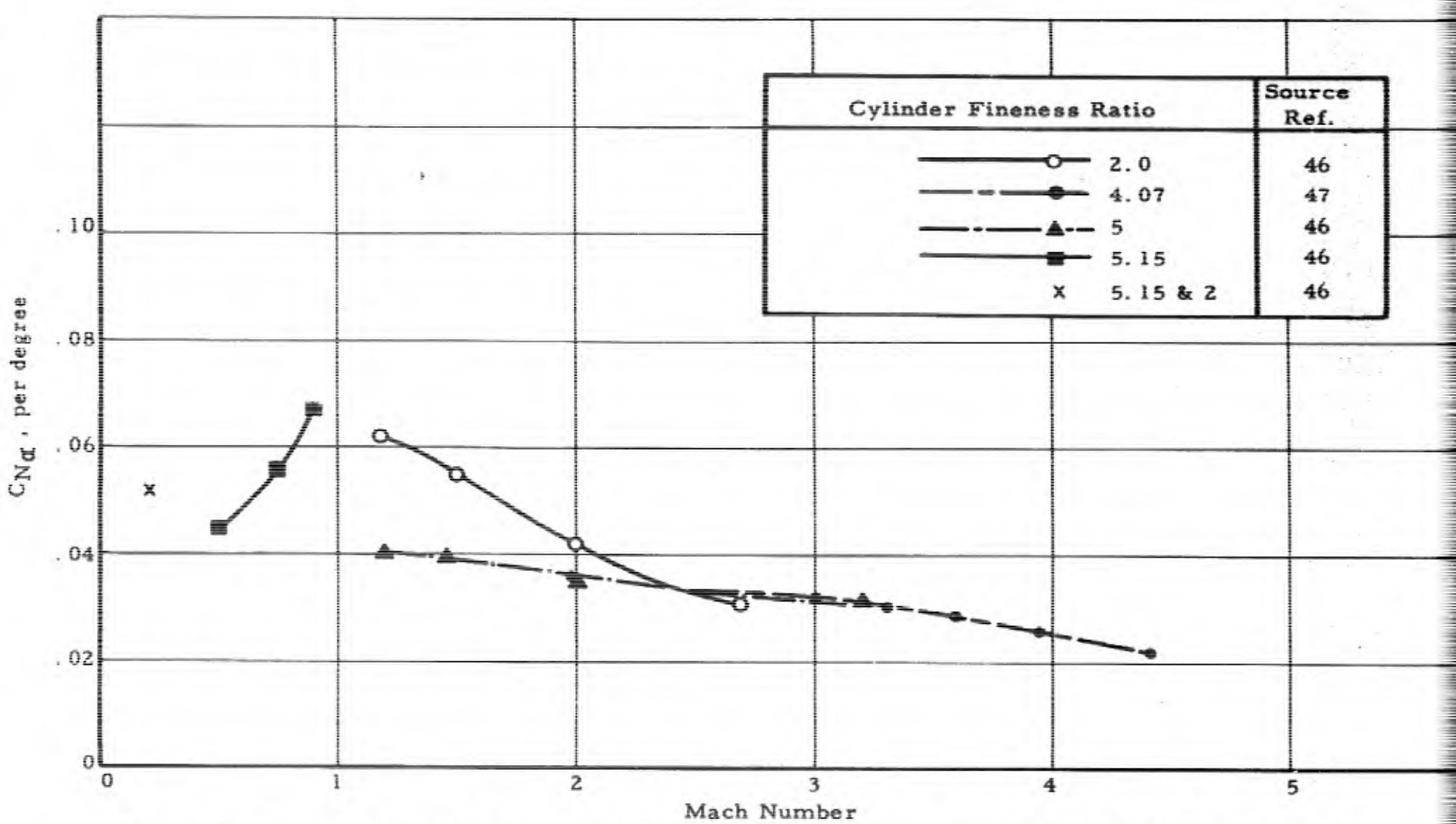

Figure 19. Slope of Normal Force Coefficient Curve, C_{N_α}, for Blunt Cylinder at Zero Angle of Attack as Function Mach Number and Fineness Ratio

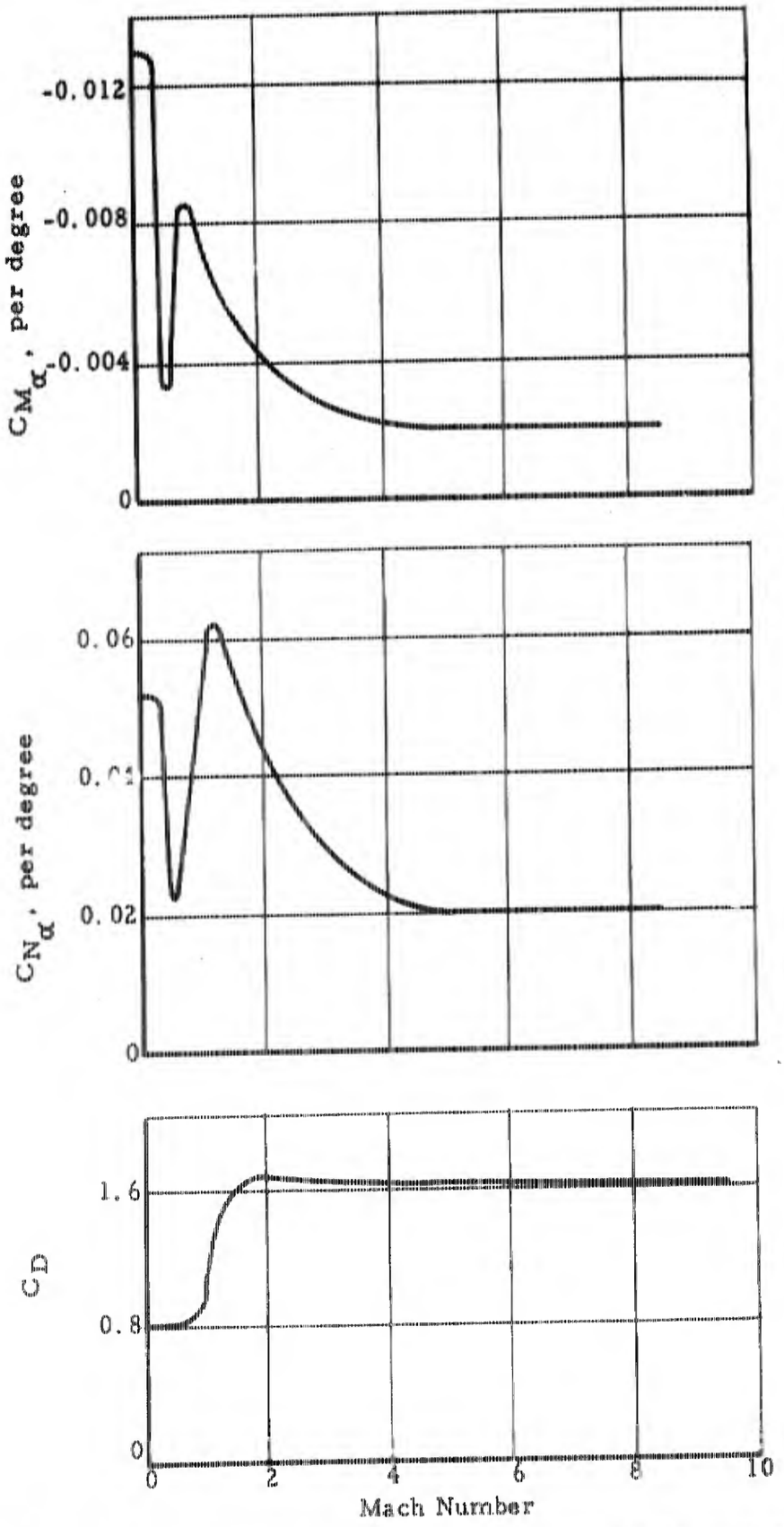

Figure 20. Variation of Pitching Moment Curve Slope, $(C_{M_\alpha})_{0.4L}$, Normal Force Curve Slope, C_{N_α}, and Drag Coefficient, C_D, with Mach Number for a Cylinder of Fineness Ratio 2 at Zero Angle of Attack

NOTE: Coefficients based on base area and capsule length (where applicable)

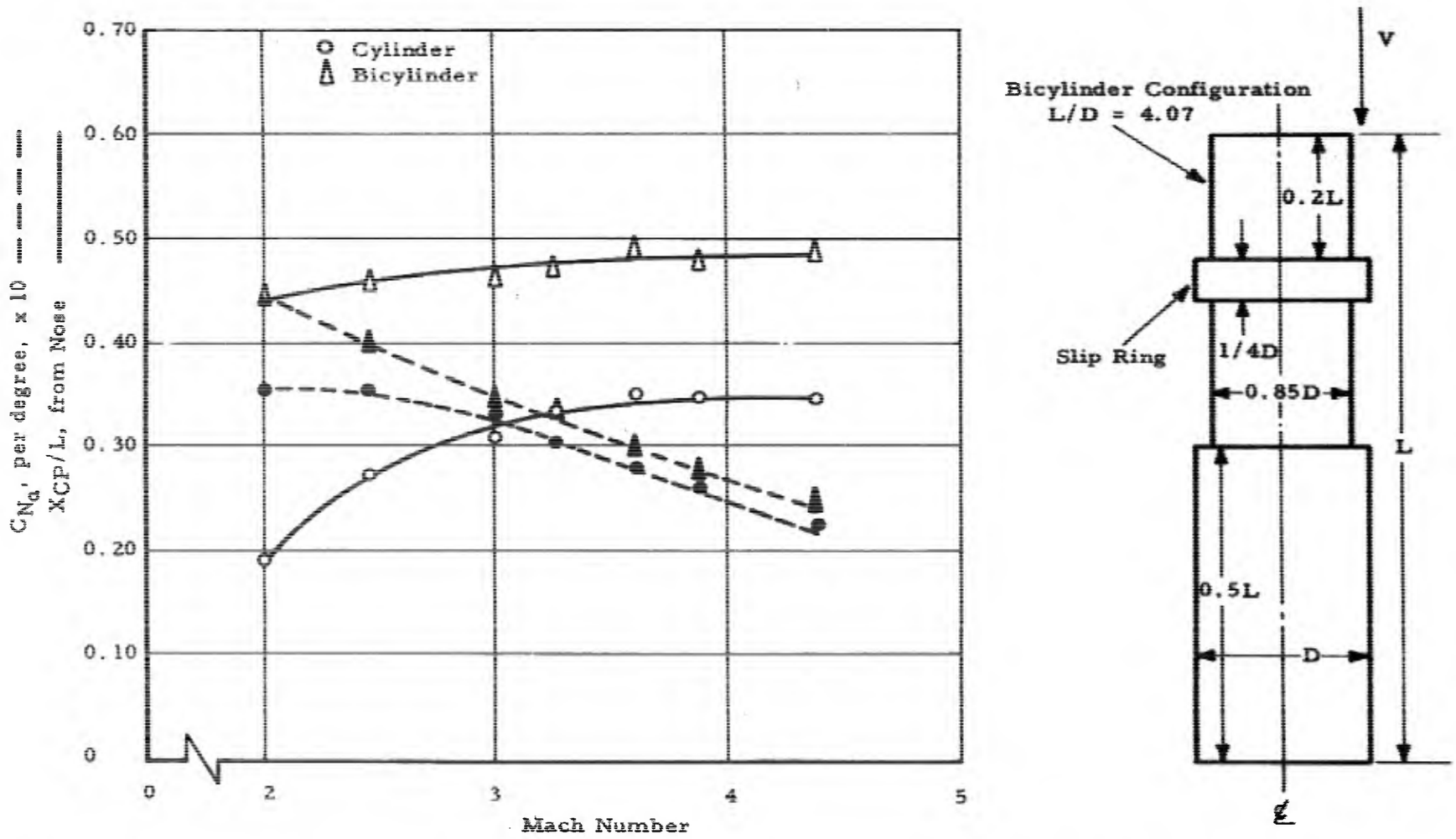

Figure 21. Variations of Center of Pressure Location, X_{CP}/L, and Slope of Normal Force Coefficient Curve, C_{N_α}, with Mach Number for Cylindrical and Bicylindrical Bodies, Zero Angle of Attack; Bodies of Equivalent Fineness Ratio

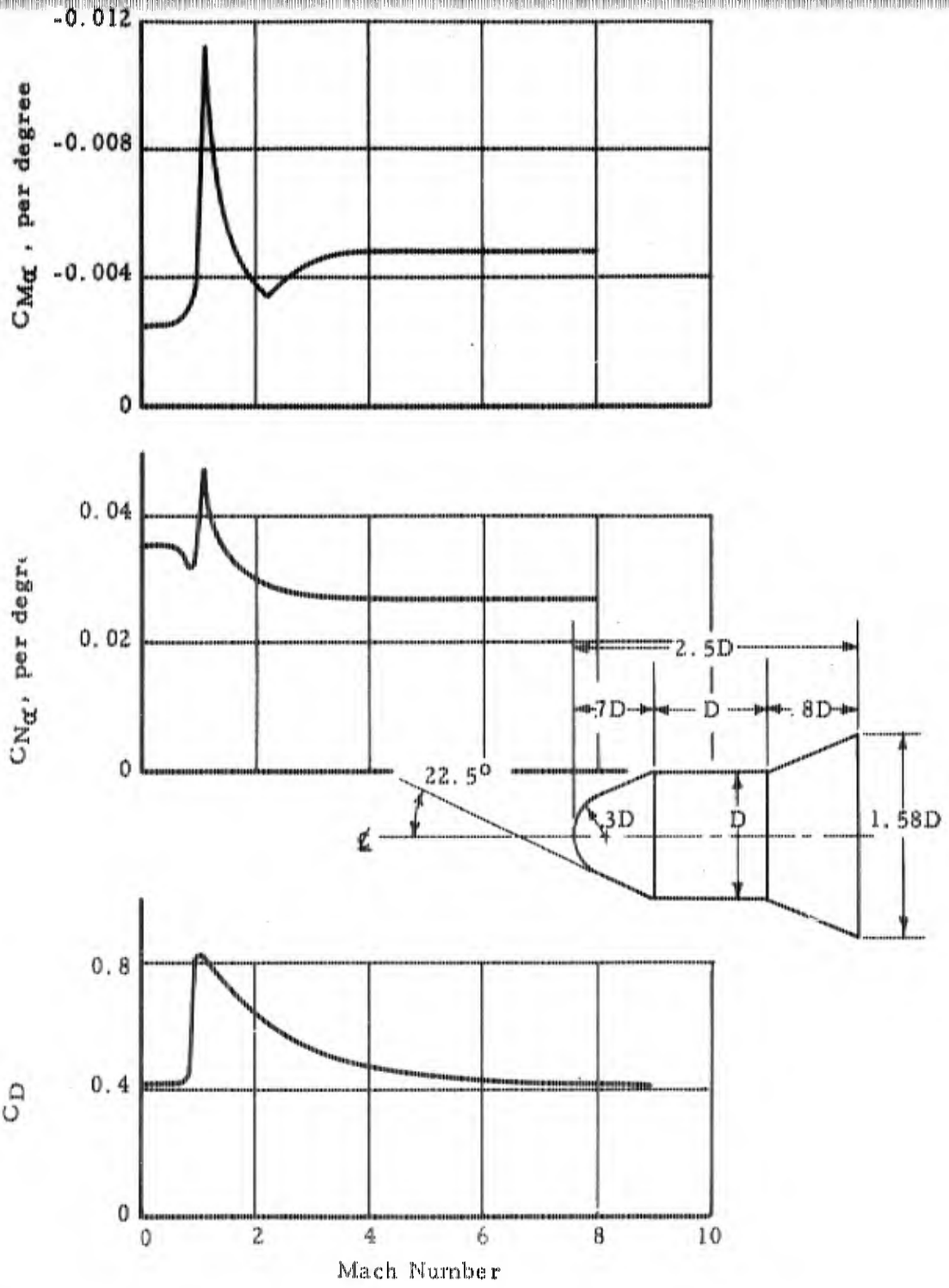

NOTE: Coefficients based on base area and capsule length (where applicable)

Figure 22. Variation of Pitching Moment Curve Slope $(C_{M_\alpha})_{0.5L}$, Normal Force Curve Slope, C_{N_α}, and Estimated Drag Coefficient, C_D, with Mach Number for a Flared Body of Fineness Ratio 2.5 at Zero Angle of Attack

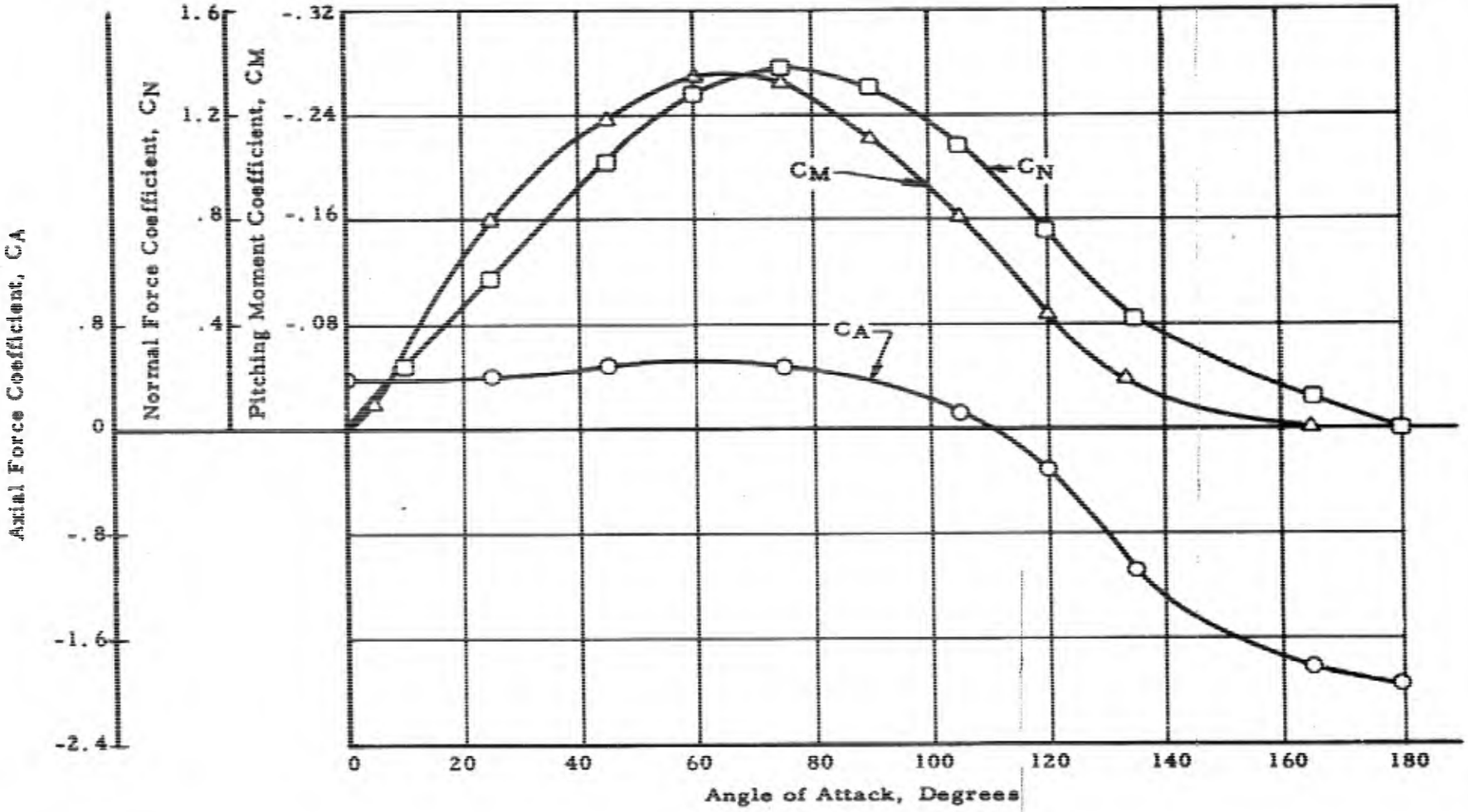

Figure 23. Variation of Pitching Moment Coefficient, C_M; Normal Force Coefficient, C_N; and Axial Force Coefficient, C_A, as Functions of Angle of Attack, for Flared Body Predicted by Newtonian Flow Theory

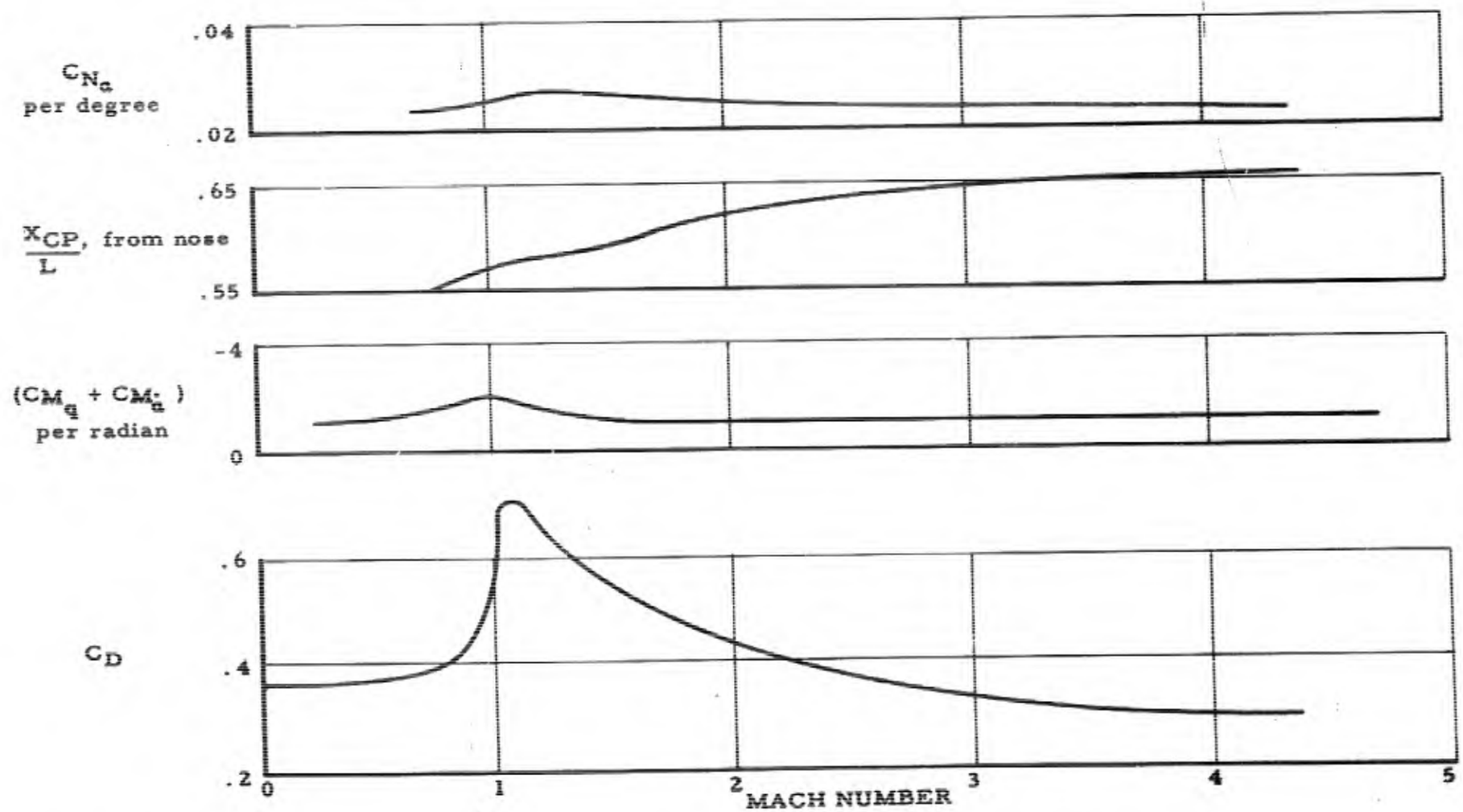

Figure 24. Variation of Normal Force Curve Slope, C_{N_α}, Center of Pressure Location $\frac{XCP}{L}$, Dynamic Stability Derivatives, $(C_{M_q} + C_{M_{\dot{\alpha}}})$, and Drag Coefficient vs Mach Number for a Representative Blunted Cone at Zero Angle of Attack

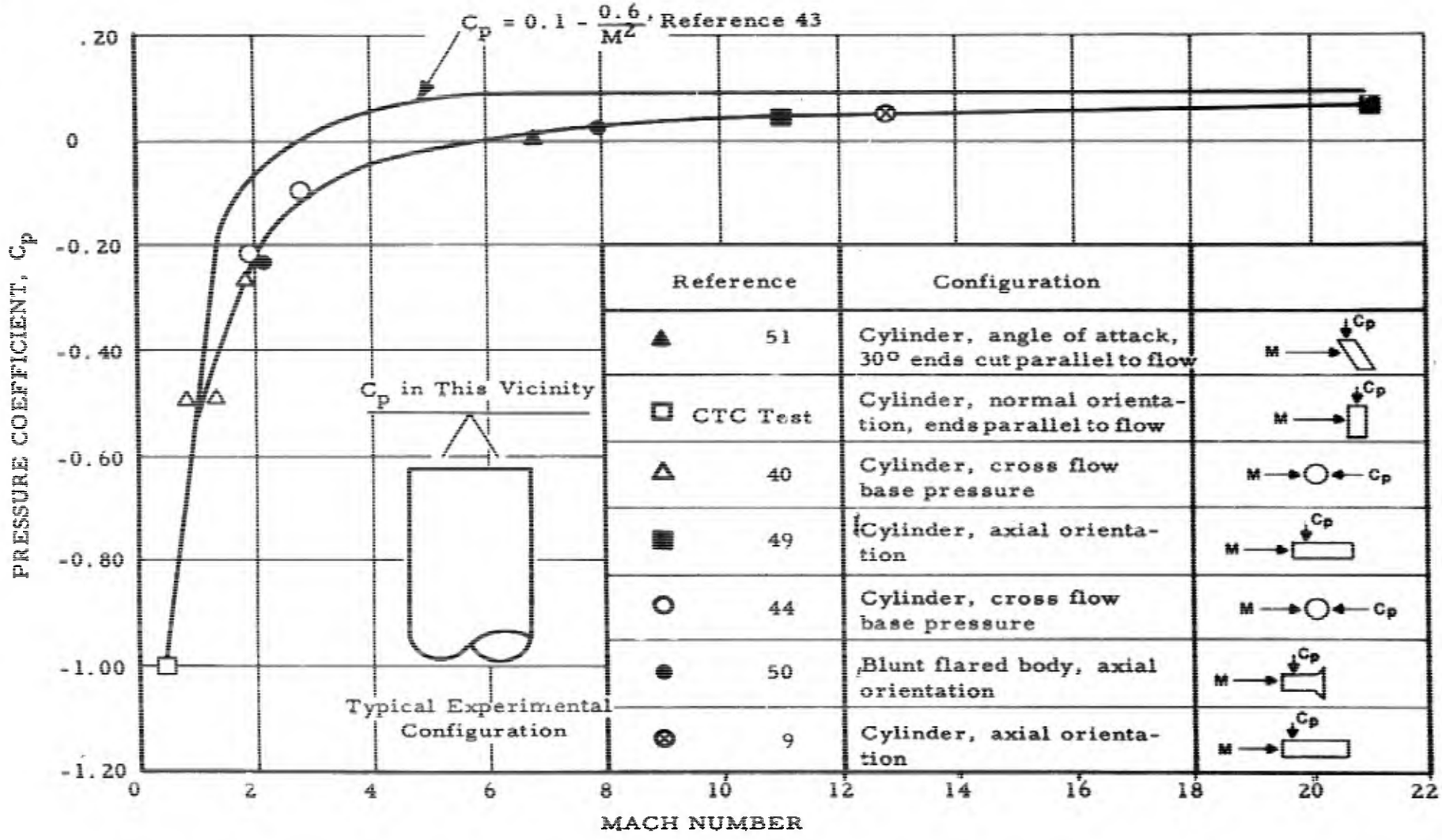

Figure 25. Pressure Coefficient Immediately Behind Shoulder of Blunt Body in Supersonic Flow

SECTION V

SEPARATION TRAJECTORY CALCULATIONS

In order to gain insight into the mechanics of the separation process and the requirements on the separation system, calculations of representative separation trajectories have been made. In each instance that capsule type or types considered most pertinent to the particular carrier ejection field has been examined.

Of principal interest is the capsule trajectory relative to the carrier vehicle while in the influence of the carrier flow field. The investigation embraces nose, base, and side field ejections and includes conical, cylindrical, spherical, and flared capsule configurations. Free-flight capsule trajectories have also been considered in limited extent with respect to the flared body configuration.

The characteristics of carrier flow fields as discussed in section IV. A and D and of representative capsules, section IV. B, have been adopted as the basis for the trajectory investigation. Carrier trajectory conditions at separation are selected as representative of conditions which may be encountered in practice, and which provide critical elements of the ejection environment.

Base separation is akin to a carrier vehicle which is decelerating under the influence of high aerodynamic loads, i. e., no rocket motor is attached at the base, thus allowing the deployment of a separable capsule from the base. Nose separation is pertinent under conditions of both carrier vehicle deceleration and acceleration (vehicle in powered flight). Side separation of a capsule is considered more pertinent to conditions where the carrier is accelerating, and the base of the vehicle is taken up by propulsion components. With respect to side separation and the associated restraint system that must be employed during ejection of the capsule, a qualitative discussion is made on the possible effects of the configuration of this component which can be important in determining the resultant separation characteristics of the capsule.

Capsule free-flight trajectories are discussed in the first subdivision of this section and the separation process, organized according to the carrier ejection field, is considered in the second subdivision.

A. Capsule Free-Flight Trajectories

Of academic interest with respect to the flared body configuration capsule free-flight trajectories were computed to determine the damping qualities of the flared capsule and to assess the effect of a moderate tail wind on its impact dispersion. From a trajectory computation initiated at Mach 10 and an altitude of 300,000 feet with a re-entry angle of 45 degrees below local horizontal, the initial conditions for the dynamic stability analysis and wind dispersion estimate were obtained.

Assuming a 10 knot tail wind acting from 60,000 feet down, the impact dispersion of the flared body configuration was estimated. (Above 60,000 feet the high velocity of the capsule indicated that wind effects would be negligible.) It was determined from this analysis that the imposition of this moderate tail wind on the flared capsule trajectory had small effect on range dispersion.

The dynamic stability of the flared body configuration was investigated using the aerodynamic data presented in a previous section of this report. The initial conditions employed for the wind dispersion estimates were also used as initial conditions for this analysis, i.e., approximately 60,000 feet and Mach number 3. Above this altitude the effect of increasing dynamic pressure coupled with the favorable aerodynamic damping and lift curve slope parameters would cause the capsule to converge on its stable trim point quite quickly. At the above initial conditions the capsule was assumed to have an initial total disturbance of 14 degrees angular displacement, a combination of a 10 degree yaw angle and 10 degree pitch angle. The six-degree-of-freedom program was utilized to compute the capsule response in this range where the unfavorable influence of decreasing dynamic pressure is realized. Figure 26 presents the angle of attack history of this simulation, indicating that under the conditions imposed the damping of this configuration is quite satisfactory.

B. Separation Process

The separation of capsules pertinent to given carrier regions is discussed in the subdivisions of this section. With respect to the nose region, the nose cone itself (blunt cone) is the configuration of interest. The cylinder is employed for the base region, while for the carrier side field the cylinder and flared body types are considered. Also, for the side field, the sphere is included for purposes of comparison with the more practical shapes.

In all instances, the computational procedure was to perform single parameter variations on a "standard" problem configuration, thereby to determine the effects of given parameters. The objective of the computations was to establish or to indicate minimum requirements on ejection thrust or ejection velocity under the criterion of successful ejection for all combinations of the problem parameters. In this manner, the relative significance of the parameters and – in the case of side field ejection – the effect of capsule type on ejection requirements are indicated.

1. Nose Separation Process

The standard problem configuration for nose separation has the following values of the basic parameters:

Altitude - 5,000 ft

Mach number - 5.0

Trajectory path angle - 45 degrees below horizontal

Ejection thrust angle with respect to carrier axis - 0.2 radians

Thrust axis lever arm with respect to nose cone c.g. - 0.133 nose cone base diameter

Carrier angle of attack - 0

Contact friction coefficient - 0.15

In addition, variations were made individually of altitude and Mach number, and – by a process of trial and error – the required ejection thrust levels were computed for each parameter set. Characteristics of a typical separation trajectory are presented in Figure 27 for conditions of the standard problem configuration.

The effects of Mach number (at an altitude of 50,000 feet) and altitude (at a Mach number of 5.0) on required thrust are presented in Figure 28 As might be expected, that these effects are – in essence – an effect of dynamic pressure variation in a region where Mach number has relatively little effect on the value of aerodynamic coefficients is illustrated in the same figure, where a linear correlation is exhibited. Not specifically documented in this report are the effects of carrier angle of attack and

thrust angle. It is found that required thrust levels are very sensitive to these parameters. Especially in cases where the thrust vector is displaced off the nose center of gravity to produce displacement by rotating as well as translating the capsule in the desired direction of motion, the rotational moments are resisted by the inherent static stability of the nose. Under this consideration, use of thrust in this manner is generally inefficient.

A recommended technique in nose separation is to utilize thrust directed through, or nearly through, the nose center of gravity transverse to its axis such as to produce translation only. Use of a track or rail and of roller bearing contacts appears feasible with this technique. However, it is noted, parenthetically, that the thrust levels established for "angular" (thrust vector off center of gravity) ejection are within the capabilities of available explosive devices, and that such devices are suggested for many applications in view of the short thrust durations involved.

On the other hand, in certain cases the employment of short duration or "explosive" thrust devices for separation may not be possible. In situations where a human occupant or sensitive instrumentation is involved, the separation impulse required to displace a safe distance from the carrier may have to be spread out over a relatively length period of time due to g limitations. Also, in certain cases where the carrier vehicle is an active or potentially active booster, the use of a directly lateral separation (transverse to carrier vehicle) may result in undesirable normal or lateral g loading requirements to achieve an adequate separation distance in the desired time, or - conversely - in a nose cone position too close to the carrier vehicle during that portion of the separation when the carrier (booster) passes up the nose section such that danger of damage to capsule due to booster explosion is possible. This case discussed above would be pertinent to conditions that can be achieved by a space vehicle during boost where a mission abort is necessitated. In such a situation use of separation thrust directed approximately through the nose center of gravity but at some angle less than 90 degrees (and generally more than 0 degrees) from the nose cone longitudinal axis may be optimum. In this case, the nose cone is projected well forward of the carrier to avoid explosion hazard (or in addition, for off-the-pad aborts, to an altitude where a successful recovery can be initiated), and also laterally to insure that the parent vehicle does not pass dangerously near the capsule later when the carrier overtakes the nose cone, it being assumed that the carrier vehicle W/C_DA is greater than that of the separated nose.

The use of thrust axis orientation slightly displaced off the nose cone center of gravity can in some similar cases be worthwhile to aid in the relative lateral displacement of the nose section. The extent of this thrust axis displacement must be weighed in the light of nose cone aerodynamic stability and the tolerance that can be maintained on actual alignment of the thrust axis such that the possibility of achieving angles of attack that would impose excessive air and g loads on the nose structure, instrumentation, or occupant during separation would be avoided.

2. Base Separation Process

Ejection of a cylindrical capsule from the base of a carrier vehicle at an angle to the carrier vehicle axis has been studied in a general manner by means of a parametric analysis based upon the following standard problem configuration:

Altitude - 50,000 ft

Mach number - 5.0

Ejection angle measured from wake axis - 22.5 degrees

Capsule initial position relative to carrier axis center of gravity - on axis (capsule axis at 22.5 degrees from carrier axis)

Ratio carrier-to-capsule weight-to-drag area ratios - 16

Carrier weight-to-drag area ratio - 700

The case of axial ejection was investigated in considerable detail for the effects of variations in weight-to-drag area ratio of carrier and of capsule.

The results of the axial ejection analysis are presented in Figure 29; the parametric investigation is summarized in Figures 30 and 31. Values of parameters held constant for the variation of another parameter correspond to conditions stated for the standard problem configurations. Requirements on the base ejection system are interpreted in terms of ejection velocity; the significance of each of the problem parameters is discussed in the following paragraphs.

In the instance of axial ejection (down the wake centerline), the following effects may be noted from Figure 29.

(1) Required ejection velocity increases with increasing free-stream Mach number. Since the capsule in axial ejection, is not required to negotiate abrupt changes in flow conditions (as, e.g., in crossing the wake boundary), the effect of Mach number becomes to a great degree an effect of dynamic pressure. Consequently, ejection requirements become more severe as Mach number and dynamic pressure increase.

The dynamic pressure effect is a result of the increased incremental deceleration of the carrier vehicle with increased dynamic pressure, while the increment in magnitude of capsule deceleration with respect to space is not nearly so affected by a dynamic pressure change during that initial portion of the capsule trajectory when it is immersed in the reduced intensity environment aft of the carrier vehicle, i.e., in the wake of the carrier. Consider the hypothetical case of the wake dynamic pressure recovery being insignificant or zero for a certain distance aft of the carrier. The carrier deceleration would double if the free-stream dynamic pressure is doubled; and, neglecting such pure effects as Mach number, the local wake dynamic pressure would also double. However, if the initial value is negligible or zero the capsule deceleration while in this region will be unaffected. Correspondingly, the ejection velocity required to displace the capsule relative to the carrier out of this insignificant dynamic pressure region would be increased, by a square root function in this case. Though this case is unrealistic, it can be approached to some degree in practice.

(2) Required ejection velocity decreases with increasing ratio of carrier-to-capsule weight-to-drag ratios. The effect to carrier weight-to-drag ratio increasing is more powerful than the similar effect of capsule weight-to-drag ratio decreasing for a fixed value of $(W/C_DA)_{carrier}/(W/C_DA)_{capsule}$. This is a result of the same circumstances discussed in (1), pertaining to the fact that the capsule while in the reduced intensity wake of the carrier is less affected by changes in dynamic pressure or W/C_DA than in the carrier vehicle which is at all times exposed to free-stream flow. In either case it is a result, of course, of relative vehicle decelerations.

The generalized parameteric investigation yields the following

results (see Figures 30, 31).

(1) Referring to Figure 30, curve (a), it is seen that the ejection velocity required to separate the capsule is significantly less if the capsule is ejected at such an angle to penetrate the wake boundary ahead of the wake throat, as compared to the wake core ejection. Once the angle of ejection becomes large enough to cause penetration ahead of the throat, the effect on ejection velocity of further increasing the angle of ejection is relatively small. Increments of 10 feet per second were employed to approximate the velocity requirements for wake penetration and the lowest value which resulted in successful separation was employed. To emphasize the difference between the wake penetration ejection and wake core, it must be stated that the criterion employed for a successful wake penetration run in determining minimum ejection velocity was that, in addition to successfully separating, the capsule must be completely out of the convergent portion of the carrier wake when it passed the wake throat longitudinally. In the case of wake core ejection, the only criterion employed was that the capsule successfully separate from the carrier. The comparison shown in Figure 30 reflects this difference in criteria as well as in the fact that 10 feet per second increments were employed in the wake penetration case. Thus, the difference shown between wake core and wake penetration velocity requirements should be conservative. On curve (a) no fairing is shown between the data at zero angle of ejection (wake core) and the 22.5 degree approximation (wake penetration) since the shape of this portion of the curve has not been determined and may be subject to certain inflections. Reasoning for the superiority of the wake penetration mode of base ejection is that upon passing through the wake boundary significant dynamic pressure immediately aids in carrying the capsule downstream; whereas for ejection down the wake centerline, a gradual recovery of free-stream dynamic pressure exists from the wake throat to points downstream of the throat.

(2) Correspondingly, the effect of initial capsule lateral position (Figure 30, curve (b)) is negligible as long as ejection angle is large enough for wake boundary penetration. Presumably, if an effect of capsule lateral or vertical position exists, it will arise at small ejection angles.

(3) Referring to Figure 30, curve (c), it is seen that the required

ejection velocity for a significant ejection angle (wake boundary penetration) increases with increasing ratio of carrier-to-capsule weight-to-drag area ratio, contrary to the case of axial ejection. It is noted that these data were obtained by varying the capsule weight-to-drag area ratio at a fixed value of carrier weight-to-drag area ratio. Under this particular condition, it is reasoned that since in angular ejection the wake boundary is penetrated and the capsule immediately encounters a dynamic pressure field which approaches free-stream values, the higher drag and/or lower inertia (lower W/C_DA) capsule which is associated with larger values of carrier-to-capsule weight-to-drag area ratio is resisted from entering the free-stream field more effectively than is the capsule with a higher weight-to-drag ratio. On the other hand, if the ratio of carrier-to-capsule weight-to-drag area ratios is varied by holding the capsule W/C_DA fixed and varying the carrier W/C_DA, it is conceivable that little effect of changing the ratio of these W/C_DA ratios can be realized. In fact, the ejection velocity required for separation should even reduce slightly at increasing values of the ratio so obtained since the carrier would decelerate less relative to the capsule during that small portion of the trajectory where the capsule is within the convergent portion of the carrier wake. The effect of reduced carrier deceleration with respect to the capsule after the capsule is immersed in free-stream flow is of no consequence on ejection velocity requirements since it is assumed that the carrier weight-to-drag area ratio is significantly larger than that of the capsule in all cases. If the carrier density (and therefore weight) is changed to produce the varying W/C_DA, no effect on the wake structure is realized. Changing the carrier geometry to vary W/C_DA is not herein considered as a parameter.

Figure 30, curve (d), presents the effect of carrier W/C_DA on required ejection velocity for a fixed value of $(W/C_DA)_{carrier}/(W/C_DA)_{capsule}$ equal to 16. This curve reflects the change in ejection velocity requirements with a change in both the carrier and capsule ballistic coefficients, W/C_DA. Assuming, as discussed before, that the effect of changing carrier ballistic coefficient is quite small at a fixed capsule W/C_DA, the main variation of these data results from the fact that the capsule W/C_DA is increased (as the carrier value increases to maintain a constant value of the ratio of their ballistic coefficients). In other words, the increasing value of capsule W/C_DA effects the main reduction in ejection velocity requirements due to the resultant decreased sensitivity of the capsule to airloads.

(4) The Mach number effect at a constant altitude (Figure 30, curve (e)) and the altitude effect at a fixed Mach number (Figure 30, curve (f)) for the wake penetration exhibit trends similar to that observed in nose separation, an increase in required ejection velocity or force (for nose separation) with increasing free-stream dynamic pressure. In the case of nose separation, the force required was shown to be approximately a linear function of dynamic pressure. In the case of base separation, where the velocity required for ejection was employed as the parameter of interest, the ejection velocity squared would be proportional to the dynamic pressure if a pure dynamic pressure effect were present. This is a result of the fact that the required velocity is proportional to the square root of applied net force. However, the data of Figure 30, curves (e) and (f), and Figure 31 indicate that direct correlation of required ejection velocity as a function of the square root of dynamic pressure is prohibited. Taking curve (e) and dividing through by the square root of dynamic pressure indicates that a reduction in required ejection velocity at a fixed dynamic pressure would result between Mach 5.0 and Mach 10.0. Taking curve (f), which is for a fixed Mach number of 5.0, and dividing through by the square root of dynamic pressure indicates that the required ejection velocity varies approximately with the square root of dynamic pressure at a fixed Mach number. Also, according to the carrier deceleration correlation exhibited in Figure 31, which depends on free-stream dynamic pressure, required ejection velocity does increase with deceleration, but at a fixed value of carrier deceleration (dynamic pressure) a reduction in required ejection velocity is found with increasing Mach number. Because of the assumed penetration criteria such that capsule attitude angle with position aft of the carrier becomes critical, and because rather gross velocity increments were employed to approximate the ejection velocity requirements, it can be misleading to assess quantitatively the actual magnitude of ejection velocity sensitivity to Mach number at a fixed dynamic pressure. However, it may be stated that the data indicate the favorable effect of a pure Mach number increase, all other parameters being held constant. The rationalization for this favorable pure Mach effect lies in the fact that, as free-stream Mach number is increased in the hypersonic range, the local Mach number just forward of the base of the carrier is reduced. Since available information indicated that the ambient pressure in this region is near the free-stream value, the dynamic pressure just forward of the base of the vehicle is reduced as a function of the

ratio of the local Mach number to free-stream Mach number squared. Thus, at a fixed level of free-stream dynamic pressure, an increase of free-stream Mach number will reduce the local dynamic pressure outside the wake near the vehicle base. The resistance of the local flow to penetration of the capsule is thereby reduced with a pure increase of free-stream Mach number.

(5) When the capsule penetrates the wake boundary in angular ejection large angular velocities, accelerations, and loadings are imposed on the capsule due to its attitude at penetration and the fact that, as it penetrates, various portions of the capsule are exposed to the flow outside the convergent wake boundary. This consideration would be of importance if structurally weak or sensitive instrumentation is packaged in the capsule. Furthermore, as dynamic pressure is reduced or as vehicle weight-to-drag area ratio is increased (carrier deceleration reduced), the ejection velocity requirements for wake core and wake penetration ejection approach each other. Thus, under the above conditions and/or in a situation where relatively high angular accelerations or rates on the capsule are to be avoided, the employment of the wake centerline mode of ejection may be advisable.

3. Side Separation Process

The side separation process is analyzed in two steps, namely

(1) Determination of ejection force-ejection velocity dependency during the partial exposure phase of the ejection process wherein the capsule is restrained in longitudinal translation and rotational freedom

(2) Calculation of capsule relative trajectory when physically free of the carrier vehicle, initial conditions interpreted in terms of ejection velocity with zero longitudinal and angular displacement and zero angular velocity.

The standard problem configuration has the following values of the basic parameters:

Altitude - 50,000 ft

Mach number - 5.0

Carrier acceleration - 5 g's

Capsule weight-to-drag ratio - 100

Coefficient of friction - 0.05

Capsule types represented in the partial exposure computations include the sphere, the cylinder in "normal" orientation, and the flared body in both "normal" and "parallel" orientation. The cylinder in parallel orientation is included for the complete exposure computations. Treated as a special case was the flared capsule in parallel orientation at Mach 15.0, altitude 85,000 feet, other parameters above. The partial exposure and complete exposure analyses are discussed in the following two subdivisions of this section.

a. Partial Exposure Phase

(1) Method of Restraint and Associated Effects

An investigation of various restraint system configurations and ejection systems to be employed by a carrier vehicle to implement the separation of a capsule was not made as a part of this study effort. However, a qualitative discussion of certain aspects of these systems and their effects on the initial conditions of the capsule complete exposure phase is warranted.

With respect to ejection systems, the force-supplying component may be an inherent part of the carrier system such as a gas generator powered piston or compressed spring mechanism, or the thrusting device may be incorporated with the capsule, for example a rocket motor. The design of the restraint system will in many cases be premised on the type of ejection mechanism chosen, or vice versa. Choice of particular hardware components will depend on many parameters such as capsule type and size and ejection environment. The restraint system may be simply a means of holding a self-powered capsule in a fixed position prior to ejection (vehicle contact is prevented by use of a sufficiently large opening in the carrier vehicle), or it may be a relatively complex arrangement wherein the capsule is held in a desired axial and angular position until emergence is nearly completed. In either case the ejection and/or restraint system can have

important effects on the angular attitude and rate of the separated capsule as it initiates the complete exposure phase of its trajectory.

Assuming a capsule in parallel orientation prior to ejection, if the capsule is allowed to tip-off the rear restraint of the carrier when nearly separated, a nose-up moment will be generated that could induce a significant angle of attack and/or pitch rate on the capsule. If the aerodynamic frequency of the capsule were such that approximately one-half cycle of motion would be achieved during that time in which the capsule traverses to the base of the carrier, the normal force on the capsule during this critical time would be such as to displace the capsule away from the carrier, or at least tend to cancel out the effect of any carrier field in-flow. In such a case, the actual flow field existing around the parent vehicle may even be relatively insignificant, and the only parameter of real importance would be the ejection velocity required to cause capsule emergence against a possible adverse aerodynamic force distribution during partial exposure. Even if no tip-off occurs the ejection thrust device may be employed in such a way as to provide a preprogrammed angular attitude or rate at emergence. Thus the ejection and restraint systems and their possible effects on establishing capsule initial conditions for complete exposure are other important parameters that must be weighed when analyzing the dynamics of a particular body in side separation.

The restraint system employed for the study of side separation in this report is one in which no axial or rotational translation with respect to the carrier is allowed during th partial exposure phase. As indicated in the following sketch, the rear restraint is fixed relative to the carrier; the forward restraint is fixed axially to restrain the capsule longitudinally and in pitch but is allowed to move vertically with the capsule such that its contact point is maintained until release of restraint. The ejection force was applied to the capsule mass as a step input until release of restraint, except in the case of the sphere. For the sphere the ejection force was applied throughout partial exposure but the restraint was assumed to be removed at approximately half exposure.

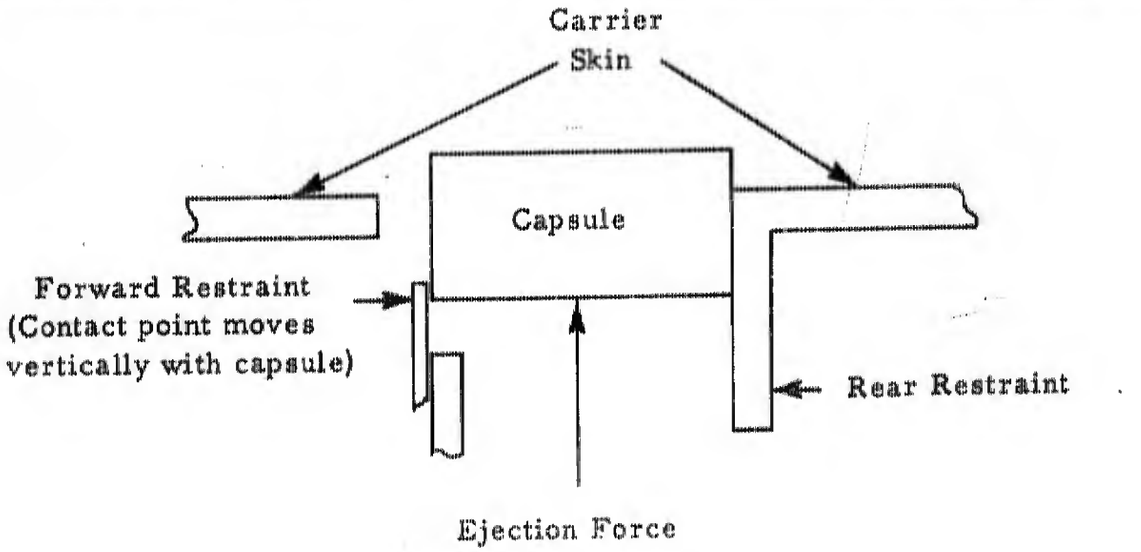

(2) Capsule Motion During Partial Exposure

Capsule motion under the influence of carrier restraint with incomplete exposure to the flow field was calculated as a function of ejection thrust level. Constant thrust is assumed to be applied during the entire ejection event, instantaneously falling to zero at the moment of complete capsule exposure. As the ejection velocity is increased by increasing the ejection force level, the time which the ejection force is applied is reduced, since this force acts only to the point where complete exposure is established.

Partial results of this analysis are plotted in Figure 32, which presents ejection thrust required as a function of capsule velocity at the instant of complete exposure. The plot exhibits the effect of capsule type on ejection thrust requirements for the "standard" set of problem parameters and for the particular type of restraint assumed. In the case of the sphere, no friction force was assumed to act during emergence. For the flared capsule and cylinder in normal orientation, the capsule-restraint contact was a line contact, i.e., a cylindrical surface against a flat surface. For the flared capsule in parallel orientation, the contact surfaces were flat, i.e., the capsule base against a flat restraint surface. It is immediately evident that the flared capsule in normal orientation (flare first) has the most favorable ejection force-velocity characteristics. This circumstance is ascribed to the flare surface pressure distribution,

which assists in the ejection process, and which causes ejection velocity at the instant of complete exposure to be finite at all force levels. Intermediate force requirements apply for the cylindrical capsule ejected in normal orientation, while the flared capsule in parallel orientation and the sphere have approximately the greatest, and equivalent, force requirements due, primarily, to the pressure distributions which oppose the ejection during the partial exposure phase.

In order to examine the effects of individual problem parameters, the arbitrary criterion of a minimum or near minimum (within the resolution of the computational process) ejection velocity at the instant of complete exposure was imposed on the ejection system, and the force requirements for that condition were determined for all the parameter sets. In the determination of the required force levels, 100 pound increments or greater were used in general. In view of this rather gross increment, minor effects of some of the parameters may be obscured or lost but important trends are nevertheless exhibited. Minimum required ejection velocities were, with this force increment, not obtained in certain instances. What has been used, then, to represent "minimum" required velocity is some nominally low value characteristic of the given capsule type.

The results of this single parameter variation analysis are summarized in Figure 33, wherein is plotted as a function of the respective parameters the ejection force corresponding to the "minimum" accepted ejection velocity. The following observations are drawn relative to this analysis.

(1) Altitude and Mach number (to 5.0) effects (Figure 33, (a) and (b)) tend to correlate as a free-stream dynamic pressure effect. However, a representative Mach 15.0 calculation for a flared at 85,000 feet altitude yields a similar ejection force requirement as for the same capsule at Mach 2.0, 50,000 feet altitude. Apparently the large loss in dynamic pressure associated with the bow shock at hypersonic speeds invalidates the correlation on free-stream dynamic pressure in the hypersonic regime. In that range a correlation on the local dynamic pressure field may likely be found to exist.

(2) For the particular type of restraint assumed, it is seen that friction coefficient has a substantial effect on force requirements for the cylinder in normal orientation and the flared capsule in parallel orientation (Figure 33 (c)). For the sphere a friction coefficient of zero was employed so no variation is shown. The data of Figure 33 (c) at a value of zero for the coefficient of friction indicate the relative magnitudes of aerodynamic forces resisting ejection during the partial exposure phase. It is seen that the sphere and flared capsule in parallel orientation have the greatest resistance to emergence during the partial exposure phase. As stated previously, the flared capsule in normal orientation requires only a small force to initiate ejection; thereafter the aerodynamic force distribution on the capsule insures that ejection will be completed.

(3) Further approximations have indicated that, in the manner in which it was varied, capsule weight-to-drag area ratio has a moderate effect on ejection force requirements. With constant geometry and increasing mass, the effect is to increase force requirements somewhat. At a given value of carrier acceleration this effect can be attributed to increased capsule bearing force on the rear restraint due to the increased inertial force with increasing mass. Thus, the frictional resistance to ejection is increased at a constant value of friction coefficient as the mass is increased. A moderate effect on ejection force can also be attributed to carrier acceleration where again the inertial bearing force of the capsule on the carrier rear restraint in an axial direction will produce increased resistance to ejection through friction as the carrier acceleration is increased.

(4) If the capsule is to be restrained during the partial exposure phase, the aerodynamic moments imposed by exposure of the capsule to the carrier flow field must be taken out by internal restraint moments. As would be expected the normal orientation mode in partial exposure imposes the greatest bending moments on the capsule. As a typical example, under the conditions stated for the standard problem configuration the aerodynamic moment

(referred to the capsule center of gravity) of the flared body in parallel orientation was calculated to be approximately 600 foot-pounds. Under identical circumstances the aerodynamic moments of the flared body in normal orientation and the cylinder in normal orientation were approximately 3,800 foot-pounds. Over the range of cases considered (Mach 2 and 5, altitudes of 50,000 and 100,000 feet), the bending moments in normal orientation are consistently about six times greater than those characteristic of parallel orientation.

In summary, it may be stated that under the influence of high aerodynamic loads, the deployment of a flared capsule in normal orientation, flare first, requires relatively the lowest ejection force; however, during ejection the bending moment on the capsule associated with the normal orientation mode is correspondingly great and requires, therefore, that the capsule and its restraint system be proportionately strong.

b. Complete Exposure Phase

The relative trajectory of an ejected capsule commencing from the instant of complete exposure (and removal of carrier physical restraints) is discussed in this section, and comparisons are made among the several capsule types considered. Trajectories are presented pictorially in Figures 34 through 40; environmental conditions and computational results are summarized in Table VIII. Zero angular velocity is assumed as an initial condition of the parametric analysis; the effect of finite initial angular velocity is examined in a particular case. Ejection velocity was taken as a parameter of the computations with the minimum value of the parameter taken to be consistent with those accepted as nominal "minimums" of the partial exposure force analysis. Favorable high pressures, which exist between the carrier and capsule when the capsule is in close proximity to the carrier vehicle are neglected; hence, the ejection velocities herein presented may be conservative.

Flow nonuniformity was considered in a representative hypersonic case (Mach 15.0). The results of the nonuniform flow field computations are compared to those of the same case (Table VIII) where the flow field was assumed uniform at averaged values of the

flow variables. In all other cases (Mach 5.0), the assumption of flow uniformity (except for shock encounter) is reasonably valid, according to section IV. A. 1. Free-stream conditions were assumed in the carrier side flow field for these cases. The significant observations relative to the complete exposure side separation calculations are discussed in the following paragraphs.

(1) Due to the inherent static stability of the flared capsule large angular displacements, velocities, and accelerations arise in the instance of normal orientation. This consideration may be of importance if sensitive or structurally weak instrumentation or components are part of the capsule system. The 90 degree angle of attack condition is one which would not be encountered at any other time during the trajectory of the capsule to ground impact, and as such might require a capsule structural strength well in excess of that which would be necessary for the other portions of its trajectory.

(2) The assumption of flow uniformity in the hypersonic case does not seriously affect the prediction of displacement of capsule center of gravity from the carrier vehicle base (see Table VIII and Figures 39 and 40). It does, however, lead to a probable underprediction of angular displacement and angular acceleration. (Since the restraint and ejection systems were assumed not to disturb the capsule in pitch, the assumption of a uniform field allows the capsule, ejected in parallel orientation, to remain at zero angle of attack through its trajectory.) The slight turning of the capsule trajectory toward the carrier base, which is observed at an ejection velocity of 7.73 feet per second (low), is ascribed to the local in-flow in the region near the vehicle. Further from the vehicle, the local flow turns outward. A capsule ejected at twice the above velocity encounters this out-flow with resulting absence of the tendency to turn its trajectory toward the carrier base. The angular motion in the latter instance is substantially greater than that at the lower ejection velocity.

(3) Since the investigation of restraint and ejection was not a basic part of the present program, the assumption of zero initial angular displacement and velocity was made. It is not to be inferred that an ejection system which can yield this initial condition is necessarily practical. In order to ascertain,

to some degree, the consequences of an initially finite angular velocity a case has been examined in which initial pitch rate is a parameter. Fixed conditions were as follows:

Mach number - 15.0

Altitude - 85,000 ft

Carrier flow field - Averaged uniform

The results of this investigation are shown in Figure 41 where the pitch rate parameter has values of 0, -0.1, -1.0, -5.0 radians per second with initial angular displacement zero. These data indicate that at an initial favorable pitch rate of -5 radians per second (nose away from carrier vehicle), the lateral displacement at the vehicle base is increased by approximately 25 percent over that of the zero initial pitch rate condition. The capsule frequency is such that slightly more than one and one quarter pitch cycles were experienced in traversing the distance from the capsule stowed position to the vehicle base. Thus, the initially favorable effect of angle of attack disappears after a time and becomes unfavorable as the angle of attack becomes positive. Ideally, the capsule frequency characteristic which results in one half cycle or less of angular motion during transit along the carrier is optimum from the point of view of separation. In those instances in which this frequency characteristic exists it would be desirable to employ a restraint-ejection system which can provide an appropriate initial angular rate and/or displacement.

To supplement the pitch rate investigation, for which a uniform flow field was assumed, a case was calculated for a nonuniform field with an initial pitch rate of 5 radians per second. The resulting trajectory is plotted in Figure 40 along with the equivalent trajectory at zero initial pitch rate. The in-flow characteristics of the nonuniform flow field reduce the favorable effects of initial pitch rate, though a small advantage of pitch rate still accrues.

TABLE VIII

SIDE FIELD EJECTION TRAJECTORY CHARACTERISTICS
CAPSULE FREE OF CARRIER

Figure	34	35		36		37		38		39	40	
Capsule Type	Sphere	Flared Body		Flared Body		Cylindrical		Cylindrical		Flared Body	Flared Body	
Orientation	-	Parallel		Normal, Flare First		Parallel		Normal		Parallel	Parallel	
Mach Number	5.0	5.0		5.0		5.0		5.0		15.0	15.0	
Altitude (ft)	50,000	50,000		50,000		50,000		50,000		85,000	85,000	
Interference Effects	(1)	(1)		(2)		(1)		(1)		(1)	(3)	
Ejection Velocity (ft/sec)	13.47	11.42	34.26	41.5	81.5	6.47	31.0	6.47	31.0	7.73	7.73	15.45
Capsule Center of Gravity Clearance at Base (ft)	1.3	1.5	4.5	3.2	6.5	0.95	3.0	(4)	2.3	2.23	1.86	4.75
Maximum Angle of Attack (deg.)	N.A.	(5)	(5)	80	123.3	(5)	(5)			0.09	37.8	67.7
Maximum Angular Acceleration (rad/sec^2)	N.A.	(5)	(5)	4870	4940	(5)	(5)			1.74	338	960
Maximum Angular Velocity (rad/sec)	N.A.	(5)	(5)	104	115	(5)	(5)					

(1) Uniform Field, Shock not Encountered - (2) Uniform Field, Shock Encountered - (3) Shock not Encountered, Moskowitz Method Interference Field - (4) Strikes Carrier - (5) Consequence of Restraint Assumption.

Capsule Weight-to-Drag Area Ratio - 100
Carrier Acceleration - 5 g's

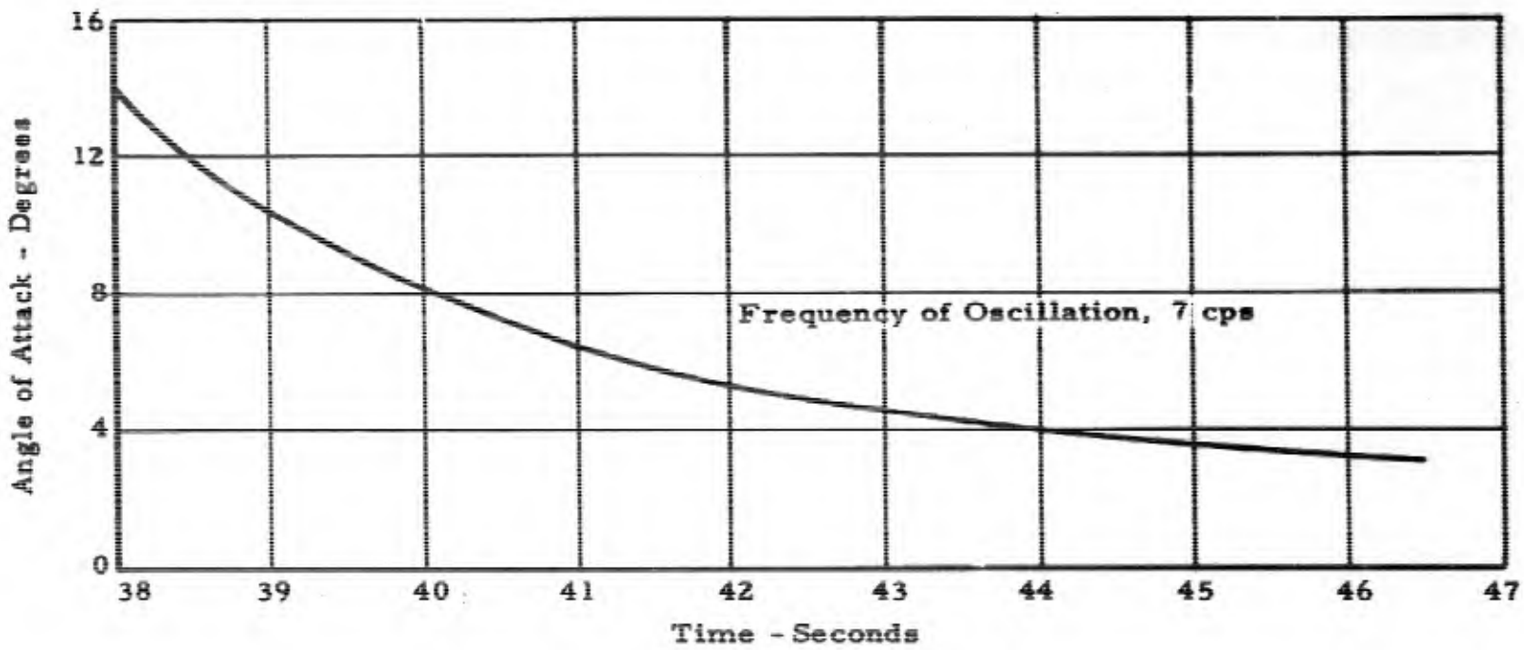

Figure 26. Angle of Attack Magnitude History for Stable Flared Capsule on Re-entry Trajectory

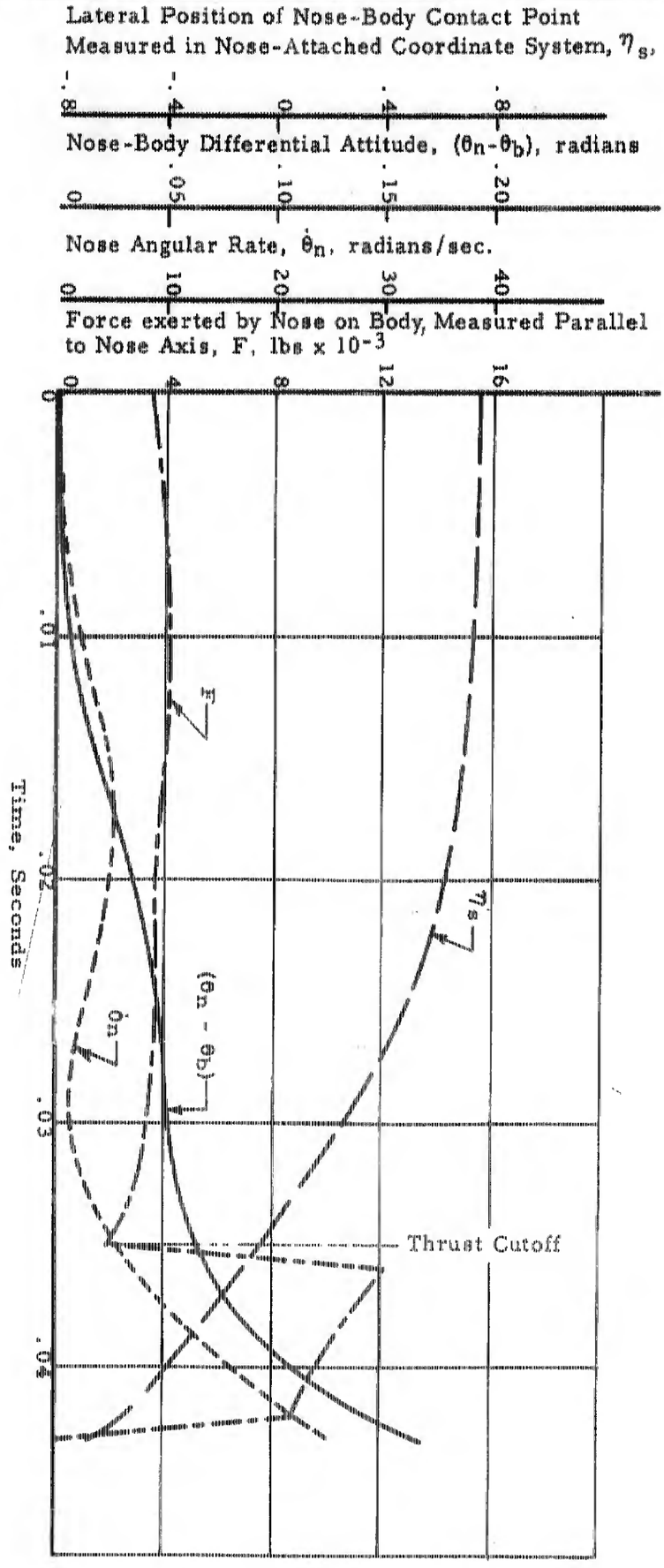

Figure 27. Characteristics of a Typical Nose Separation Trajectory, Standard Problem Configuration, Thrust Level 12,000 Pounds, Afterbody Diameter = 1.5 ft

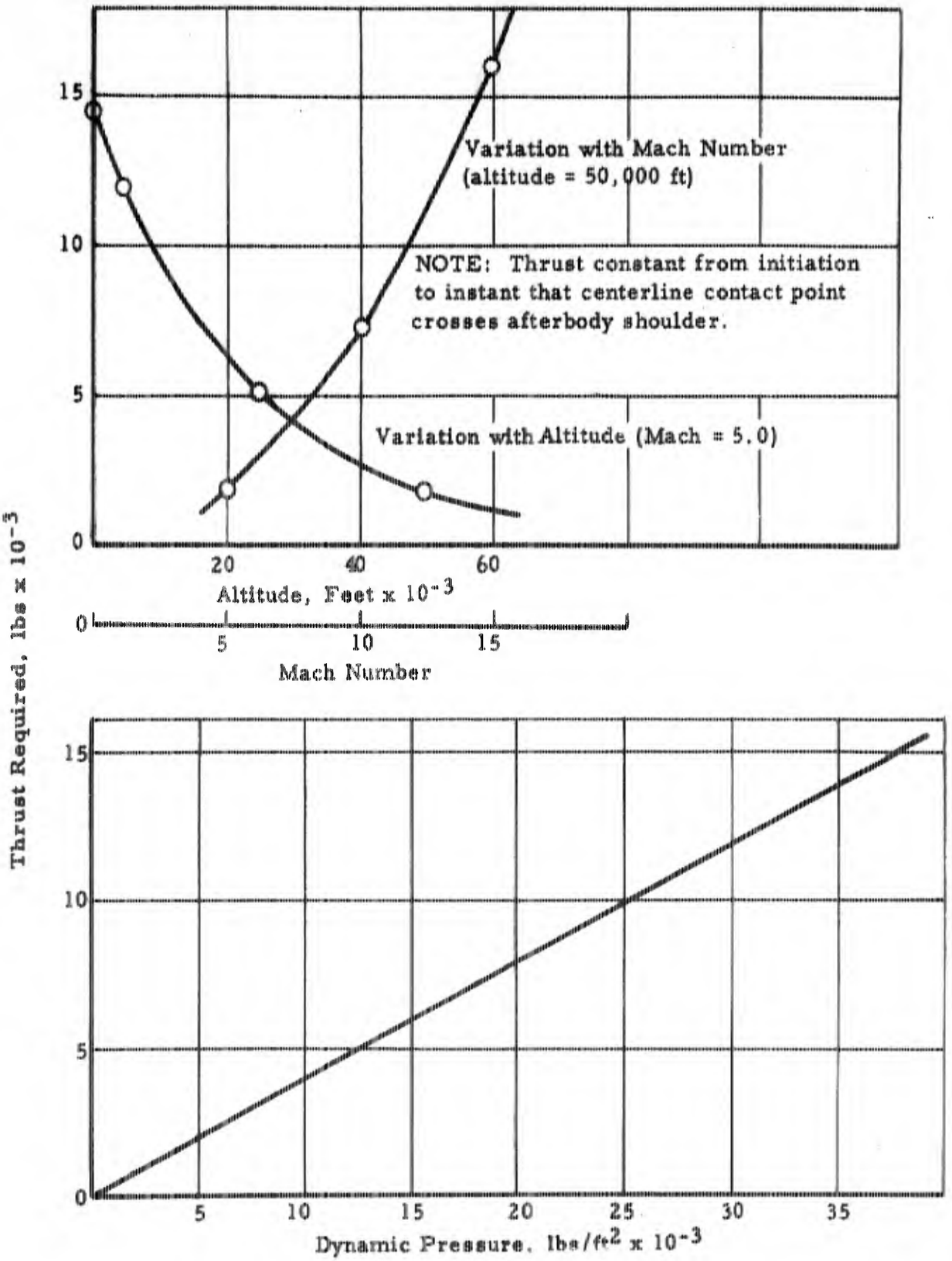

Figure 28. Correlation of Mach Number, Altitude Effects on Thrust Required as a Dynamic Pressure Effect in Nose Separation; Ejection Thrust Angle, 0.2 Radian, Carrier Angle of Attack, Zero Degrees

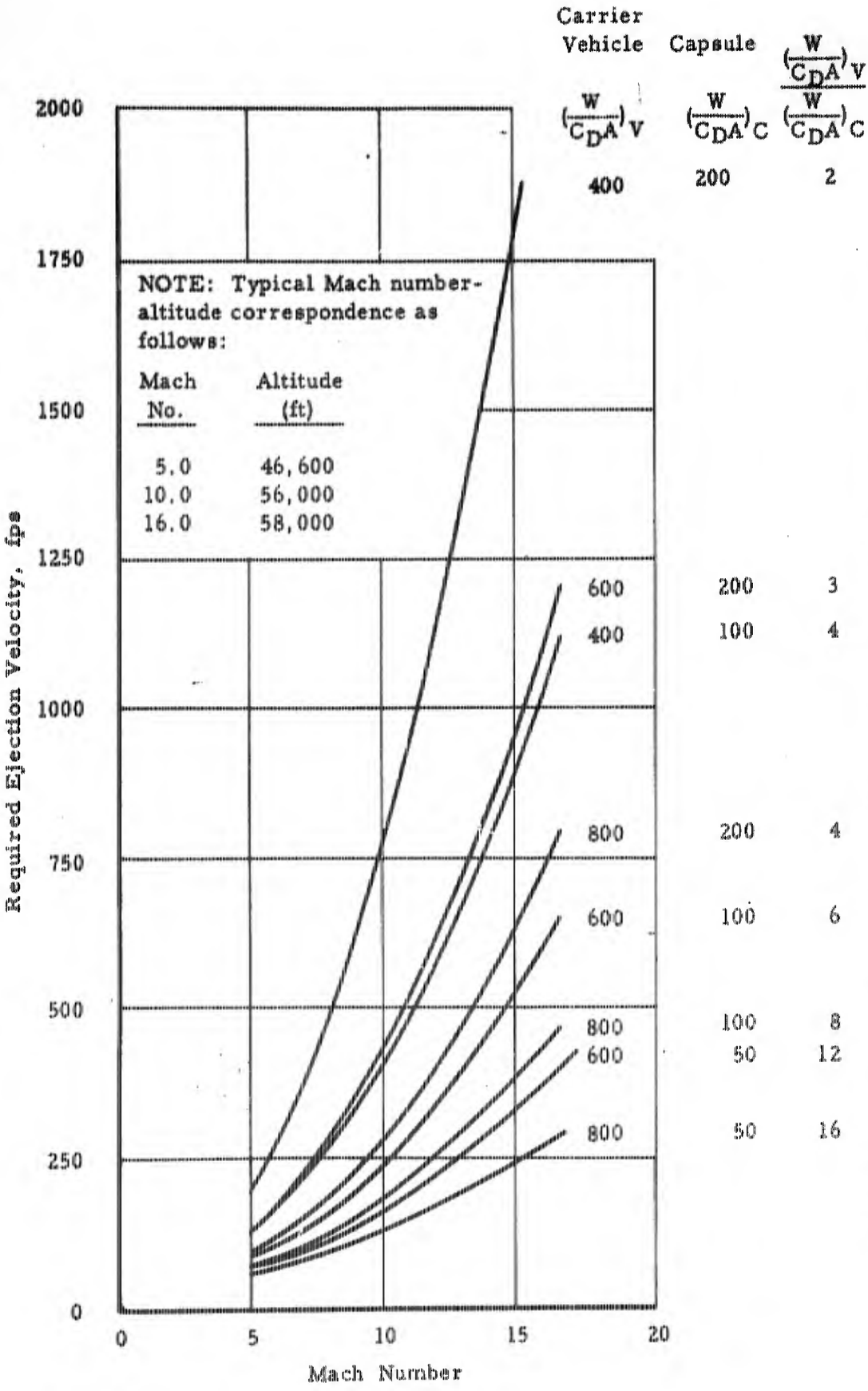

Figure 29. Base Ejection Along Wake Core: Required Ejection Velocity as a Function of Mach Number and Ratio Carrier-to-Capsule Weight-to-Drag Area Ratios

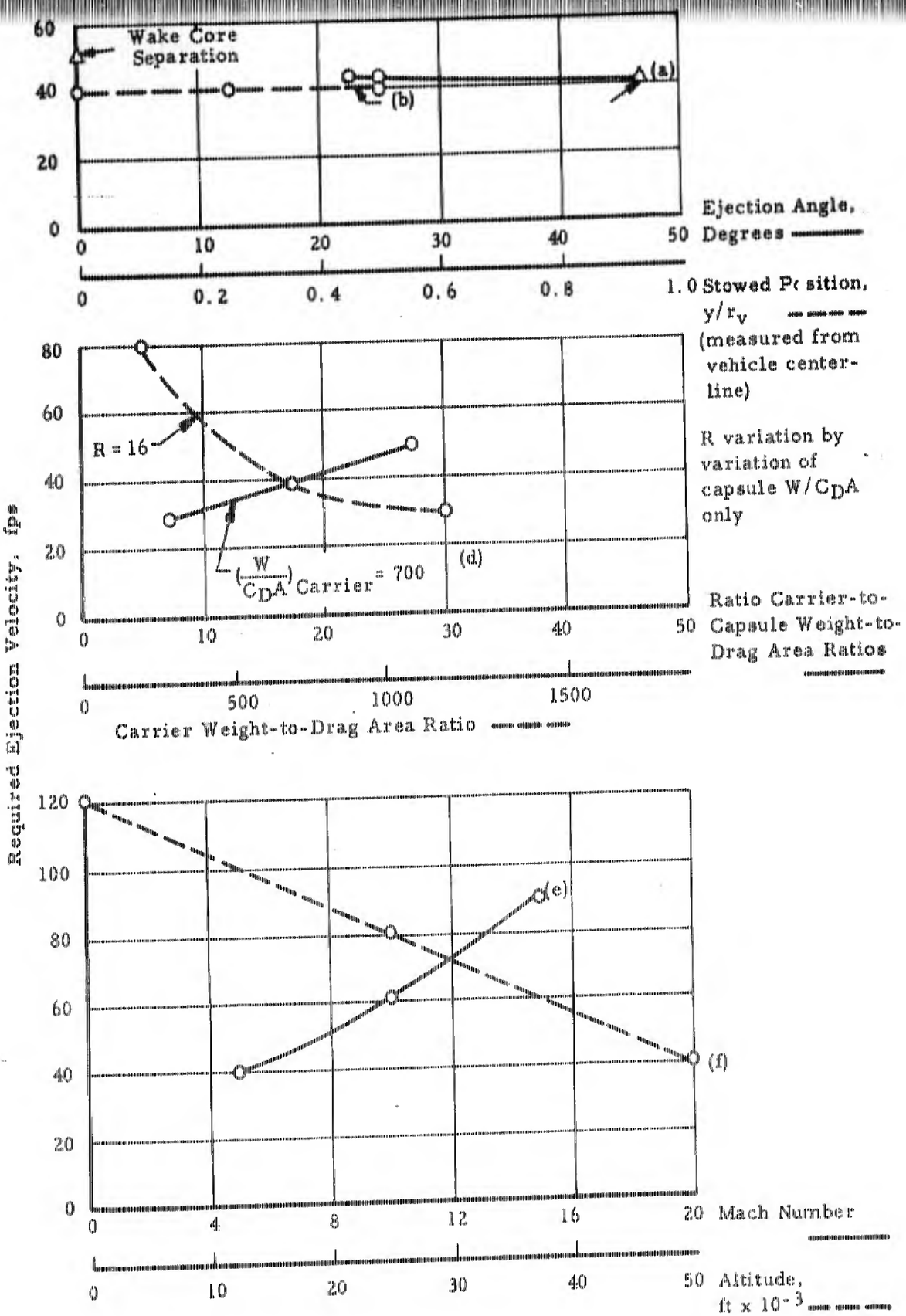

Figure 30. Variation of Required Ejection Velocity in Base Ejection with the Several Parameters of the Analysis; Standard Problem Configuration Except as Noted

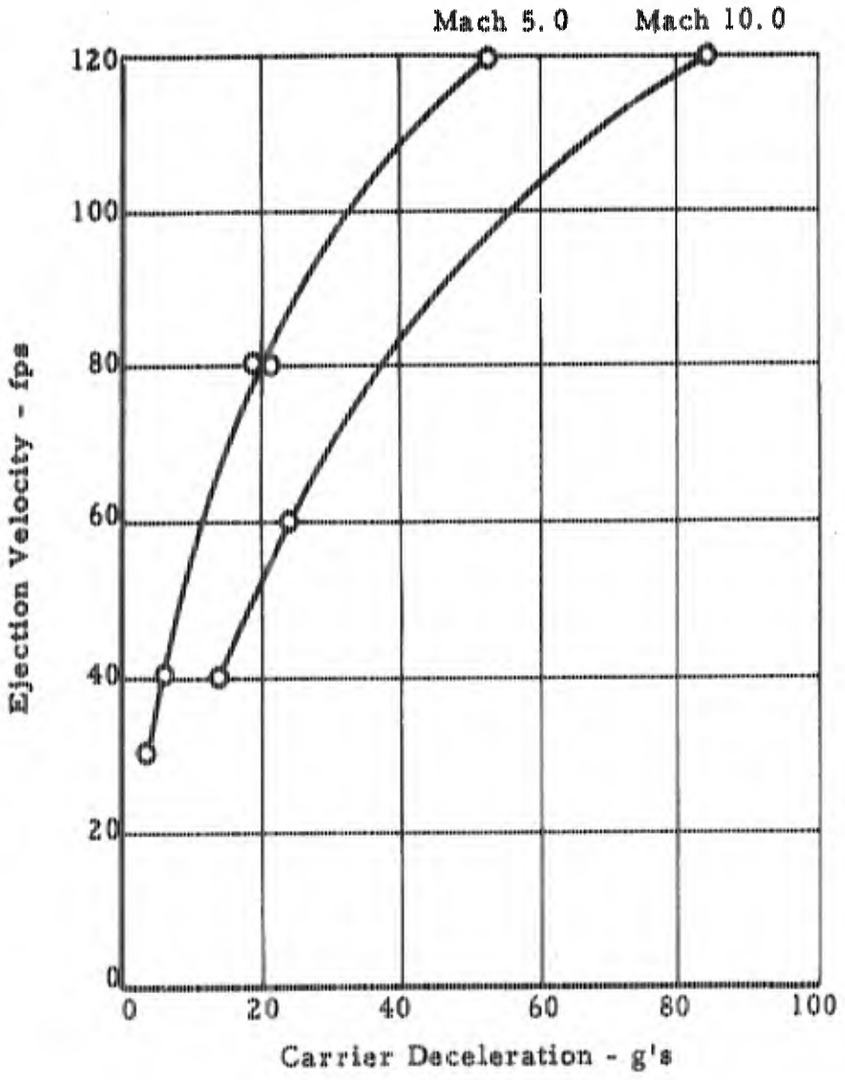

Figure 31. Effects of Carrier Deceleration and Mach Number on Required Ejection Velocity in Angular (Wake Boundary Penetration) Base Separation

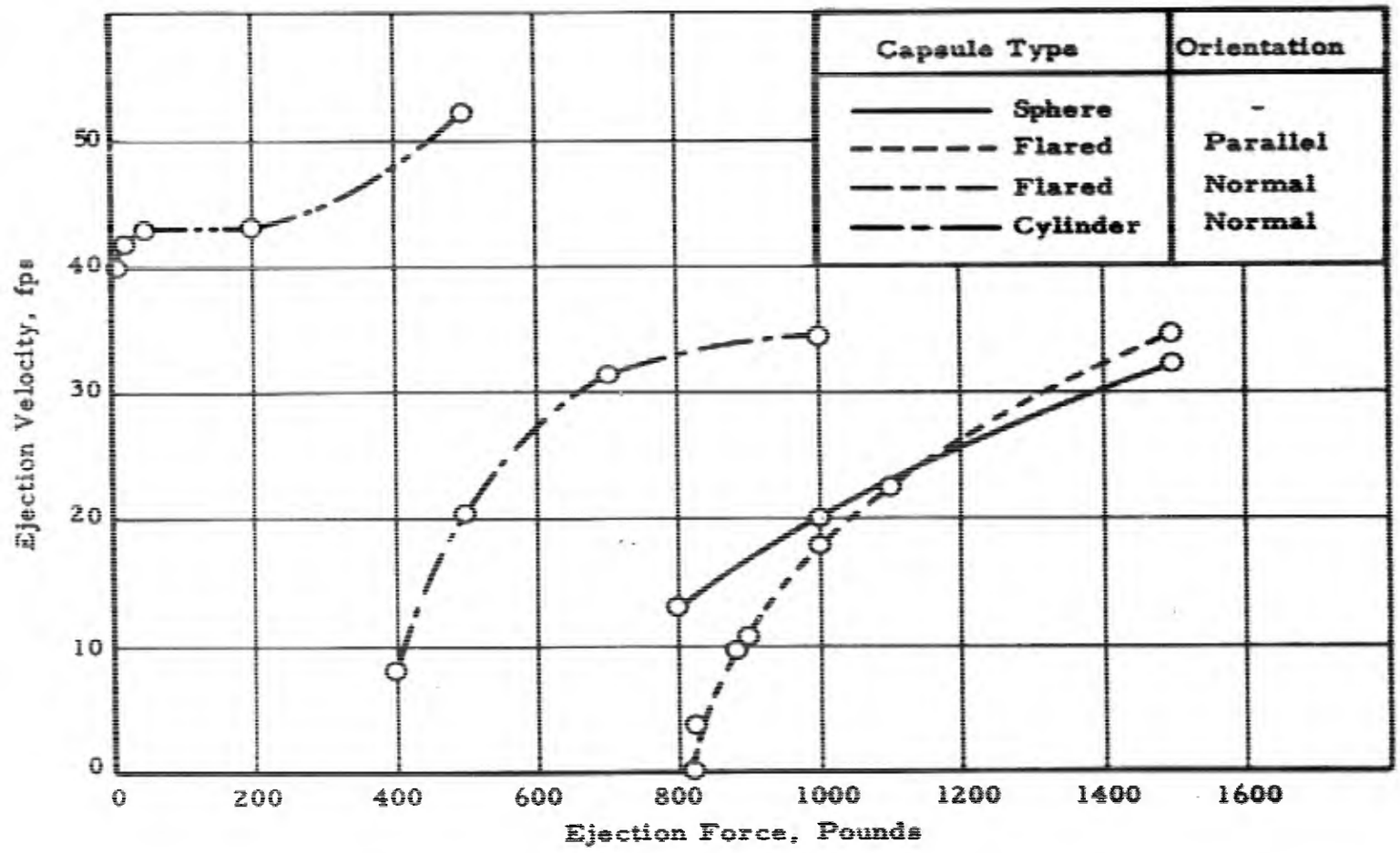

Figure 32. Velocity of Ejection at Instant of Complete Exposure as a Function of Ejection Thrust Level for Several Capsule Types and Orientations in Side Ejection; Standard Problem Configuration

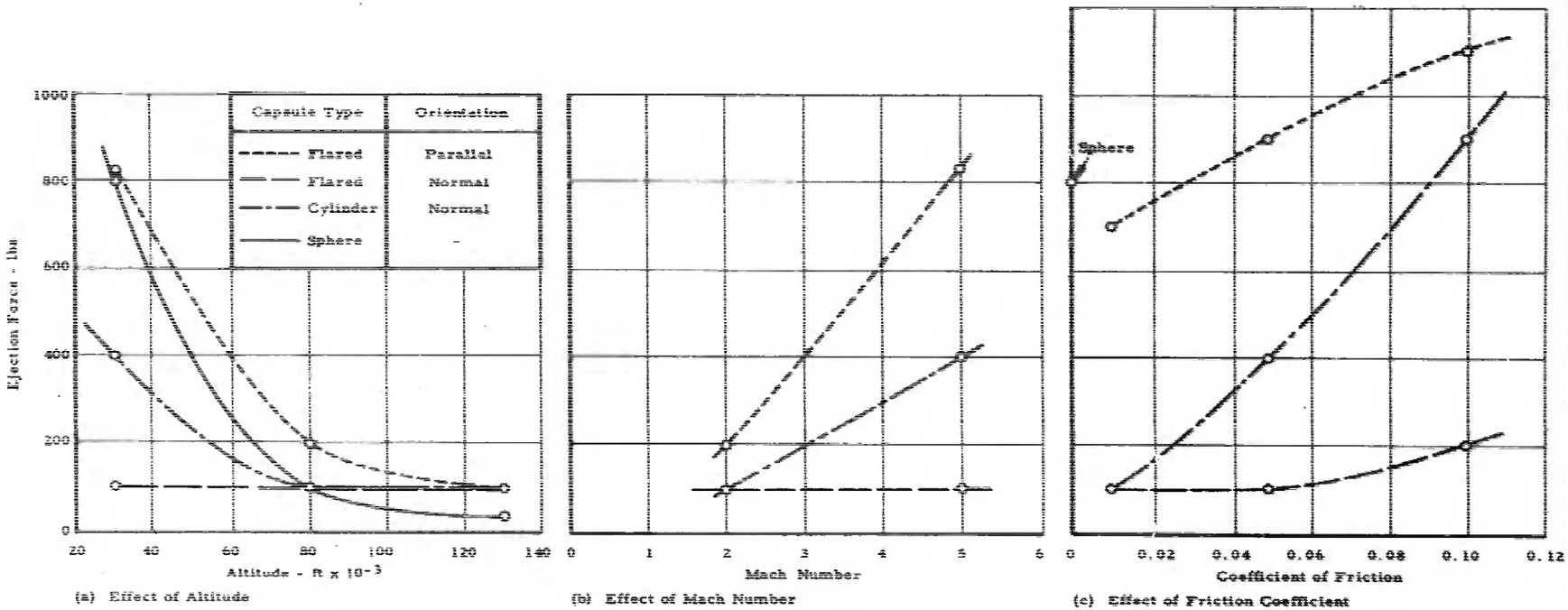

Figure 33. Ejection Force Required for Nominal "Minimum" Ejection Velocity at Instant of Complete Exposure in Side Ejection as a Function of the Several Problem Parameters and of Capsule Type and Orientation; Nonexhibited Parameters from Standard Problem Configuration

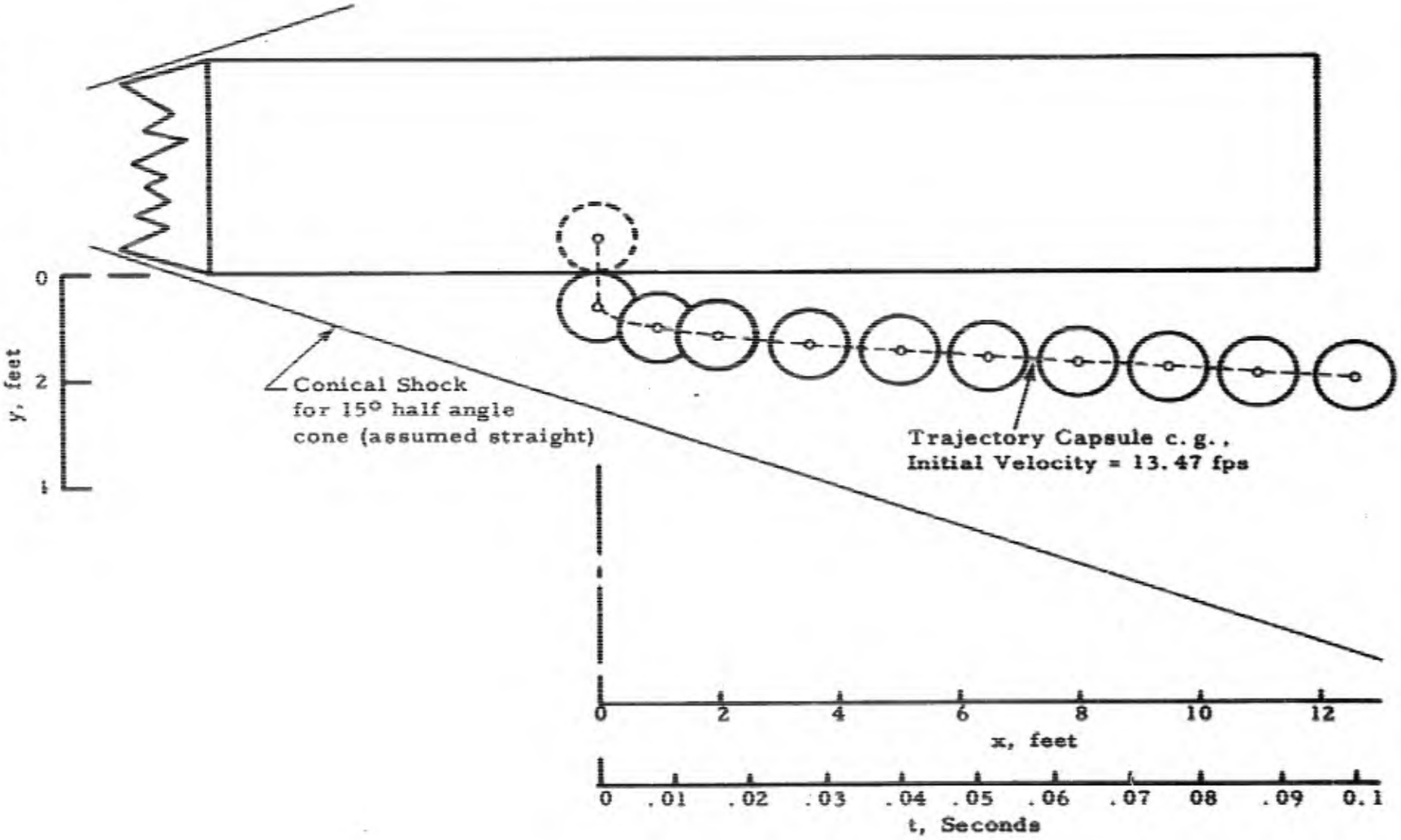

Figure 34. Separation Trajectory Side Ejection of Spherical Capsule, Standard Problem Configuration

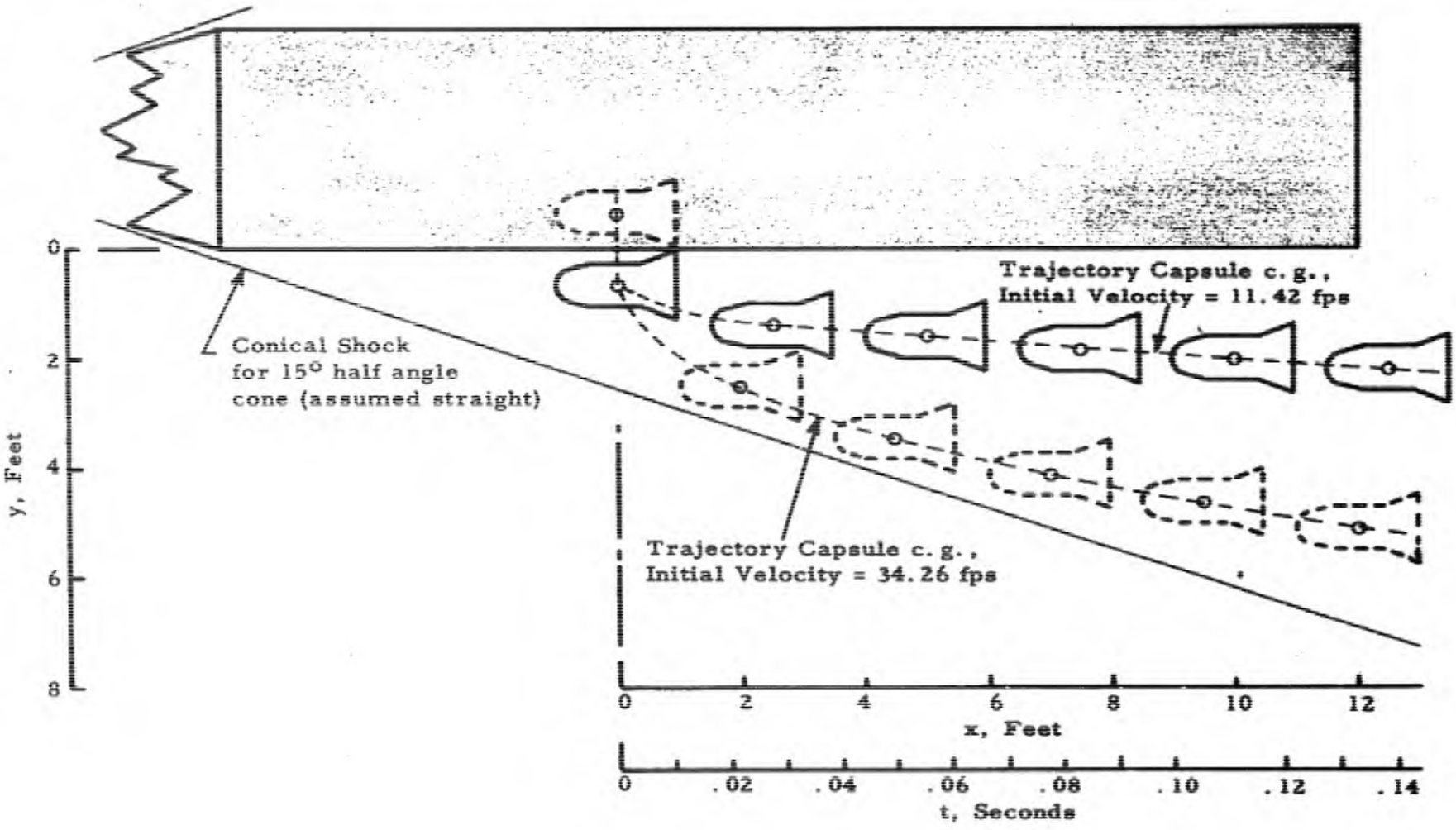

Figure 35. Separation Trajectories Side Ejection of Flared Capsule in Parallel Orientation, Standard Problem Configuration

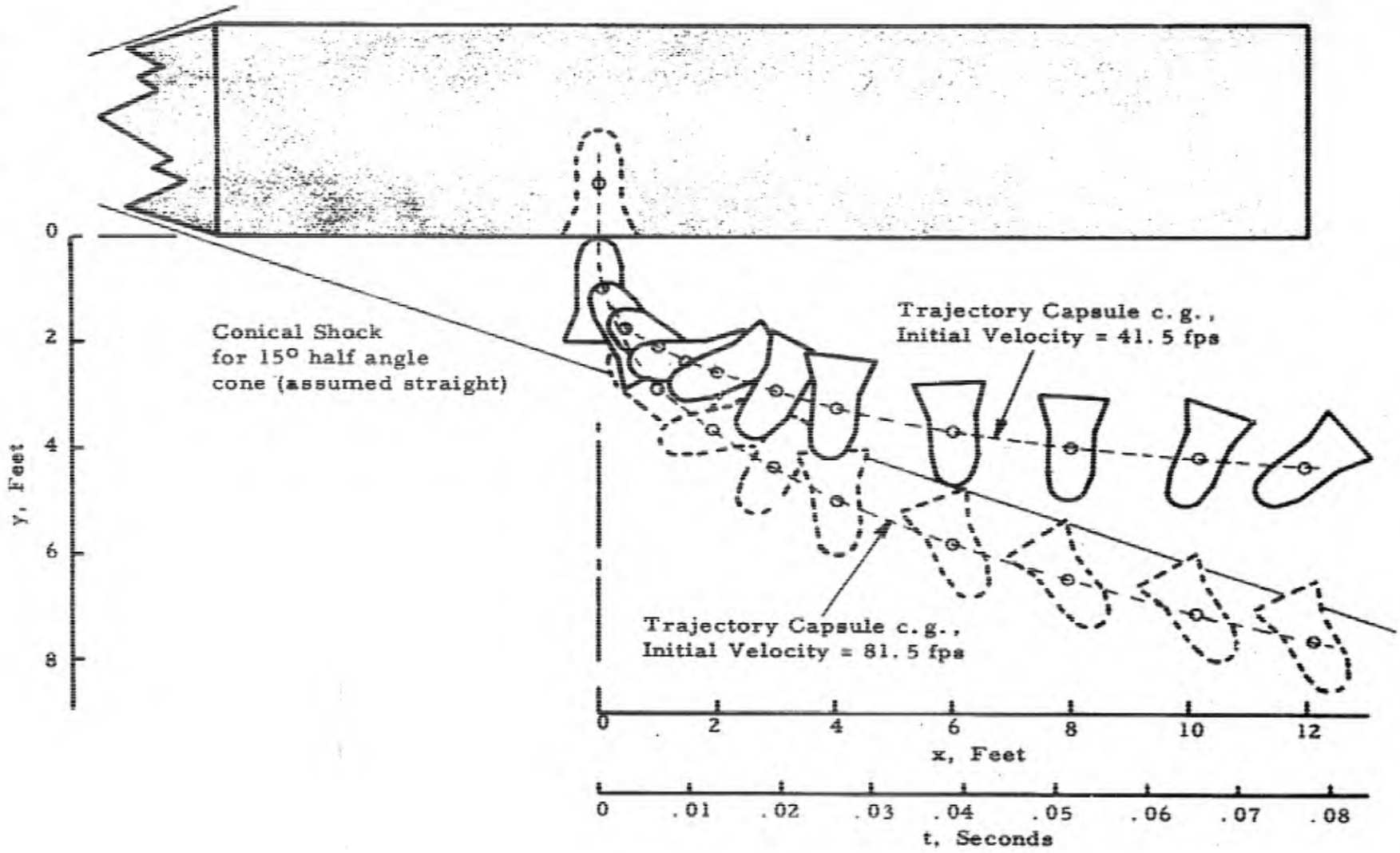

Figure 36. Separation Trajectories Side Ejection of Flared Capsule in Normal Orientation, Standard Problem Configuration

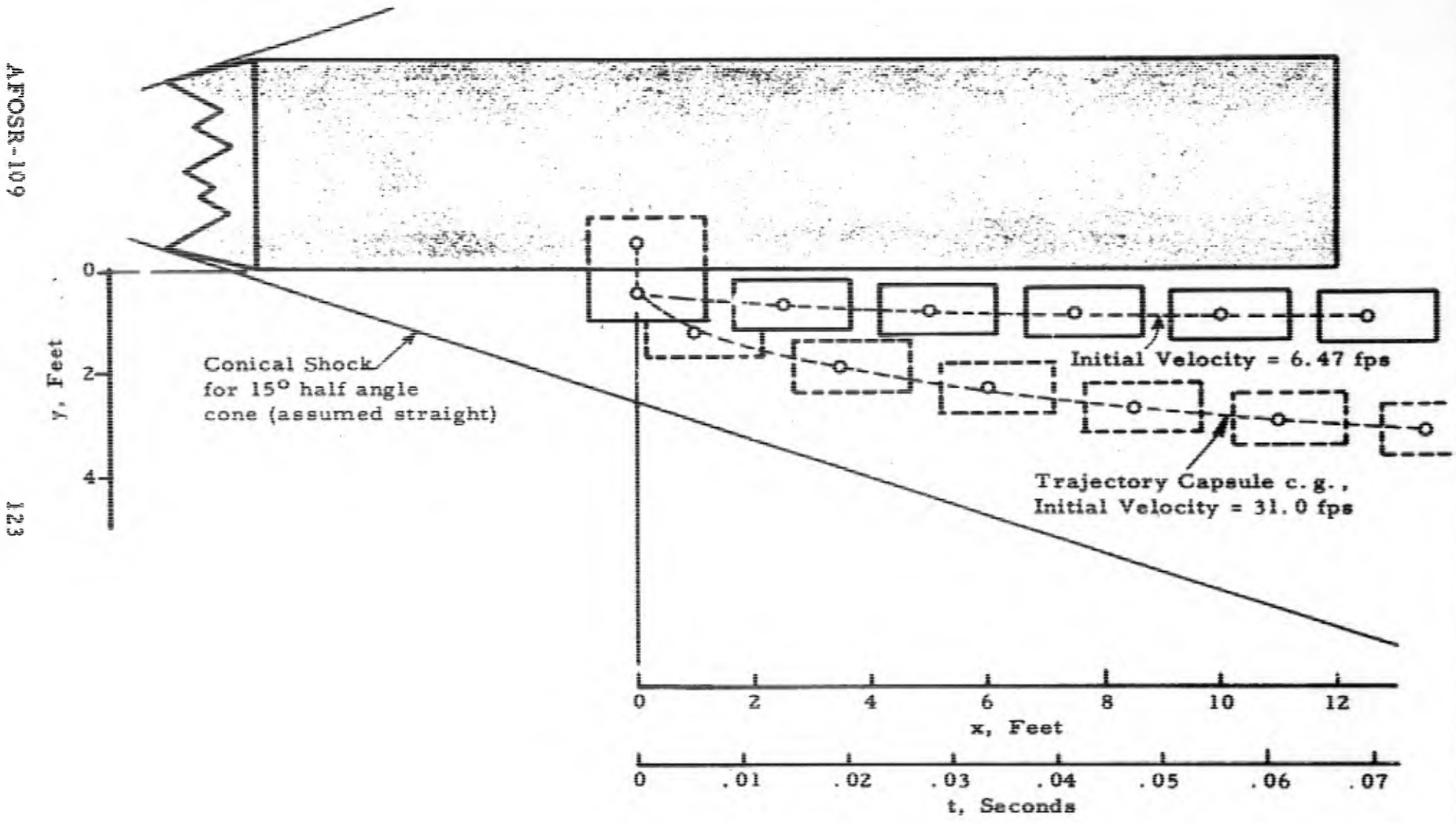

Figure 37. Separation Trajectories Side Ejection of Cylindrical Capsule in Parallel Orientation, Standard Problem Configuration

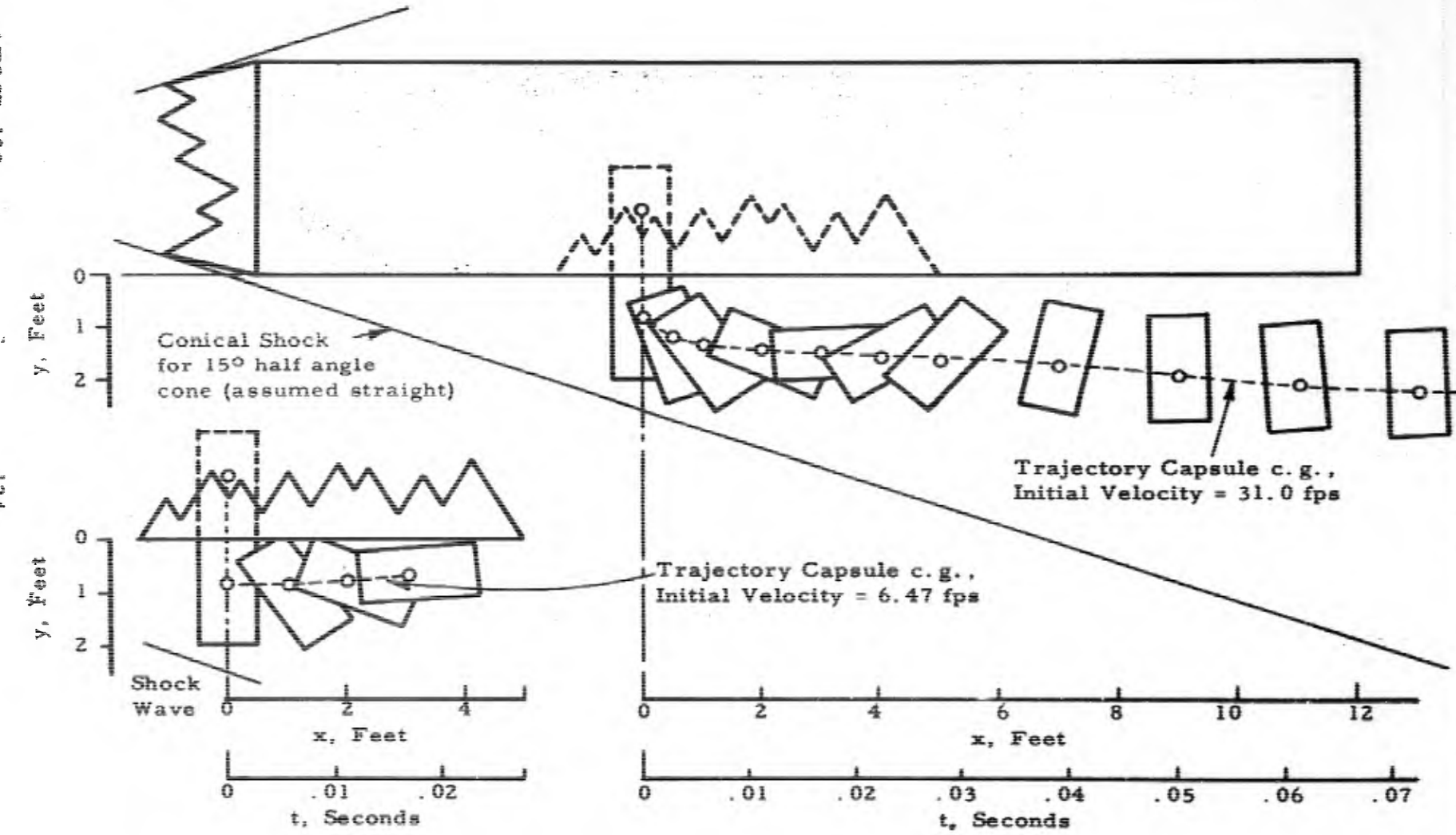

Figure 38. Separation Trajectories Side Ejection of Cylindrical Capsule in Normal Orientation, Standard Problem Configuration

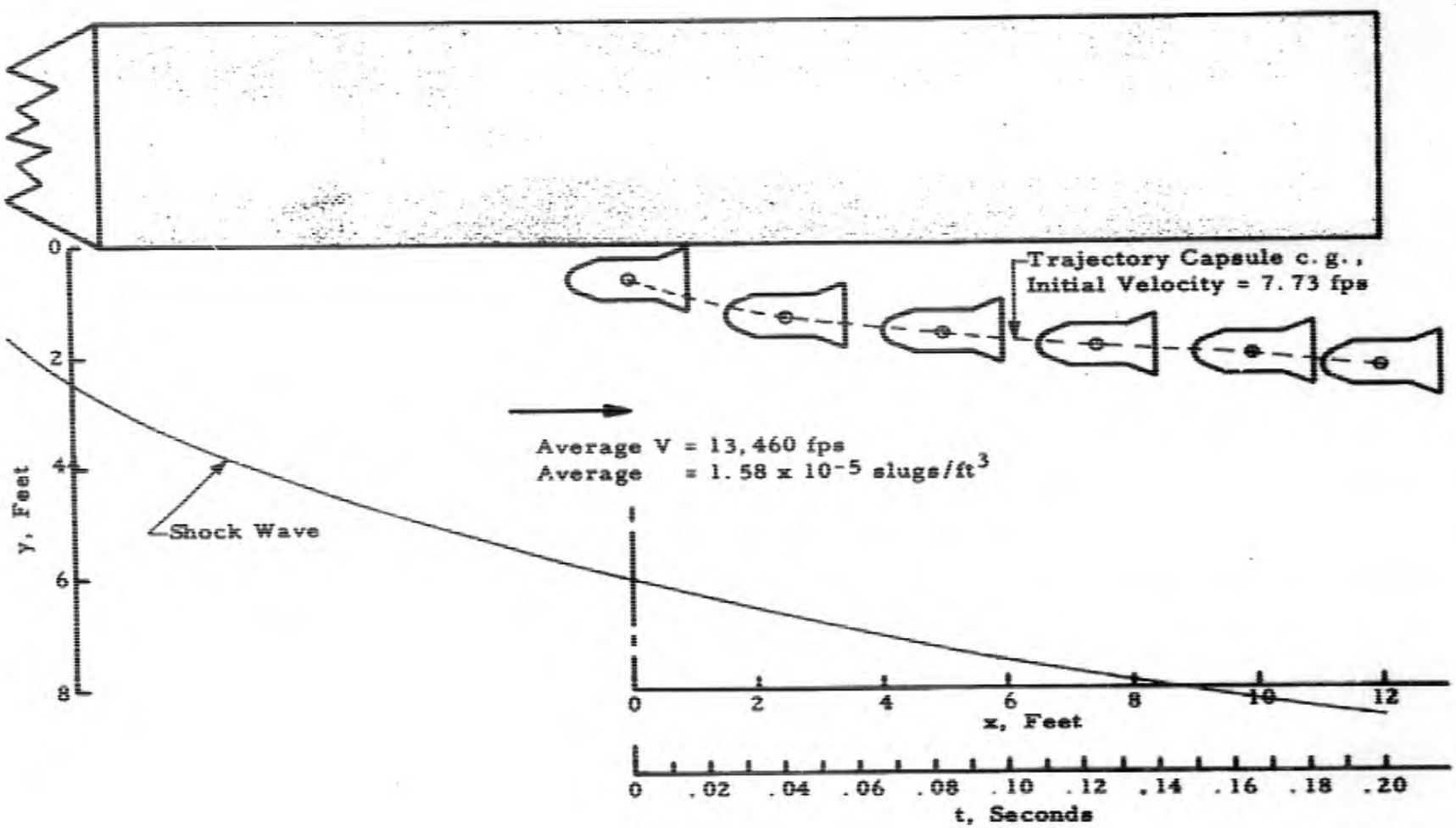

Figure 39. Separation Trajectory Side Ejection of Flared Capsule in Parallel Orientation, Mach 15.0 Problem Configuration, Uniform Flow Field Assumed - Blunt Nosed Carrier Vehicle

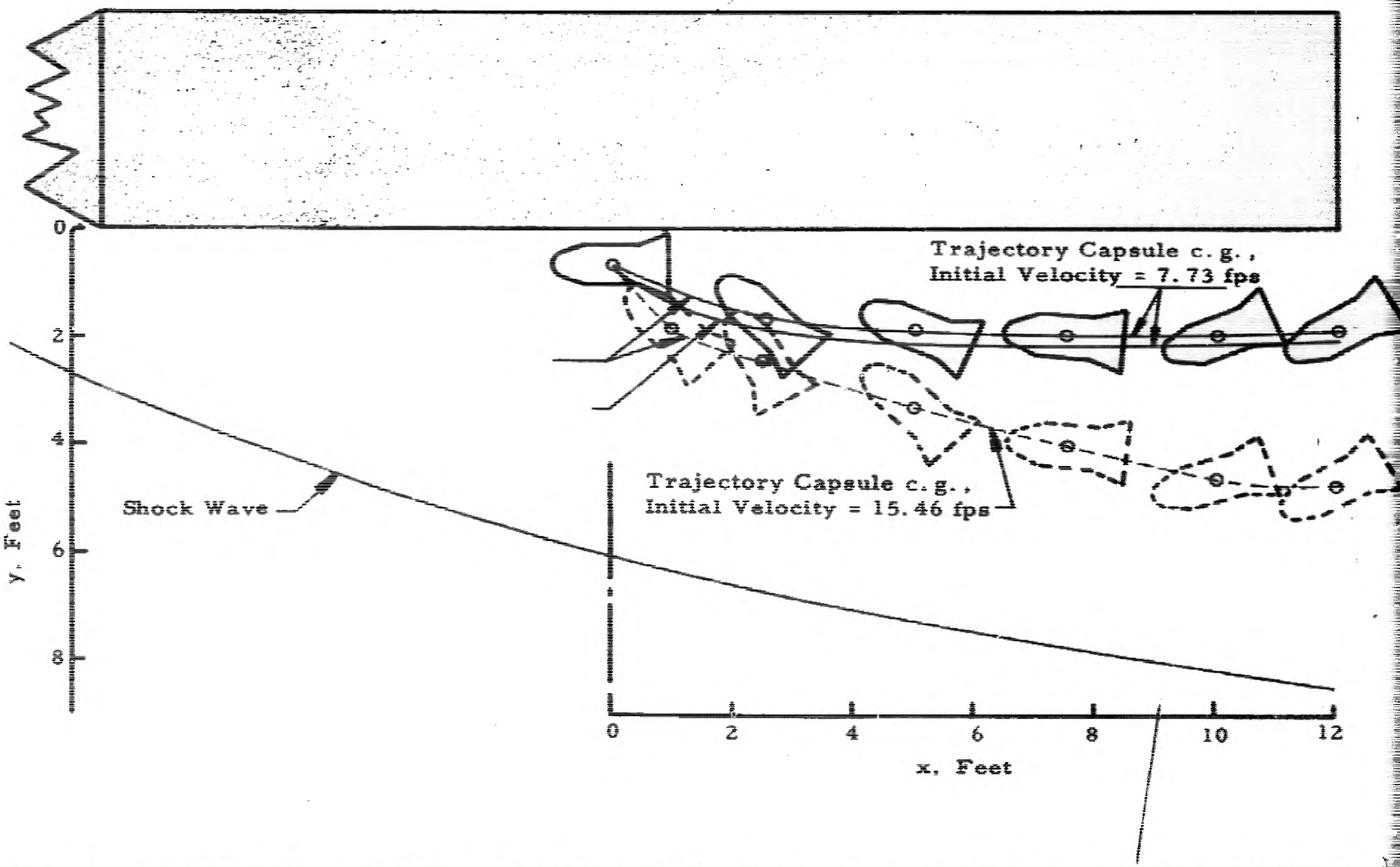

Figure 40. Separation Trajectories Side Ejection of Flared Capsule in Parallel Orientation, Mach 15.0 Problem Configuration, Nonuniform Flow Field, Blunt Nosed Carrier Vehicle

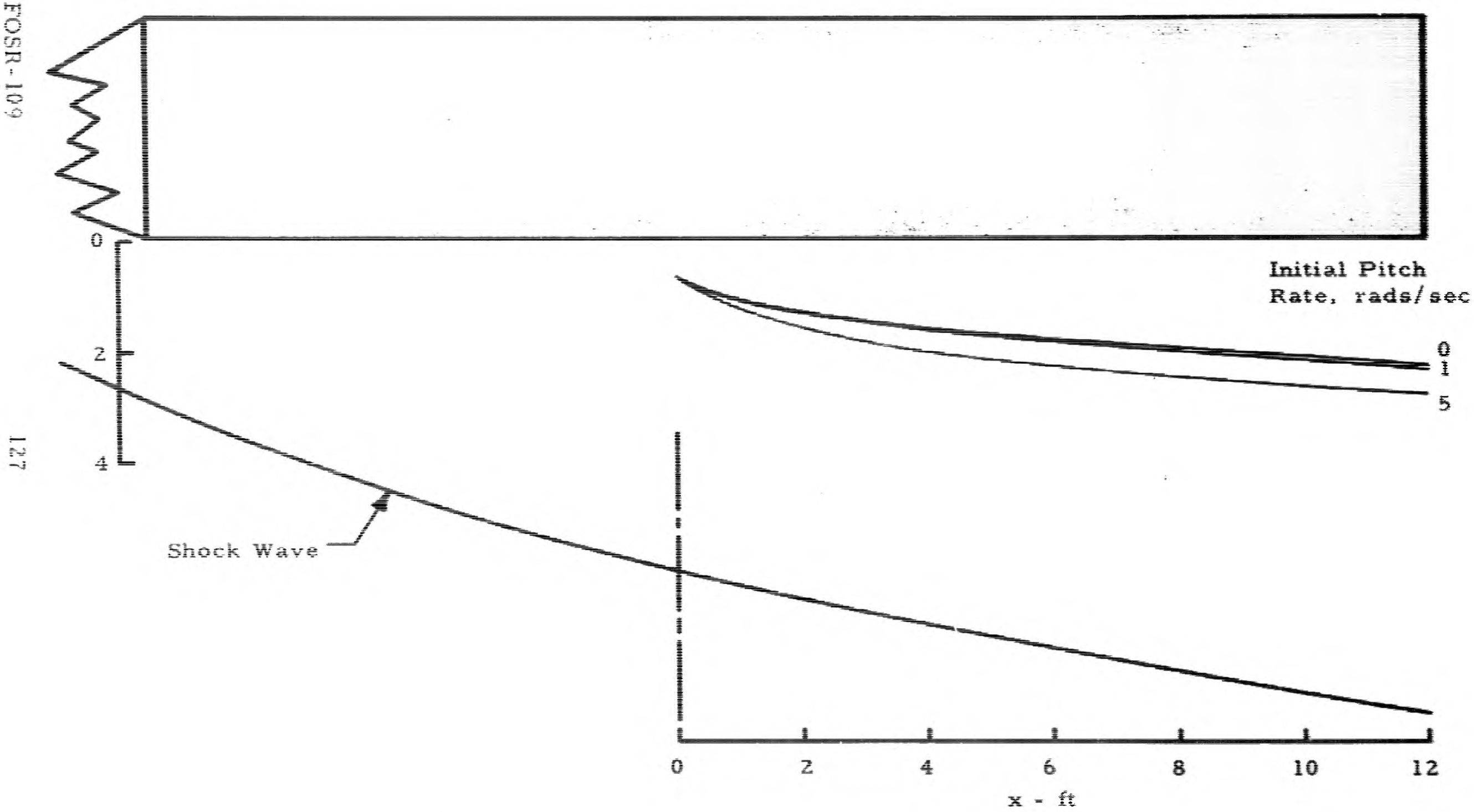

Figure 41. Trajectories of Flared Capsule Center of Gravity as Function of Initial Pitch Rate; Parallel Orientation, Nonuniform Flow Field, Blunt Nosed Body Initial Ejection Velocity, 7.73 ft/sec.

SECTION VI

CONCLUSIONS

Conclusions which have been derived from the theoretical study of separation dynamics are summarized in this section. The results reported herein are indicative of realistic trends and are amenable to (recommended) experiment and improvement. Characteristics of the ejection environment are first summarized. The ejection and separation process is discussed in terms of the problem parameters relative to pertinent combinations of capsule type and carrier ejection region.

In the supersonic range, say up to Mach number 7.0, flow fields around pointed bodies approach uniform conditions at distances aft of the body nose of 4 to 6 body diameters, with values of Mach number and dynamic pressure slightly reduced from free stream values. Blunt nosed body flow fields approach approximately free stream static pressures at distances aft of the nose of about 6 body diameters. At hypersonic Mach numbers, for blunt nosed bodies of practical length, the Mach number in the side flow field does not appreciably exceed 5.0 at any point.

Of chief interest are two capsule types, the cylinder and the hemisphere-cone-flared cylinder. Conical configurations have been considered in nose separation. The flared capsule is pertinent in nose separation and in side and base ejections; it has been treated in detail in the side ejection case. The cylinder has been examined both in side and base ejections.

The thrust required for nose separation is within the capability of feasible explosive devices. When directed through the nose center of gravity at an angle which is neither axial nor transverse such explosive thrust may be inefficiently employed. A preferred alternative is to direct this thrust transversely to the nose axis if lateral acceleration limits are not exceeded by such a technique. Friction, which would arise between the nose-carrier vehicle contact surfaces, would be minimized by means of roller bearings, for example. A linear correlation on dynamic pressure is found to exist in establishing thrust requirements in nose separation.

In base separation the angle of ejection is again critical. The greatest requirements on the ejection system (thrust) occur for ejection along the wake core, especially at large values of carrier deceleration. Required ejection velocity decreases materially if the combination of ejection angle and capsule stowed position results in wake penetration ahead of the wake throat. In wake

core ejection the relative deceleration effects of carrier weight-to-drag ratio increasing and capsule weight-to-drag decreasing act to reduce ejection velocity requirements, the carrier effect being greatest. When ejection results in wake penetration ahead of the throat the capsule weight-to-drag ratio effect reverses at a fixed value of carrier weight-to-drag ratio, since the external dynamic pressure field acts to resist more effectively entry of the higher drag and/or lower inertia configuration. Less positive, but nevertheless favorable, is the effect of increasing carrier weight-to-drag ratio.

Altitude and Mach number effects in axial base separation tend to correlate as a dynamic pressure effect. In angular ejection, however, a favorable Mach number effect arises. At constant free stream dynamic pressure increasing Mach number results in greater carrier vehicle shock losses and hence reduced intensity of the field exterior to the carrier vehicle wake. Penetration, therefore, is less difficult.

A model of the base flow field, which has not been reflected in the analyses which led to the above (nevertheless valid) conclusions, but which is deserving of further consideration and experimental verification has been advanced in this report. Within the recirculation region of the wake reverse flow occurs which is most significant at low Mach numbers. A buoyancy effect arises most importantly when base pressaure is zero and recompression pressure is a maximum. If the integrated effect (with time) of reverse flow and adverse pressure gradient becomes comparable to the margin provided an ejected capsule by a given ejection velocity then these factors may not be disregarded in assessing ejection system requirements.

The prominent aspect of side separation is its sensitivity to initial conditions of ejection, i.e., to capsule angle of attack and pitch rate at completion of the partial exposure phase. If the technique of ejection and/or related ejection devices can be designed to provide, initially, an angle of attack or an angular rate favorable for separation the resultant effect could override the unfavorable effects of locally non-uniform flow fields. The framework of initially zero angle of attack and pitch rate has been employed in the analyses of the effects of other parameters in side ejection.

Effects of capsule orientation in side ejection are compared for cylindrical and flared capsules. The latter configuration has the less severe ejection system requirements at moderate to high dynamic pressure. Normal orientation imposes, in terms of ejection velocity (and force) the lowest requirement on the ejection system. However, the moments imposed on a capsule when ejected in attitude normal to the carrier vehicle motion are very

much greater than those characteristic of parallel orientation. Consequently capsule strength requirements in beriding (and the strength of the restraint system) are proportionately high and may be crucial in selection of orientation mode.

Capsule type is more or less important with respect to the other side separation parameters. The effect of carrier acceleration is negligible for all types. Capsule weight-to-drag ratio affects force required moderately in the upper range of the parameter, principally through the weight term. Friction coefficient is most significant for the cylinder in normal orientation and for the flared body in parallel orientation. Mach number and altitude effects tend to correlate as a free stream dynamic pressure effect in the supersonic range around Mach 5.0. At hypersonic Mach numbers the loss in dynamic pressure suffered across the carrier vehicle bow shock wave invalidates this correlation.

The effect of flow non-uniformity, which arises importantly in the hypersonic range, is small measured in terms of capsule trajectory characteristics. Large angular motion is revealed, however, when the assumption of flow uniformity is removed.

REFERENCES

1. Von Karman, T.H., and Moore, N.B., "Resistance of Slender Bodies Moving with Supersonic Velocities with Specific Reference to Projectiles," Transactions ASME 54, 1932

2. Van Dyke, M., "First and Second Order Theory of Supersonic Flow Past Bodies of Revolution," JIAS, Vol. 18, p 161, 1951

3. Sears, W.R., Editor, High Speed Aerodynamics and Jet Propulsion, Vol. VI, Princeton University Press, 1954

4. Ferri, A., Elements of Aerodynamics of Supersonic Flows, 1949

5. Gravalos, F.G., Edelfelt, I.H., and Emmons, H., The Supersonic Flow About a Blunt Body of Revolution for Gases at Chemical Equilibrium, 9th Annula Congress, International Astronautical Federation, Amsterdam, August 25-29, 1958

6. Liepmann, H.W., and Lapin, E., Summary of Characteristic Methods for Steady State Supersonic Flows, Douglas Aircraft Co., Report No. SM-13343, May 1949

7. Clippinger, R.F., Giese, J.H., and Carter, W.C., "Tables of Supersonic Flows About Cone Cylinders," Part II, Complete Flows, BRL Report No. 730, August 1950

8. Lees, L., "Recent Developments in Hypersonic Flow," Jet Propulsion Vol. 27, November 1957

9. Bogdonoff, S.M., and Vas, I.E., "Preliminary Investigations of Spiked Bodies at Hypersonic Speeds," JIAS, Vol. 26, February 1959

10. Wang, C.T., Applied Elasticity, McGraw-Hill Book Co., 1953

11. Powers, W.E. Stetson, K.F., and Adams, M.C., "A Shock Tube Investigation of Heat Transfer in the Wake of a Hemisphere-Cylinder, with Applications to Hypersonic Flight," IAS, Report No. 59-35, January 1959

REFERENCES (cont'd)

12. Chapman, D. R., An Analysis of Base Pressure at Supersonic Speeds and Comparison with Experiment, NACA TN2137, July 1950

13. Chapman, D. R., Kueh, D. M., and Larson, H. K., Investigation of Separated Flows in Supersonic and Subsonic Streams with Emphasis on the Effect of Transition, NACA TN 3869, March 1957.

14. Crocco, L., and Lees, L., "A Mixing Theory for the Interaction Between Dissipative Flows and Nearly Isentropic Streams", JIAS, Vol. 19, No. 10, October 1952

15. Korst, H. H., "A Theory for Base Pressures in Transonic and Supersonic Flow", Journal of Applied Mechanics, Vol. 23, 1956

16. Love, E. S., Base Pressure at Supersonic Speeds on Two-Dimensional Airfoils and on Bodies of Revolution, with and without Fins Having Turbulent Boundary Layers, NACA TN 3819, January 1957

17. Fuller, L., and Reid, J., Experiments on Two-Dimensional Base Flow at M = 2.4, ARC Tech, Rep. R & M No. 3064, February 1956.

18. Rouse, H., "Diffusion in the Lee of a Two-Dimensional Jet", Proceedings IXth International Congress of Applied Mechanics, Vol. I, Brussels, 1957.

19. Charwat, A. F., and Yakura, J. K., "An Investigation of Two-Dimensional Supersonic Base Pressures", JIAS Vol. 25, No. 2, February 1958.

20. Hastings, R. C., A Note on the Interpretation of Base Pressure Measurements in Supersonic Flows, RAE Tech, Note Aero 2572, June 1958

21. Napolitano, L. G., Critical Study of the Adequacy of Integral Methods in Plane Mixing Problems, Polytechnic Institute of Brooklyn, PIBAL Report No. 425, December 1957

22. Boehler, G. D., and Spindler, R. J., Aerodynamic Theory of the Annular Jet, Part I, Aerophysics Company Report AR 581-R, Washington, D. C., December 1958

23. Pai, S. I., Fluid Dynamics of Jets, D. Van Nostrand Company, New York, 1954

24. Birkhoff, G., and Zarantonello, E. H., Jets, Wakes, and Cavities, Academic Press, New York, 1957

25. Townsend, A. A., The Structure of Turbulent Shear Flow, Cambridge University Press, 1956

26. Goldstein, S., "Concerning Some Solutions of the Boundary Layer Equations in Hydrodynamics," Proc. Cambridge Phil. Soc., Vol. 26, 1930

27. Napolitano, L. G., Libby, P. A., and Ferri, A., "Recent Work on Mixing at the Polytechnic Institute of Brooklyn," Combustion and Propulsion, Third Agard Colloquium, Pergamon Press, New York, 1958

28. Bogdonoff, S. M., "A Preliminary Study of Reynolds Number Effects on Base Pressure at M = 2.95," JIAS, Vol. 19, No. 3, March 1952

29. Kavanau, L. L., "Base Pressure Studies in Rarefied Supersonic Flows," JIAS, Vol. 23, No. 3, March 1956

30. Kavanau, L. L., "Results of Some Base Pressure Experiments at Intermediate Reynolds Numbers with M = 2.84," JIAS, Vol. 21, No. 4, April 1954

31. Van Hise, V., Investigation of Variation in Base Pressure Over the Reynolds Number Range in Which Wake Transition Occurs for Nonlifting Bodies of Revolution at Mach Numbers from 1.62 to 2.62, NACA TN 3942, January 1957

32. Lehnert, R., and Schermerhorn, V. L., "Correlation of Base Pressure and Wake Structure of Sharp and Blunt Nose Cones with Reynolds Number Based on Boundary Layer Momentum Thickness," JIAS, Vol. 26, No. 3, March 1959

33. Nicholson, H. M., and Fields, J. P., "Some Experimental Techniques to Investigate the Mechanism of Flame Stabilization in the Wake of Bluff Bodies," Third Sumposium on Combustion, Flame and Explosion Phenomena, Williams and Wilkins Company, 1949

34. Westenberg, A. A., Berl, W. G., and Rice, J. L., Studies of Flow and Mixing in the Recirculation Zone of Baffle Type Flameholders, Proceedings of the Gas Dynamics Symposium on Aerothermochemistry, Northwestern University, 1955

35. Lange, R. H., Present Status of Information Relative to the Prediction of Shock-Induced Boundary-Layer Separation, NACA TN 3065, February 1954

36. Chapman, D. R., Laminar Mixing of a Compressible Fluid, NACA Rep. 958, 1950

37. Schlichting, H., Boundary Layer Theory, Pergamon Press, New York, 1955

38. Liepmann, H. W., and Laufer, J., Investigations of Free Turbulent Mixing, NACA TN 1257, August 1947

39. Korst, H. H., Page, R. H., and Childs, M. E., A Theory for Base Pressures in Transonic and Supersonic Flow, TN 392-2, University of Illinois, Engr. Exp. Sta., Mech. Engr. Dept., March 1955

40. Howarth, L., Editor, "Modern Developments in Fluid Dynamics," High Speed Flow, Vol. II, Oxford at the Clarendon Press, 1953

41. Heinrich, H. G., Theoretical Parachute Investigations, Progress Report 7, University of Minnesota, Aeronautical Engineering Department, November 1958

42. Anonymous, "Design for Survival," Machine Design, Vol. 31, pp. 22 to 25, March 5, 1959

43. Hoerner, S. F., Fluid Dynamic Drag, 1958

44. Broderick, M. A., and Turner, R. D., Design Criteria and Techniques for Deployment and Inflation of Aerodynamic Drag Devices, ASD Technical Report 61-188, Cook Research Laboratories, May 1961

45. Swain, L. M., On the Turbulent Wake Behind a Body of Revolution, Proc. Roy. Soc. London, A 125, 1929

46. Potter, Leith J., Murphree, William D., and Shapiro, Norman M., "Normal Force and Center of Pressure on Right Circular Cylinders," JIAS, (Readers' Forum) Vol. 22, No. 3, pp. 214-215, March 1955

47. Felix, R. A., and Lundy, T. E., Static Stability Characteristics of a High Drag Re-entry Configuration, ABMA Report No. DA-TN-72-5B

48. Dennis, David H., The Effects of Boundary-Layer Separation Over Bodies of Revolution with Conical Tail Flares, NACA RM A57130

49. Tobak, Murray, Reese, Jr., David E., and Beam, Benjamin H., Experimental Damping in Pitch of 45° Triangular Wings, NACA RM A50J26

50. Moeckel, W. E., Flow Separation Ahead of Blunt Bodies at Supersonic Speeds, NACA TN 2418

51. Penland, J. A., Aerodynamic Characteristics of a Circular Cylinder at Mach Number 6.86 and Angles of Attack up to 90°, NACA TN 3861

52. Armes Research Staff, Equations, Tables, and Charts for Compressible Flow, NACA TR 1135

53. Moskowitz, B., Approximate Theory for Calculation of Lift of Bodies, Afterbodies, and Combinations of Bodies, NACA TN 2669.

APPENDIX

EQUATIONS OF MOTION

The separation conditions and trajectories pertinent to the present study are sufficiently diverse and unconventional as to make expedient the development of equations of motion specifically appropriate in the particular case. In base separation, for example, the motion of the ejected body is analyzed either in one-degree-of-freedom or three-degree-of-freedom depending upon the angle of ejection. This appendix presents the motion equations employed in the study of:

(1) Nose separation

(2) Capsule ejection from the carrier vehicle base

(3) Capsule ejection from the carrier vehicle side.

A. Nose Separation Equations of Motion

Separation of the nose of a missile from the afterbody is initiated by a thruster unit mounted at the nose base. The force provided by the thruster can operate in any arbitrary direction from any point in the base.

The calculation of the separation dynamics involves three-degree-of-freedom computations for the nose and for the afterbody. The force between the nose and afterbody is calculated while they are in contact and appears in each set of motion equations. In addition, friction forces which result from the sliding of the nose against a shoulder of the afterbody are included.

Aerodynamic force coefficients for both the nose and the afterbody are computed as functions of angle of attack. The change in Mach number during the separation process is small so that change of these coefficients with Mach number can be neglected. As separation proceeds, the front face of the afterbody becomes exposed. The aerodynamic force coefficients associated with the afterbody vary, therefore, as functions of the linear and angular displacements of the nose and afterbody.

The motion is represented with respect to earth fixed coordinate axes, x horizontal and y positive upward. The origin of the inertial frame can be chosen for simplicity. For convenience, a second moving frame, (ξ, η), is employed.

This frame is rigidly attached to the nose center of gravity, with ξ lying along the longitudinal axis, positive forward, and η, completing a right-handed system in the plane of rotation. These axes are indicated in Figure A-1.

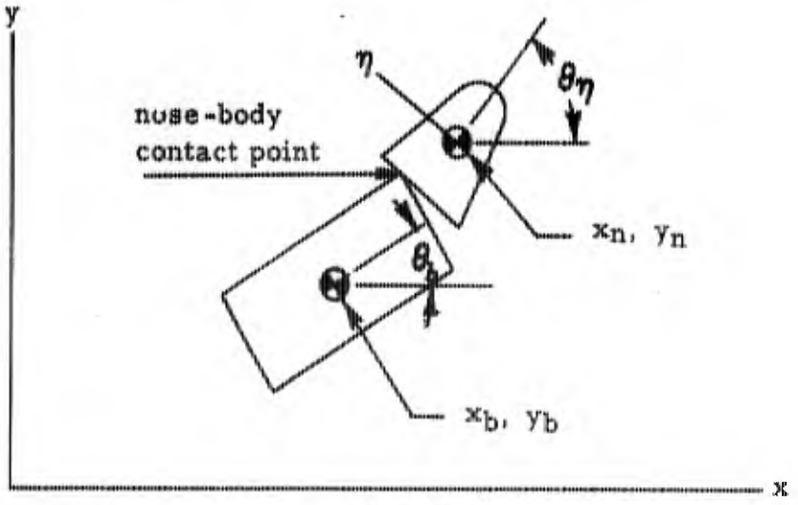

Fig. A-1

The equations of motion of the nose are:

$$m_n \ddot{x}_n = - C_{A_n} A_n \frac{\rho}{2} V_n^2 \cos \theta_n - C_{N_{a_n}} a_n \frac{\rho}{2} V_n^2 A_n \sin \theta_n$$

$$+ F_{n_b} (\cos \theta_n + \mu \sin \theta_n) + T \cos (\theta_n + \tau_T)$$

$$m_n \ddot{y}_n = - C_{A_n} A_n \frac{\rho}{2} V_n^2 \sin \theta_n + C_{N_{a_n}} a_n \frac{\rho}{2} V_n^2 A_n \cos \theta_n$$

$$- m_n g + F_{n_b} (\sin \theta_n - \mu \cos \theta_n) + T \sin (\theta_n + \tau_T)$$

$$I_n \ddot{\theta}_n = + C_{M_{a_n}} a_n A_n \frac{\rho}{2} V_n^2 d_n + C_{M_{q_n}} \frac{\dot{\theta}_n d_n}{2V_n} A_n d_n \frac{\rho}{2} V_n^2$$

$$+ C_{M_{\dot{a}_n}} \frac{\dot{a}_n d_n}{2V_n} A_n d_n \frac{\rho}{2} V_n^2 - F_{n_b} (\eta_s + \mu \xi_s)$$

$$+ T (\xi_T \sin \tau_T - \eta_T \cos \tau_T)$$

where F_{n_b} is the contact force between the nose and afterbody, and

$$V_n = (\dot{x}_n^2 + \dot{y}_n^2)^{1/2}$$

The equations of motion for the unpowered afterbody are represented in terms of the same fixed coordinate system. These equations are:

$$m_b \ddot{x}_b = -(C_{A_b} + \Delta C_{A_b})\, A_b \frac{\rho}{2} V_b^2 \cos\theta_b - (C_{N_{a_b}} \alpha_b + \Delta C_{N_b})\, A_b \frac{\rho}{2} V_b^2 \sin\theta_b$$

$$- F_{n_b} (\cos\theta_n + \mu \sin\theta_n)$$

$$m_b \ddot{y}_b = -(C_{A_b} + \Delta C_{A_b})\, A_b \frac{\rho}{2} V_b^2 \sin\theta_b + (C_{N_{a_b}} \alpha_b + \Delta C_{N_b})\, A_b \frac{\rho}{2} V_b^2 \cos\theta_b$$

$$- m_b g - F_{n_b} (\sin\theta_n - \mu \cos\theta_n)$$

$$I_b \ddot{\theta}_b = +(C_{M_{a_b}} \alpha_b + \Delta C_{M_b})\, A_b d_b \frac{\rho}{2} V_b^2 + (C_{M_{q_b}} + \Delta C_{M_{q_b}})\, A_b d_b \frac{\rho}{2} V_b^2 \frac{\dot{\theta}_b d_b}{2V_b}$$

$$+ (C_{M_{\dot{\alpha}_b}} + \Delta C_{M_{\dot{\alpha}_b}})\, A_b d_b \frac{\rho}{2} V_b^2 \frac{\dot{\alpha}_b d_b}{2V_b}$$

$$+ F_{n_b} \left\{ \left[\cos(\theta_n - \theta_b) + \mu \sin(\theta_n - \theta_b) \right] \frac{d_b}{2} \right.$$

$$\left. + \left[\mu \cos(\theta_n - \theta_b) - \sin(\theta_n - \theta_b) \right] h_b \right\}$$

where, in this case, all moment coefficients are referenced to the nose or vehicle diameter, and:

$$V_b = (\dot{x}_b^2 + \dot{y}_b^2)^{1/2}$$

The symbols employed in the above equations are defined in the List of Symbols. If the afterbody is powered, appropriate thrust terms can be added

to the afterbody equations. Certain remarks about these representations of the motion equations and the kinematical relations employed follow.

The aerodynamic force coefficients employed in both body and nose equations are conventional. The differential coefficeint terms involved in the body equations represent the effects of nose displacement. For example, consider axial force coefficient of the body, $(C_{A_b} + \Delta C_{A_b})$. With the nose in its normal position, the quantity C_{A_b} represents the entire axial force acting on the afterbody; ΔC_{A_b} is zero. As the nose is removed from the afterbody, the term, ΔC_{A_b} becomes finite, increasing in magnitude in proportion to the amount of afterbody frontal area which becomes exposed. For computational purposes ΔC_{A_b} has been taken proportional to $(\theta_n - \theta_b)$, the difference in attitude angles, and to η_s, the lateral position of the nose-afterbody contact point measured in the nose-attached coordinate system. Similar considerations apply to the other differential coefficients. Some of the incremental terms in the above expression, such as $\Delta C_{M_{t_b}}$, are almost impossible to determine or will be of such a magnitude to allow them to be neglected. A discussion of interference effects is contained in section IV.C.1 of this report.

The magnitude of the thrust which is employed to initiate separation is represented by the term T. The thrust axis is assumed to be inclined at an angle, τ_T, to the longitudinal axis, and the quantities, (ξ_T, η_T), are coordinates of the point at which the thrust is effective (see Figure A-2).

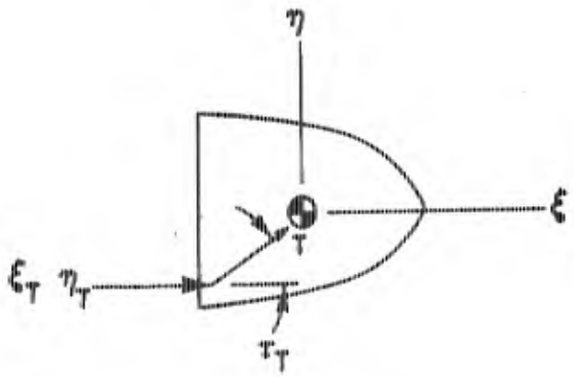

In general, as the nose slides on the afterbody, contact is maintained between the flat, rear face of the nose and the edge (shoulder) of the afterbody. In the absence of friction the force between the afterbody and the nose is normal to the flat rear face of the nose, i.e., parallel to the longitudinal axis

of the nose. The sign on the friction force, μF_{n_b}, is determined from the velocities along the η axis of the contact points on nose and shoulder of the afterbody, positive when the velocity in the inertial frame of the contact point on the nose is greater than that of the contact point on the afterbody, negative when otherwise. When there is no relative velocity, the friction force is zero.

At each step of the computation the absolute value of the coordinate of the afterbody shoulder, $|\xi_s|$, is computed. When this absolute value exceeds the distance from the nose center of gravity to the nose base, separation has occurred and the force F_{n_b} becomes zero. Also, the η coordinate of the afterbody shoulder is computed at each step. When the absolute value of this coordinate exceeds the radius of the nose base, separation has also occurred and the force F_{n_b} drops to zero.

The coordinates of the shoulder of the afterbody are given by

$$x_s = x_b + l_b \cos(\theta_b + \tau_b)$$

$$y_s = y_b + l_b \sin(\theta_b + \tau_b)$$

where

$$\tau_b = \tan^{-1} \frac{d_B}{2h_B},$$

a constant for a fixed afterbody center of gravity location and l_b is the distance from the center of gravity of the afterbody to the shoulder of the forward end where contact with the nose cone is established:

$$l_b = \sqrt{h_B^2 + \left(\frac{d_B}{2}\right)^2}$$

where h_B is the distance from the center of gravity to the forward end of the afterbody measured along the longitudinal axis and d_B is the afterbody diameter.

The ξ and η coordinates of the afterbody shoulder are given by

$$\xi_s = (x_s - x_n)\cos\theta_n + (y_s - y_n)\sin\theta_n$$

$$\eta_s = (y_s - y_n)\cos\theta_n - (x_s - x_n)\sin\theta_n$$

while contact is maintained.

The force F_{n_b}, the "knife-edge" contact force between the nose and afterbody normal to the base of the nose, is computed by employing kinematical relationships to relate the components of acceleration of the contact points. The accelerations of the contact points in the direction of the longitudinal axis of the nose are equated yielding a relationship between accelerations of the nose and of the body. Substitution of the nose and body equations in this relation yields an equation for F_{n_b} in terms of velocities and position coordinates. This relation is solved for F_{n_b} and employed to compute the normal force between nose and afterbody at each step of the computations.

The force F is given by

$$\begin{aligned}
F_{n_b} = \Bigg\{ & (C_{A_b} + \Delta C_{A_b}) \frac{\rho}{2m_b} V_b^2 A_b \cos(\theta_n - \theta_b) \\
& - (C_{N_{a_b}} a_b + \Delta C_{N_b}) A_b \frac{\rho}{2m_b} V_b^2 \sin(\theta_n - \theta_b) \\
& + \sin(\theta_n - \theta_b - \tau_b) \frac{l_b}{I_b} \Big[(C_{M_{a_b}} a_b + \Delta C_{M_b}) A_b d_b \frac{\rho}{2} V_b^2 \\
& + (C_{M_{q_b}} + \Delta C_{M_{q_b}}) \frac{\dot\theta_b d_b}{2V_b} \frac{\rho}{2} V_b^2 A_b d_b + (C_{M_{\dot a_b}} + \Delta C_{M_{\dot a_b}}) \frac{\dot a_b d_b}{2V_b} \frac{\rho}{2} A_b d_b V_b^2 \Big] \\
& + l_b \dot\theta_b^2 \cos(\theta_n - \theta_b - \tau_b) - C_{A_n} A_n \frac{\rho}{2m_n} V_n^2 + \frac{T\cos\tau_T}{m_n} \\
& - \frac{l_{n_s}}{I_n} (C_{M_{a_n}} a_n \frac{\rho}{2} V_n^2 A_n d_n + C_{M_{q_n}} \frac{\dot\theta_n d_n}{2V_n} \frac{\rho}{2} V_n^2 A_n d_n \\
& + C_{M_{\dot a_n}} \frac{\dot a_n d_n}{2V_n} \frac{\rho}{2} V_n^2 A_n d_n - T\eta_T) \sin\tau_s + l_{n_s} \dot\theta_n^2 \cos\tau_s \Bigg\} \div \\
& \Bigg\{ \frac{l_b}{I_b} \sin(\theta_n - \theta_b - \tau_b) \Bigg(\Big[\cos(\theta_n - \theta_b) + \mu \sin(\theta_n - \theta_b) \Big] \frac{d_b}{2} \\
& + \Big[\mu\cos(\theta_n - \theta_b) - \sin(\theta_n - \theta_b) \Big] h_b \Bigg) - \frac{1}{m_n} - \frac{1}{m_b} + \frac{l_{n_s}}{I_n} \sin\tau_s (\eta_s + \mu\xi_s) \Bigg\}
\end{aligned}$$

where l_b and τ_b were previously defined and

$$l_{n_s} = \sqrt{\eta_s^2 + \xi_s^2},$$

the distance from the nose center of gravity to the contact point on the afterbody.

$$\tau_s = \tan^{-1} \frac{\eta_s}{\xi_s},$$

the angle between the nose longitudinal axis and the line of contact to the center of gravity of the nose.

B. Base Separation Equations

Base separation is accomplished in one of two ways. In the first procedure, the separating body is deployed down the wake core through the low energy portions of the wake. In the other procedure, the deployment angle is such that the separating body contacts the wake boundary between the vehicle base and the wake throat. The attempt in this case is to penetrate the wake boundary. The equations of motion pertinent in these cases are derived in the two subdivisions of this section.

1. Ejection Along Wake Core

This ejection process is described as one-dimensional linear motion. The equations derived for this case are general and provide for various combinations of ejected bodies. They are written for two (or possibly more) ejected bodies with the possibility of elastic interconnection between these bodies. In this case the equations representing the motions of the various bodies are solved simultaneously by numerical integration. In addition, provision has been made for elastic connection between the ejected body and the carrier vehicle. In cases where no interconnection exists, the spring constant associated with the elastic connection is taken as zero. Where only a single body is ejected, the differential equation for the second body is suppressed.

Of particular importance in the computations in this case are the wake flow static pressure and density variation. The variations of wake velocity, static pressure, and density with position relative to the vehicle

base are described by algebraic expressions. In the process of the computation, the density, static pressure and wake velocity are computed as a function of body position. The dynamic pressure is then obtained as a combination of these quantities and the body absolute velocity. A discussion of this representation is contained in sections IV. A. a. c and IV. D of this report.

The motion of the carrier vehicle, and all ejected bodies, is assumed to be along a line making a constant angle, θ_o, with the horizontal. The origin for the x axis is taken to be the point at which separation begins and is fixed in space. The equations of motion are now considered.

The equation for the carrier vehicle is:

$$m_v \ddot{x} = -(C_D A)_v \frac{\rho_\infty}{2} \dot{x}_v^2 + m_v g \sin\theta_o - K_p (x_v - x_p - \lambda_p)\left(1 + \frac{\dot{x}_v - \dot{x}_p}{k_p}\right)$$

$$- K_c (x_v - x_c - \lambda_c)\left(1 + \frac{\dot{x}_v - \dot{x}_c}{k_c}\right)$$

where

K_p is used if a pilot device is attached by lines to the vehicle

K_c is used if the capsule is attached by lines to the vehicle

θ_o is positive when measured downward from the horizontal.

These tension terms are zero except during line stretch, i.e., the interconnecting line cannot supply force to separate the bodies. The damping is taken proportional to both the separation velocity and the line tension.

The equation of motion for an ejected pilot device which is attached to a vehicle or capsule is given by

$$\left[m_p + \rho_p (x - x_p)\right] \ddot{x}_p = -(C_D A)_p \frac{\rho_w}{2} (\dot{x}_p - W)^2$$

$$+ \left[m_p + \rho_p (x - x_p)\right] g \sin\theta_o + K_p (x - x_p - \lambda_p)\left(1 + \frac{\dot{x} - \dot{x}_p}{k_p}\right)$$

where

$x = x_v$ when the vehicle is at the opposite end of the line

$x = x_c$ when the capsule is at the end of the line

ρ_p is the line density per unit length, slugs/ft

ρ_w is the air density of the flow field environment in the wake, slugs/ft^3

W is the local velocity of the wake relative to the space-fixed coordinate system.

When lines are employed, the mass term $\rho_p(x - x_p)$ is maximum at λ_p, or is equal to $\rho_p \lambda_p$ at the time when full extension of the unstretched length occurs. However, during the period of line stretch, $(x - x_p) \gg \lambda_p$, the effective mass of the lines is taken as $1/2\ \rho_p \lambda_p$. It should be noted that during the time of line extension the derivative

$$\frac{d}{dt}\left[m_p + \rho_p (x_v - x_p)\right] \dot{x}_p$$

has been taken as

$$\left[m_p + \rho_p (x_v - x_p)\right] \ddot{x}_p$$

since the lines are pulled out of the pack rather than being pushed out by a reaction force. The term $K_p(x_v - x_p - \lambda_p)$ is zero unless $(x_v - x_p - \lambda_p) > 0$.

If the pilot device is to increase its effective drag area, as - for example – with a small parachute or balloon, this increase in drag area can be initiated either at a predetermined time or at a predetermined distance aft of the carrier vehicle. The increase in drag or effectiveness can be made instantaneously or at a prescribed rate.

When this pilot device is employed to extract a capsule, the motion equation of the capsule is written:

$$\left[m_c + \rho_c (x_v - x_c)\right] \ddot{x}_c = - (C_D A)_c \frac{\rho_w}{2} (\dot{x}_c - W)^2$$

$$+ \left[m_c + \rho_c (x_v - x_c)\right] g \sin\theta_o - K_p (x_c - x_p - \lambda_p)(1 + \frac{\dot{x}_c - \dot{x}_p}{k_p})$$

$$+ K_c (x_v - x_c - \lambda_c) (1 + \frac{\dot{x}_v - \dot{x}_c}{k_c})$$

The terms $\rho_c (x_v - x_c)$ and $K_c (x_v - x_c - \lambda_c)$ are inserted to permit attachment of the capsule to the carrier vehicle or to a second capsule if desired. Considerations similar to those mentioned previously apply to these terms.

It should be mentioned that the terms representing tension forces in the connecting lines provide for a linear variation of tension with elongation. This can be varied to provide a quadratic variation during unloading thus representing a hysteresis loop in the connecting line material such as is common with nylon.

2. Ejection with Wake-Penetration

The physical circumstance which is represented is that of a capsule ejected rearward from the base of a carrier vehicle such that it encounters the wake boundary and attempts to cross it. As the capsule penetrates the wake boundary, the dynamic and static pressures to which it is exposed change. In particular, the principal resistance to penetration of the wake boundary results from the large static and dynamic pressure on those portions of the capsule which are external to the wake boundary. Hence, in the motion equations it is important to obtain accurately the areas exposed to these high pressure fields. In addition, it is necessary to represent accurately the wake density, velocity components, and static pressure as functions of position relative to the carrier vehicle base. This variation is represented in terms of distance aft of the vehicle base and distance above or below the vehicle longitudinal axis. The area exposed to the high pressure region is obtained by computing the coordinates of the points at which the capsule crosses the wake boundary. From these coordinates the projected areas of the capsule faces, both interior and exterior to the wake, are computed. In addition, the centroids of these areas are also computed for purposes of moment calculations.

As parts of the separating capsule emerge from the low energy region of the wake, large moments are imposed upon it. Consequently,

large angular accelerations may be anticipated. These large angular accelerations can seriously affect the relative velocity of air with respect to the faces of the separating body, depending of course on the exposure time and the moment of inertia of the body. This is considered in the formulation of the computation procedures. Eight faces of the body are considered, and the total relative velocity of these faces with respect to the air is computed as the vector sum of the velocity of the center of gravity of the capsule, the linear velocity of the face induced by rotation, and the wake velocity at the centroid of the face.

The equations representing three-degree-of-freedom motion of a capsule in the wake of a carrier vehicle are of themselves relatively straightforward. However, the representation of forces and moments on such a capsule is complex.

The notation used is similar to that given previously. In addition, the angle θ represents the angle between the capsule longitudinal axis and the space-fixed x axis. As before, the carrier vehicle motion is uniform along the x axis; Figure A-3 shows the axis system.

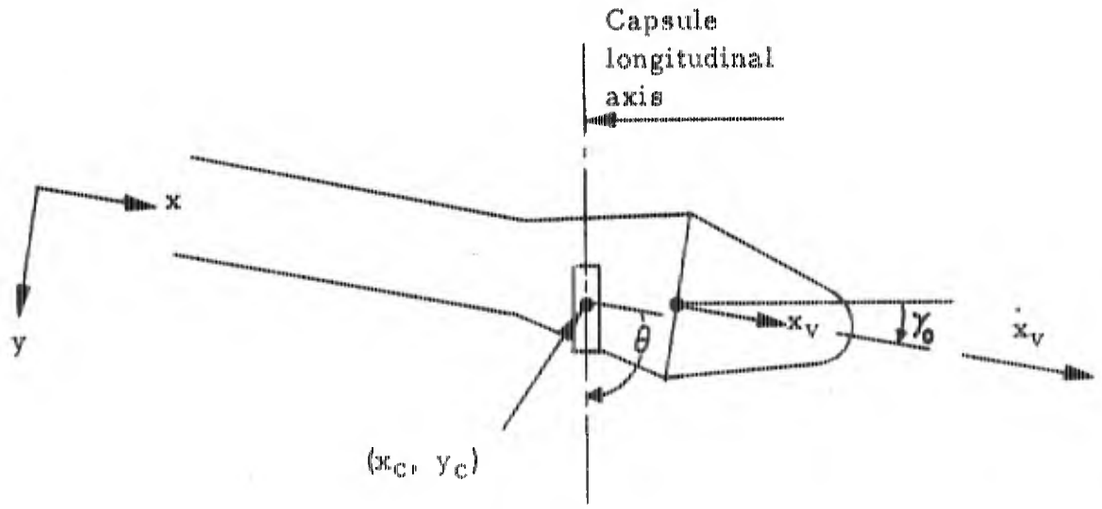

Fig. A-3

The equations of motion then become:

For the vehicle

$$m_v \ddot{x}_v = - (C_D A)_v \frac{\rho_\infty}{2} \dot{x}_v^2 + m_v g \sin \gamma_o$$

For the capsule

$$m_c \ddot{x}_c = F_x + m_c g \sin \gamma_o$$

$$m_c \ddot{y}_c = F_y$$

$$I_c \ddot{\theta} = M_{cg}$$

Again, in this case, motion is assumed to be along a fixed path angle. The direction of positive θ and positive moment M is assumed downward.

As mentioned previously, considerable complexity occurs in representing the forces and moments on the capsule during wake-penetration. Preliminary calculations indicate that high angular velocities of the capsule are to be anticipated during wake-penetration. Hence, in computing the linear velocity of each face of the capsule, account must be taken of the velocity induced by rotation. This rotationally-induced velocity will vary appreciably across a face. In the representation of forces and moments, this variation in velocity is accounted for by dividing the surface of the capsule into eight half faces. These half faces are determined by a plane normal to the x-y coordinate plane which includes the longitudinal axis and a second plane at right angles and passing through the capsule center of gravity which divides the capsule in halves longitudinally. The result is a capsule with two half faces each on the forward and aft ends and, for a cylindrical capsule, four half faces formed by the cylindrical section, each half the length of the body and semicircular in the other dimension - two half faces on the bottom of the capsule and two on the top. The velocity of each half face is taken to be the velocity of the centroid of the half face. The angle of attack of each half face is the angle of attack at the centroid. This analysis was conducted for bodies whose planes of symmetry are characterized by right angles between all faces, i.e., cylinders and rectangular shapes.

This involves, then, determining at each step of the calculation eight attitude angles, eight velocities, and at least eight angles of attack. Faces are designated 0, 1, 2, 3 and half faces by a plus or minus. In this notation, the absolute velocity of the centroid of half face j+ or j- is given by

$$\dot{x}_j = \dot{x}_c - K_j \dot{\theta} \sin(\theta + r_j)$$

$$\dot{y}_j = \dot{y}_c + K_j \dot{\theta} \cos(\theta + r_j) \qquad (j = 0, 1, 2, 3)$$

where K_j is the distance from the centroid of the half face to the capsule center of gravity and r_j is the angle between the longitudinal axis and the line from the center of gravity to the centroid of half face j+ or j-.

The air flow angle as seen at the centroidal points will vary depending upon whether the point is inside or outside the wake. Hence, it is necessary to compute these flow angles and angles of attack for conditions both inside - designated by a subscript w, and external to the wake - designated by a subscript E. Thus, for half face j+ or j-, the air flow angle, γ_{aj}, is given outside the wake by

$$\tan \gamma_{aj_E} = \frac{\dot{y}_j - W_y}{\dot{x}_j - W_x} \qquad (j = 0, 1, 2, 3)$$

and inside the wake by (assuming that transverse wake velocities are negligible)

$$\tan \gamma_{aj_w} = \frac{\dot{y}_j}{\dot{x}_j - W} \qquad (j = 0, 1, 2, 3)$$

Here W_x and W_y are velocity components of the air outside the wake at the centroid and W is the wake velocity along x at the centroid. These velocities, determined by a study of the wake structure, are programmed into the computation as functions of Mach number, distance aft of the parent vehicle, and distance from the wake boundary. Similar variations in static pressure, P_s, and density, ρ, were employed. The angles of attack of face j+ or j- are given by

$$a_{j_E} = \gamma a_{j_E} - (\theta + j\,\pi/2)$$

$$(j = 0,\ 1,\ 2,\ 3)$$

$$a_{j_W} = \gamma a_{j_W} - (\theta + j\,\pi/2)$$

The forces of each half face are obtained as the product of area, the component of pressure normal to the half face, and a pressure coefficient. Flow parallel to a face is assumed to contribute no force. Thus, the net forces along x and along y are composed of eight parts.

$$F_x = F_{x_0} + F_{x_{0^-}} + F_{x_{1^+}} + \text{etc.}$$

$$F_y = F_{y_0} + F_{y_{0^-}} + F_{y_{1^+}} + \text{etc.}$$

For face j+ or j-

$$F_{x_j} = -\left[\begin{Bmatrix} P_{B_{j_E}} \\ P_{F_{j_E}} \end{Bmatrix} A_{j_E} + \begin{Bmatrix} P_{B_{j_W}} \\ P_{F_{j_W}} \end{Bmatrix} (A_j - A_{j_E})\right] \cos(\theta + j\,\pi/2)$$

thus:

$$F_{x_j} = -\left[B_{j_E} + B_{j_W}\right] \cos(\theta + j\,\pi/2), \text{ and}$$

$$F_{y_j} = -\left[B_{j_E} + B_{j_W}\right] \sin(\theta + j\,\pi/2) \qquad (j = 0,\ 1,\ 2,\ 3)$$

where the negative sign denotes the drag direction. The term $P_{B_{j_E}}$ is used if $\pi/2 < a_{j_E} < 3\,\pi/2$. $P_{F_{j_E}}$ is used otherwise. This change is associated with the use of base or frontal surface pressure coefficients associated with the appropriate type of surface, i.e., whether the surface is flat or curved.

Similarly a_{j_W} is associated with $P_{B_{j_W}}$ and $P_{F_{j_W}}$. A_j is the total

area of the half face and A_{j_E} is the area of the half face which is external to the wake boundary.

The terms P_B and P_F are defined as follows:

$$P_{B_{j_E}} = C_{D_B} \frac{\rho_E}{2} Va_{j_E}^2 \cos^2 a_{j_E} + P_{s_E}$$

$$P_{F_{j_E}} = C_{D_F} \frac{\rho_E}{2} Va_{j_E}^2 \cos^2 a_{j_E} + P_{s_E}$$

$$P_{B_{j_w}} = C_{D_B} \frac{\rho_w}{2} Va_{j_w}^2 \cos^2 a_{j_w} + P_{s_w}$$

$$P_{F_{j_w}} = C_{D_F} \frac{\rho_w}{2} Va_{j_w}^2 \cos^2 a_{j_w} + P_{s_w} \qquad (j = 0, 1, 2, 3)$$

where P_{s_E} and P_{s_w} are static pressures at the centroid. The velocities employed above are given by

$$Va_{j_E} = \left[(\dot{x}_j - W_x)^2 + (\dot{y}_j - W_y)^2 \right]^{1/2}$$

$$Va_{j_w} = \left[(\dot{x}_j - W)^2 + \dot{y}_j^2 \right]^{1/2}$$

In terms of the above notations, the moments are simply obtained:

$$M = M_{0^+} + M_{0^-} + M_{1^+} \text{ etc.}$$

$$M_{j^-} = - B_{j^-_E} \cdot a_{j^-_E} - B_{j^-_w} \cdot a_{j^-_w}$$

$$M_{j^+} = B_{j^+_E} \cdot a_{j^+_w} + B_{j^+_w} \cdot a_{j^+_w} \qquad (j = 0, 1, 2, 3)$$

where a_{j_E} is the moment arm of the centroid of the exposed portion of half face j^- and a_{j_w} is the moment arm to the centroid of the portion of half face j^- within the wake. A similar statement applies to half face j^+.

The details of the computation of the quantities a_{j_E} and a_{j_W} are not given here. The areas associated with partial exposure of the flat faces of a cylinder are determined as part of a circle cut by a chord, while the appropriate centroid of this area is computed to obtain the center of pressure. The projected area of the curved faces when partially across the wake boundary is obtained by approximating this area as a trapezoid. The centroid of the trapezoid is obtained for the moment calculations.

C. Side Separation Equations

The motion of a capsule during side separation is analyzed in two phases, namely

(1) That during which exposure is incomplete, and the capsule is subject to restraints imposed by the carrier vehicle

(2) That in which the capsule is free of the carrier vehicle but is subject to the interference forces and moments due to the locally varying flow field.

In the case of the equations associated with partial exposure, particular attention is required in representing the areas and effective forces of the parts of the separating body which are exposed to the air stream in the vicinity of the carrier vehicle. The forces are obtained in terms of pressure coefficients and exposed areas. The exposed area is obtained by computing the position at which the axis of the emerging capsule that is normal to the air stream crosses the carrier vehicle surface. From this coordinate and the geometry of the capsule, it is possible to compute both the exposed area and the center of pressure for this area. During the partial exposure phase, the capsule is assumed restrained from pitching and axial translation. In the computations, this restraint is released at different levels of exposure. The moments on the capsule which exist during the restraint phase of emergence are calculated only to determine structural requirements on this restraint and to determine frictional forces opposing ejection.

The second phase of the separation trajectory involves the motion of the capsule in the vicinity of the carrier vehicle while under the influence of the flow field about the carrier vehicle. The equations to be employed in this part of the analysis represent three-dimensional motion and are conventional in form. Difficulty occurs in the representation of the aerodynamic forces on the capsule as it separates from the carrier vehicle. Three problem areas arise, namely: the presence of a nonuniform flow field along the sides of the carrier from one point to another in the field; the presence of a shock front with which the separating capsule may come in contact as it emerges thus causing a discontinuity in

the force on the capsule; and, finally, interference on the capsule due to a velocity gradient distribution over the capsule caused by the field nonuniformity over its extremities. As stated in section IV. C. 2, the effects of capsule interaction with the carrier flow field are neglected.

The variations in flow field intensity can be accounted for by inserting the flow field velocity deviations from free stream along and normal to the carrier axis as a function of position with respect to the vehicle, and computing the local "uniform" flow velocity as a function of capsule position with respect to the carrier.

In the process of the computation, the equation of the shock front in coordinates attached to the carrier vehicle is programmed into the computation. The coordinates of the separating body are compared with the equation of the shock front at each step of the computation to determine if the separating body was in contact with the front. At time of contact with the shock front, the body area lying on the shock front is computed. This is employed in the force and moment equations along with the pressure differential across this area. Interference effects can be obtained by a similar procedure. The interference field may be effectively represented in carrier vehicle body fixed coordinates by taking deviations from the averaged "uniform" field seen by the capsule. The coordinates of the separating body are also represented in the same axis system and the interference flow at points on the separating body can be obtained.

Formulations of the respective sets of motion equations, for partial exposure and for complete exposure, are presented in the two subdivisions of this section.

1. Partial Exposure Phase

The carrier vehicle is assumed to be initially traveling on a straight line path which is the x axis. Its acceleration, ng, is assumed constant. The origin is taken at the initial center of gravity of the separating body,

and the coordinate system is space-fixed. The separating body is restrained during a portion of the ejection phase so that rotation and differential motion with respect to the carrier longitudinal axis are not possible. This restraint is released when the differential y coordinate of the separating body is equal to some value less than or equal to that corresponding to total exposure of the separating body. Then during the period of restraint

$$\ddot{x}_c = ng$$

$$\ddot{\theta} = 0$$

$$m_c \ddot{y}_c = - \mu f_a F_{a_x} - \mu f_m m_c ng - F_{a_y} + F(y, t)$$

where μ is the coefficient of friction, F_a's are the aerodynamic forces and $F(y, t)$ is the force imparted by the ejection mechanism. No gravity force is introduced since gravity is acting equally on both bodies.

The f's are determinable from the geometry of the capsule-carrier restraint system. The subscripts a and m are used to take into account the fact that the centers of aerodynamic loads and mass will in general be different.

The quantities F_{a_x} and F_{a_y} are obtained by summing the products of pressure and projected areas of the capsule. The pressures over the parts of the capsule exposed to the air stream may be approximated with modified Newtonian coefficient times the local dynamic pressure experienced by the capsule.

In order to exclude the mathematical possibility of the frictional force aiding the ejection of the capsule in the equations of motion (i. e., the friction force acting in the desired direction of motion), the terms contributing to this force must be properly identified by sign. Thus, when the magnitude of frictional resistance due to inertial forces exceeds that due to F_{a_x}, and the carrier is decelerating, the absolute magnitude of the friction force must be employed with a negative sign in the lateral displacement equation of motion. In all other cases, since F_{a_x} is considered acting in the "drag" direction, the pure algebraic values can be used to achieve the proper vector direction of the net friction force.

When the restraint is released, the separating body is free to both rotate and translate relative to the carrier vehicle. The equations for this part of the ejection phase are as follows:

$$m_c \ddot{y}_c = - F_{a_y} + F(y, t)$$

$$m_c \ddot{x}_c = - F_{a_x} + m_c g \sin \Gamma_o$$

$$I_c \ddot{\theta}_c = F_{a_x} \bar{y} + F_{a_y} \bar{x}$$

Where $\bar{x}$ and $\bar{y}$ are the axial and normal moment arms from the center of pressure of the exposed portion of the capsule to the capsule center of gravity.

The areas exposed and centroids of these areas are computed from the geometry of the particular body and the instantaneous extent of emergence.

In some cases the longitudinal axis of the separating body is at right angles (normal) to the longitudinal axis of the carrier vehicle. In other cases, the two longitudinal axes are parallel. In the case of a sphere, the orientation is immaterial.

2. Side Separation Proximity Phase

These equations are employed to calculate separation trajectories during the phase while the separating body is free of the carrier vehicle and in the flow field altered by the parent body. The carrier vehicle is assumed to be accelerating along a straight line path, the x axis. The y axis is obtained by a counterclockwise rotation. The carrier vehicle is assumed to be accelerating at a rate of n g's, including gravity effect, in the direction of motion (along the x axis). The x and y coordinate system is attached to the carrier vehicle nose. The interference effects due to deviations from average local conditions are denoted by a subscript i. The equations of motion are:

$$m_c (\ddot{x}_c + ng) = - C_A (\alpha)\, QA \cos\theta - C_N(\alpha)\, QA \sin\theta$$

$$- mg \sin\Gamma_o - C_{L_i}\, QA \sin\gamma - C_{D_i}\, QA \cos\gamma$$

$$m_c \ddot{y}_c = - C_A(\alpha)\, QA \sin\theta + C_N(\alpha)\, QA \cos\theta$$

$$+ C_{L_i}\, QA \cos\gamma - C_{D_i}\, QA \sin\gamma$$

$$I_c \ddot{\theta}_c = C_M(\alpha)\, QAd + C_{M_q} \frac{\dot{\theta} d}{2V}\, QAd$$

$$+ C_{M_i}\, QAd$$

where

$$\alpha = \theta - \gamma$$

$$\gamma = \tan^{-1} \frac{u_y - W_y}{u_\infty + u_x - W_x}$$

ρ_1 = average local stream density

$$V_1^2 = (u_\infty + u_x - W_x)^2 + (u_y - W_y)^2$$

θ = angle measured between the carrier longitudinal axis and the capsule longitudinal axis

u_∞ is the carrier velocity, a function of time, $= u_{o_\infty} + ng(t - t_o)$

u_x and u_y are the x and y components of the relative velocity of capsule to carrier

W_x and W_y are the averaged local "interference" velocities imparted to the medium by the passage of the carrier and contributing to a determination of the local angle of attack. The moment coefficients are referenced to the capsule diameter, d, in this case.

$$Q = \frac{1}{2}\, \rho_1\, V_1^2$$

C_{L_i} and C_{D_i} are the force increments normal and parallel to the mean stream direction due to continuous stream direction gradients and curvature over the extremities of the capsule.

All aerodynamic coefficients are referred to the capsule reference area and the local average dynamic pressure.

The values of C_A, C_N, C_M, and C_{M_q} to be used in these equations are those appropriate to the capsule in a uniform flow field at an effective Mach number generated locally by the carrier. The angle of attack, α, is also with respect to the averaged local flow direction seen by the capsule.

This effective Mach number may be taken as the average of the Mach number existing over the length of the capsule when flow variations are within the limits of the linear approximations of Moskowitz (Reference 53). In this case, the additional terms C_{L_i} and C_{M_i}, due to stream curvature and direction gradients, are determinable by integrations of the velocity potential functions and are obtained in terms of velocity variations from the mean local conditions acting over the capsule extremities, and the drag term is deleted. The mean conditions may be defined as those prevailing at half the capsule length and deviations, when taken, can be referenced to these conditions.

For blunt capsule configurations or for areas of flow where large gradients exist, the strip theory would be employed in order to avoid the restrictions of linearization. The correlation of the method with wind tunnel data indicates satisfactory prediction of aerodynamic coefficients is achievable. When strip theory is used, the effect of gradients and curvature are more conveniently included in single coefficients such as $C_{A'}$, $C_{N'}$, and $C_{M'}$ with the deletion of the incremental nonuniformity terms, i.e., C_{L_i} and C_{M_i}, from the equations of motion.

The effects of flow discontinuities generated by the intersection of a shock wave with the capsule are not obtainable from the linearized approximation and must be determined by the strip method of calculation.

Geometric relations are employed to compute the coordinates of the outermost points on the base and nose of the separating capsule. At each step of the computation, these are compared to the coordinates of the side of the carrier vehicle to determine if the capsule has collided with the carrier vehicle. If collision occurs, the computation is stopped.

LIST OF SYMBOLS FOR THE APPENDIX

A	Cross-sectional area, ft^2
B	Force on capsule face, lbs
C	Force or moment coefficient, dimensionless
F	Force, lbs
I	Moment of inertia, $slugs/ft^2$
K	Spring rate of attachment lines, lbs/ft
K_j	Distance from centroid of half face to capsule c.g., ft
M	Moment, ft-lbs
P	Pressure on capsule face, lbs/ft^2
Q	Dynamic pressure, lbs/ft^2
T	Thrust force, lbs
V	Velocity, ft/sec
W	Interference velocity, ft/sec
d	Diameter, ft
f	Restraint geometry function for partial exposure phase
g	Gravitational acceleration, ft/sec^2
h	Distance measured from c.g. to nose of vehicle along longitudinal axis; ft
k	Damping constant associated with lines
l	Distance or length, ft
t	Time, seconds

m	Mass, slugs
n	Acceleration, gravity units
u	Relative velocity, ft/sec
(x, y, z)	Coordinates along trajectory, ft
$(\dot{x}, \dot{y}, \dot{z})$	Velocity components along trajectory, ft/sec
$(\ddot{x}, \ddot{y}, \dot{z})$	Acceleration components along axes, ft/sec^2
Γ_o	Initial path angle, radians
Δ	Denotes incremental term
θ	Relative attitude angle, radians
θ_o	Initial path angle and attitude angle (zero angle of attack), radians
α	Angle of attack, radians
γ	Path angle, radians; direction of local velocity with respect to carrier
γ_{a_j}	Air flow angle on capsule face
η	Ordinate of nose cone body axes systems, distance measured along this axis
λ	Unstretched length of attachment lines, ft
μ	Friction coefficient, dimensionless
ξ	Abscissa of nose cone body axes system, distance measured along this axis
ρ	Mass density of atmosphere, slugs/ft^3 - or linear mass density, slugs/ft

τ	Position angle with respect to body axes, radians
$(\dot{})$	First derivative with respect to time
$(\ddot{})$	Second derivative with respect to time

LIST OF SUBSCRIPTS FOR THE APPENDIX

A	Axial direction, axial force
B	Base or leeward face
D	Drag Force
E	Exterior to wake or dimensions and conditions of exposed portion of capsule during partial exposure phase
F	Frontal (windward) face
L	Lift force
M	Moment in pitch
N	Normal direction, normal force
T	Denotes position of application of thrust forces
a	Aerodynamic
b	Refers to afterbody section
c	With respect to capsule
cg	With respect to center of gravity
i	Interference terms
j	Denotes capsule half face
l	Local conditions
n	Refers to nose section
o	Initial conditions

p	With respect to pilot device
q	Slope of parameter with respect to pitching velocity
s	With respect to afterbody shoulder; or – in general – knife-edge contact point between nose and afterbody sections
v	With respect to carrier vehicle
w	With respect to wake conditions
α	Denotes slope of parameter with respect to angle of attack, $\frac{d()}{d\alpha}$
∞	With respect to free stream conditions
x, y, z	Refers to direction of axes, x, y, z
1, 2, 3	Along coordinate axes

AFOSR-109

Directorate of Research Analysis
Air Force Office of Scientific Research
Office of Aerospace Research
Holloman Air Force Base, New Mexico
DYNAMICS OF SEPARATING BODIES, Volume I, THEORETICAL ANALYSIS
by A. H. Solarski, R. Turner and F. Doerr
Cook Research Laboratories, a division of Cook Electric Company, Chicago, Illinois
March 1961. pp incl. illus., tables
Technical Report AFOSR-109
(Contract AF 29(600)-1711) unclassified report

The theoretical foundations of a detailed study of the dynamics of separating bodies at supersonic speeds are established. Carrier vehicle flow field characteristics are investigated to define the environment into which the ejected bodies are projected. The aerodynamic properties of representative capsule configurations in locally

(over)

UNCLASSIFIED

I. Introduction
II. Criteria of the Study
III. Equations of Motion
IV. Aerodynamics
V. Separation Trajectory Calculations
VI. Conclusions
Appendix
1. Solarski, A. H., Turner, R., F. Doerr
2. Contract AF 29(600)-1711

UNCLASSIFIED

AFOSR-109

Directorate of Research Analysis
Air Force Office of Scientific Research
Office of Aerospace Research
Holloman Air Force Base, New Mexico
DYNAMICS OF SEPARATING BODIES, Volume I, THEORETICAL ANALYSIS
by A. H. Solarski, R. Turner and F. Doerr
Cook Research Laboratories, a division of Cook Electric Company, Chicago, Illinois
March 1961. pp incl. illus., tables
Technical Report AFOSR-109
(Contract AF 29(600)-1711) unclassified report

The theoretical foundations of a detailed study of the dynamics of separating bodies at supersonic speeds are established. Carrier vehicle flow field characteristics are investigated to define the environment into which the ejected bodies are projected. The aerodynamic properties of representative capsule configurations in locally

(over)

UNCLASSIFIED

I. Introduction
II. Criteria of the Study
III. Equations of Motion
IV. Aerodynamics
V. Separation Trajectory Calculations
VI. Conclusions
Appendix
1. Solarski, A. H., Turner, R., F. Doerr
2. Contract AF 29(600)-1711

UNCLASSIFIED

AFOSR-109

Directorate of Research Analysis
Air Force Office of Scientific Research
Office of Aerospace Research
Holloman Air Force Base, New Mexico
DYNAMICS OF SEPARATING BODIES, Volume I, THEORETICAL ANALYSIS
by A. H. Solarski, R. Turner and F. Doerr
Cook Research Laboratories, a division of Cook Electric Company, Chicago, Illinois
March 1961. pp incl. illus., tables
Technical Report AFOSR-109
(Contract AF 29(600)-1711) unclassified report

The theoretical foundations of a detailed study of the dynamics of separating bodies at supersonic speeds are established. Carrier vehicle flow field characteristics are investigated to define the environment into which the ejected bodies are projected. The aerodynamic properties of representative capsule configurations in locally

(over)

UNCLASSIFIED

I. Introduction
II. Criteria of the Study
III. Equations of Motion
IV. Aerodynamics
V. Separation Trajectory Calculations
VI. Conclusions
Appendix
1. Solarski, A. H., Turner, R., F. Doerr
2. Contract AF 29(600)-1711

UNCLASSIFIED

AFOSR-109

Directorate of Research Analysis
Air Force Office of Scientific Research
Office of Aerospace Research
Holloman Air Force Base, New Mexico
DYNAMICS OF SEPARATING BODIES, Volume I, THEORETICAL ANALYSIS
by A. H. Solarski, R. Turner and F. Doerr
Cook Research Laboratories, a division of Cook Electric Company, Chicago, Illinois
March 1961. pp incl. illus., tables
Technical Report AFOSR-109
(Contract AF 29(600)-1711) unclassified report

The theoretical foundations of a detailed study of the dynamics of separating bodies at supersonic speeds are established. Carrier vehicle flow field characteristics are investigated to define the environment into which the ejected bodies are projected. The aerodynamic properties of representative capsule configurations in locally

(over)

UNCLASSIFIED

I. Introduction
II. Criteria of the Study
III. Equations of Motion
IV. Aerodynamics
V. Separation Trajectory Calculations
VI. Conclusions
Appendix
1. Solarski, A. H., Turner, R., F. Doerr
2. Contract AF 29(600)-1711

UNCLASSIFIED

AFOSR-109

varying flows are documented, and the equations of motion pertinent to the several modes and techniques of ejection and separation are stated. Trajectory computations based upon a realistic summary of the problem inputs are discussed, and the relative importance of the operational parameters assessed. Separation system requirements are compared for the several ejection modes and capsule configurations considered. Particular emphasis is given to the section describing the wake structure behind a body representative of a carrier vehicle traveling at supersonic speeds.

UNCLASSIFIED

UNCLASSIFIED

AFOSR-109

varying flows are documented, and the equations of motion pertinent to the several modes and techniques of ejection and separation are stated. Trajectory computations based upon a realistic summary of the problem inputs are discussed, and the relative importance of the operational parameters assessed. Separation system requirements are compared for the several ejection modes and capsule configurations considered. Particular emphasis is given to the section describing the wake structure behind a body representative of a carrier vehicle traveling at supersonic speeds.

UNCLASSIFIED

UNCLASSIFIED

AFOSR-109

varying flows are documented, and the equations of motion pertinent to the several modes and techniques of ejection and separation are stated. Trajectory computations based upon a realistic summary of the problem inputs are discussed, and the relative importance of the operational parameters assessed. Separation system requirements are compared for the several ejection modes and capsule configurations considered. Particular emphasis is given to the section describing the wake structure behind a body representative of a carrier vehicle traveling at supersonic speeds.

UNCLASSIFIED

UNCLASSIFIED

UNCLASSIFIED

AFOSR-109

varying flows are documented, and the equations of motion pertinent to the several modes and techniques of ejection and separation are stated. Trajectory computations based upon a realistic summary of the problem inputs are discussed, and the relative importance of the operational parameters assessed. Separation system requirements are compared for the several ejection modes and capsule configurations considered. Particular emphasis is given to the section describing the wake structure behind a body representative of a carrier vehicle traveling at supersonic speeds.

UNCLASSIFIED

UNCLASSIFIED